Aus dem
Institut for Lung Biology and Disease
Helmholtz-Zentrum München

Myeloid cells immunomodulate tissue niches in Idiopathic Pulmonary Fibrosis

Dissertation
zum Erwerb des Doctor of Philosophy (Ph.D.) an der Medizinischen Fakultät der Ludwig-Maximilians-Universität München

vorgelegt von
Sonia Valeria
Viteri Alvarez

aus
Quito/Ecuador

Jahr
2024

Mit Genehmigung der Medizinischen Fakultät der
Ludwig-Maximilians-Universität München

Erstes Gutachten:	Prof. Dr. Anne Hilgendorff
Zweites Gutachten:	Dr. Dr. Isis Fernandez Buelvas
Drittes Gutachten:	Prof. Dr. Christian Schulz
Viertes Gutachten:	Priv. Doz. Dr. Tobias Veit

Dekan: Prof. Dr. med. Thomas Gudermann

Tag der mündlichen Prüfung: 01.07.2024

"The value of a life is measured by its impact on others"

Jackie Robins

Table of Content

List of Figures

List of Tables

Glossary

A

ARG1	Arginase 1
ASCEND	A Randomized, Double-Blind, Placebo Controlled, Phase 3 Study of the Efficacy and Safety of Pirfenidone in Patients with Idiopathic Pulmonary Fibrosis
AT2	Pulmonary alveolar type II cells
ATP	Adenosine triphosphate
ATS	American Thoracic Society
α-SMA	alpha -smooth muscle actine

B

B regs	Regulatory B cells
BAL	Bronchoalveolar lavage
BSA	Bovine serum albumin

C

CAPACITY	A Randomized, Double-Blind, Placebo Controlled, Phase 3 Study of the Safety and Efficacy of Pirfenidone in Patients with Idiopathic Pulmonary Fibrosis
CCL12	Chemokine (C-C motif) ligand 12 / Monocyte chemotactic protein 5
CCL2	Chemokine (C-C motif) ligand 2/ Monocyte chemoattractant protein 1
CNT	Carbon Nanotubes
COL1A2	Collagen alpha-2(I) chain
COX-2	Cycloxygenase-2
CTLA4	Cytotoxic T-lymphocyte-associated protein 4
CXCL8	Chemokine (C-X-C motif) ligand 8

D

DAMPs	Damage associated molecular patterns
DCs	Dendritic cells
dH_2O	Distilled water
DLco	Diffusing capacity of lung for carbon monoxide
DMSO	Dimethyl sulfoxide
DNA	Deoxyribonucleic acid
DPLD	Diffuse parenchymal lung diseases

E

ECM	Extracellular matrix
EMPIRE	European MultiPartner IPF registry. A longitudinal observational registry that describes the characteristics and outcomes of IPF patients throughout Europe.
EMT	Epithelial-to-mesenchymal transition
EthD-III	Ethidium homodimer III

F

FACS	Fluorescence-activated cell sorting
FAO	Fatty acid oxidation
FATP2	Fatty acid transport protein 2
FBS	Fetal bovine serum
FFPE	Formalin-fixed paraffin-embedded
FGF	Fibroblast growth factor
FVC	Forced vital capacity of lung

G

GAP index	Gender, age, and lung physiology index to evaluate the average mortality risk of IPF
GERD	Gastroesophageal reflux disease
GM-CSF	Granulocyte/macrophage colony-stimulating factor
G-MDSCs	Granulocytic myeloid-derived suppressor cells or PMN-MDSCs

H

H&E	Hematoxylin and eosin stain
H_2O_2	Hydrogen peroxide
HIF-1	Hypoxia-inducible factor 1
HLA-DR	Human Leukocyte Antigen – DR isotype
HRCT	High-resolution computed tomography

I

IBD	Inflammatory bowel disease
IFN-α	Interferon alpha
IFN-γ	Interferon gamma
IHC	Conventional Immunohistochemistry
IIP	Idiopathic interstitial pneumonia
IL-2	Interleukin 2

ILC2	Innate lymphoid cell type 2
ILD	Interstitial lung diseases
iNOS	Nitrogen-oxygen synthase 2
INPULSIS 1 and 2	52 Weeks, Double Blind, Randomized, Placebo-controlled Trial Evaluating the Effect of Oral BIBF 1120, 150 mg Twice Daily, on Annual Forced Vital Capacity Decline, in Patients with Idiopathic Pulmonary Fibrosis
INPULSIS-ON	Extension of clinical trials INPULSIS 1 and 2
IPF	Idiopathic pulmonary fibrosis

L

LAG3	Lymphocyte-activation gene 3

M

MDSCs	Myeloid-derived suppressor cells
MeOH	Methanol
MFI	Median fluorescence intensity
mIHC	Multiplexed immunohistochemistry
M-MDSCs	Monocytic myeloid-derived suppressor cells
MMP1	Matrix Metallopeptidase 1
MMP19	Matrix Metallopeptidase 19
MMP7	Matrix Metallopeptidase 7
MMPs	Metalloproteinases
MSC	Mesenchymal stem cells

N

NK	Natural killer cells
NO	Nitric oxide

P

PASSPORT	Pirfenidone post-authorization safety registry (PASSPORT)
PBMC	Peripheral blood mononuclear cell
PCLS	Precision cut lung slice
PD1	Programmed cell death protein 1
PDL1	Programmed death-ligand 1
PFA	Paraformaldehyde
PGE2	Prostaglandin E2
phFbs	Primary human fibroblasts
PMA	Phorbol 12-myristate 13-acetate

PMA	Phorbol-12-myristate-13-acetate 8
PMN-MDSCs	Polymorphonuclear myeloid-derived suppressor cells or G-MDSCs

R

RNS	Reactive nitrogen species
ROS	Reactive oxygen species
RT	Room temperature

S

scRNA-seq	Single-cell RNA sequencing
STAT3	Signal transducer and activator of transcription 3

T

TAMs	Tumor-associated macrophages
TCR	T cell receptor
TEM	Tumor microenvironment
TGF-β	Transforming growth factor-beta
TGF-β1	Transforming growth factor beta 1
Th2	T helper 2 cell
TIGIT	T cell immunoreceptor with Ig and ITIM domains
TIM3	T cell membrane protein-3
TIMP	Tissue inhibitors of metalloproteinase
TLC	Total lung capacity
TLR2	Toll-like receptor 2
TNF-α	Tumour necrosis factor-alpha
Total MDSCs	G-MDSCs + M-MDSCs
TRM	Tissue-resident memory – cell

U

UIP	Usual interstitial pneumonia

V

VEGF	Vascular endothelial growth factor

Abstract

Idiopathic Pulmonary Fibrosis (IPF) is a progressive and life-threatening lung disease. It is characterized by alterations in the lung interstitium with excessive extracellular matrix buildup and a gradual decline in lung function. While the etiology is unclear, a combination of genetic factors, environmental triggers, and immune system dysregulation are thought to be contributing factors. Recent research in IPF has cast a strong spotlight on myeloid and monocyte-like cells, such as immature monocytes and myeloid-derived suppressor cells (MDSCs). Patients with IPF have shown elevated numbers of these cells, linked to increased progression and poorer prognoses [1,2]. Thus, further investigation is required to unravel the extent of the role played by monocytes and monocyte-like cells in the pathogenesis of IPF and understand the cellular and molecular mechanisms underlying this role.

In **Chapter 4.1**, we first characterized circulating MDSCs in IPF patients. In a previous study[1], our group described increased MDSCs counts in peripheral blood in IPF patients for the first time and found a correlation with disease progression. Here, we collected peripheral blood from a new cohort of 41 IPF patients and characterized it using flow cytometry. We found that MDSCs were increased in peripheral blood of IPF patients compared to healthy controls, validating our group's prior findings.

In **Chapter 4.2**, we delved into the immunomodulatory capacity of MDSCs. Our group had previously demonstrated that MDSCs can suppress proliferation in autologous $CD8^+$ T cells[1]. Importantly, the reduction of T lymphocyte proliferative capacity found by our group is one of the features of $CD8^+$ T cell exhaustion[3]. Here we aimed to characterize this interaction between MDSCs – $CD8^+$ T cells in IPF and its potential pro-fibrotic role. First, we demonstrated the existence of an exhausted $CD8^+$ T cell phenotype in IPF lung by analyzing the IPF atlas, as well as immunohistochemistry; thus, we validated the presence of circulating $CD8^+$ T cells, $PD1^+$, $LAG3^+$, and $TIM3^+$ using FACS-based immunophenotyping of IPF blood. We further reveal that T cells expressing PD1 are increased in the lungs of IPF

patients and are clustered near PDL1$^+$ M-MDSCs, suggesting the existence of a PD1-PDL1 axis between MDSCs and CD8$^+$ T. Finally, we showed *in vitro*, that IPF M-MDSCs promote exhaustion in autologous CD8$^+$ T cells. Altogether, we demonstrate that one of the immunostimulatory functions of MDSCs is to promote CD8$^+$ T cell exhaustion, which may be mediated by a PD1-PDL1 axis, the role of which in fibrosis demands further exploration.

In **Chapter 4.3,** we investigated the interaction between MDSCs and lung structural cells. Utilizing mass-spectrometry results, we pinpointed markers specifically expressed by MDSCs, including CD263, Neuropilin, and L1CAM. Through FACS analysis, we examined the expression of these markers in circulating MDSCs and compared them to controls. The findings showed a notably higher CD263 and Neuropilin expression in IPF MDSCs, while L1CAM expression was similar in the two groups. The validation of these MDSC-specific markers within fibrous lung tissue was achieved, by quantifying their presence in ILD lung tissue homogenates using FACS. Here we found an enhanced CD263 and L1CAM expression in M-MDSCs. Immunofluorescence staining of lung tissue slides from explanted IPF lungs further confirmed the existence of CD33$^+$CD14$^+$L1CAM$^+$ cells, which are suggestive of M-MDSCs. With MDSCs' presence confirmed in lung tissue, we proceeded to characterize their invasion capability and subtype invasion patterns. Employing a 3D collagen-based assay, we attempted to reproduce the collagen buildup during fibrosis *in vitro*. Notably, our data showed that IPF M-MDSCs display heightened invasiveness compared to control M-MDSCs, suggesting a greater intrinsic capacity to migrate/invade the lung during IPF. These last results prompted us to examine their *in situ* effect. Here, we explored α-SMA expression in primary human fibroblasts (phFbs) co-cultured with M-MDSCs for 48 hours, revealing that IPF M-MDSCs hinder myofibroblast formation when phFbs are cultured with TGF-β, as evidenced by lowered α-SMA expression. Furthermore, TGF-β concentrations were reduced in the supernatants of phFbs co-cultured with IPF M-MDSCs compared to cultures containing only phFbs (No TGF-β added). These intriguing findings suggest that M-MDSCs possess an anti-fibrotic effect. Together, our *in vitro* experiments reveal that circulating MDSCs

express exclusive markers, are capable of invasion/migration, and are detectable in IPF lungs, where they appear to exert an anti-fibrotic effect *in situ*.

1 Introduction

1.1 Idiopathic pulmonary fibrosis (IPF)

1.1.1 Definition

Idiopathic pulmonary fibrosis (IPF) is a chronic, progressive, incurable, and fatal lung condition characterized by uncontrolled cellular proliferation and scarring of unknown cause. The permanent alterations in the lung interstitium result in excessive extracellular matrix deposition, gradually impairing the patient's lung function. The prognosis for this condition is poor, with some reports indicating a three to five-year average survival time after diagnosis in the worst cases[4-6]

This clinical entity is a subtype of a group of heterogeneous parenchymal lung illnesses known as diffuse parenchymal lung diseases (DPLD) or interstitial lung diseases (ILD), which overlap some clinical manifestations and pulmonary function decline but have distinct etiologies.

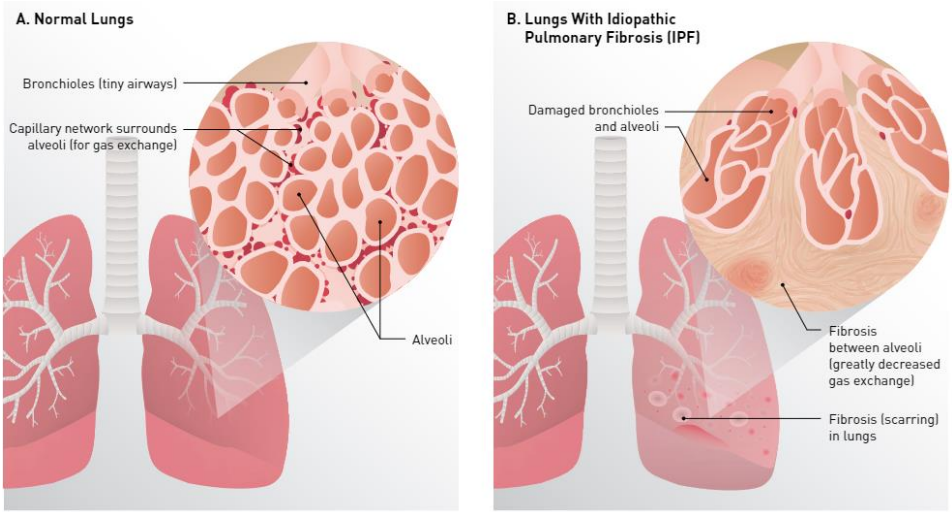

Figure 1. Alveolar damage in Idiopathic Pulmonary Fibrosis (IPF). Normal lungs versus IPF lungs (Modified from Glassberg M. 2017)

There are about 150 documented causes of ILDs, including medications, various types of dust, mold, autoimmune diseases, etc. However, because the origin of IPF is uncertain, it is classified as a variant of this group called idiopathic interstitial pneumonia (IIP) [4,7.]

1.1.2 Epidemiology

Idiopathic pulmonary fibrosis is the most common and severe type of IIP (55%). Globally, the incidence and prevalence of IPF are increasing and vary by population. Currently, it is challenging to tell whether this increase is due to genuine new cases or improved detection [8,9]. IPF is more common in men, with an annual incidence ranging from 2.8 and 19 cases per 100,000 people per year in Europe and North America, while Asia and South America have the lowest rates worldwide (1.2 to 4.16 per 100,000 and 0.26 to 0.48 per 100 000 people per year, respectively). This incidence, however, varies by age group, ranging from 6 cases per 10,000 adults aged 18 to 64 years to 94 cases per 100,000 adults aged 65 years or older. Similarly, the prevalence of IPF is 18 cases per 10,000 adults aged 18 to 64 years, while in those aged 65 years and older, the prevalence is 495 cases per 10,000 [9,10]

1.1.3 Pathophysiology

The fibrotic process in IPF is multifactorial and is characterized by excessive extracellular matrix deposition and disruption of normal pulmonary architecture, probably as a result of a dysregulated wound-healing process [8,9].

The specific trigger of IPF has not been identified. Data suggests that the pulmonary epithelia of some individuals with intrinsic (e.g. genetics, aging, etc.) or extrinsic (e.g. cigarette smoke, particles, viruses, etc.) triggers, undergoes a profibrotic epigenetic reprogramming, rendering it dysfunctional and more susceptible to premature apoptosis [8,9]. This aberrant epithelium is then activated and proliferates abnormally, particularly the alveolar epithelial cells of type A2 (AT2), affecting their progenitor functions [8,9](Figure 2).

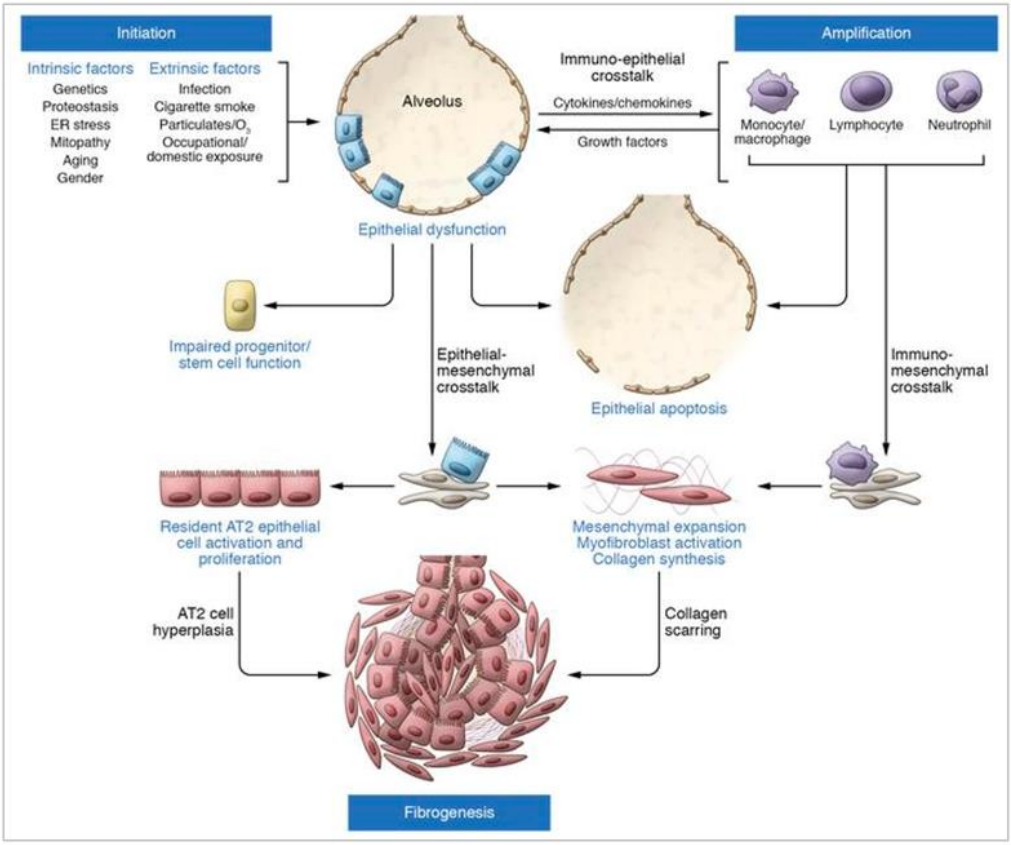

Figure 2. IPF pathogenesis occurs in three phases. *Initiation:* Intrinsic (e.g., genetic) and extrinsic (e.g., infection, air pollution) factors acting through various pathways converge to produce a vulnerable AT2 population (blue rectangular cells). Vulnerable AT2s subject of continuous cell quality controls or additional secondary injuries stimuli (often recurrent) develop functional defects with an aberrant activation of developmental programs, cell stress responses impaired progenitor function, and/or apoptosis. *Amplification*: Dysfunctional AT2 cell (red rectangular cells) start crosstalk with immune cells, which can amplify the initial injury events and promotes EMT. *Fibrogenesis*: The dysfunctional alveolar niche exhibits further feed-forward mechanisms to promote AT2 dysfunction with increased proliferation, impaired trasndifferentation to AT1 cells and upregulation of senescence. Coupled with enhanced myofibroblast activation and ECM deposition, the disrupted repair response leads to scar formation and progressive fibrotic remodeling (Modified from Katzen et al. 2020)

According to current findings, whether the pulmonary alveolus is repeatedly harmed by ex ternal forces or not, this sensitive and aberrantly activated epithelium reacts and initiates immune responses [11]. During this process, alveolar epithelial cells secrete a variety of pro-fibrotic mediators, including transforming growth factor (TGF-ß), tumor necrosis factor-alpha (TNF-α), fibroblast growth factor (FGF), platelet-derived growth factors, various

metalloproteinases (e.g. MMP1, MMP7, MMP19, etc.), chemokines (e.g CCL2, CCL12), and coagulation factors (e.g. Factor X), all of which contribute to the migration, proliferation, and activation of fibroblasts and myofibroblast, thus extracellular matrix (ECM) deposition remodeling [12,13].

TGF- ß is a strong profibrotic cytokine produced by the epithelium and other cell types such as macrophages, neutrophils, etc. Overproduction of this protein promotes the expression of fibronectin, α-smooth muscle actin (α-SMA), collagen, and N-cadherin, markers related to epithelial-to-mesenchymal transition (EMT). This occurs through Smad activation, the canonical TGF-ß downstream signaling[14–19]. During fibrosis, TGF-ß crosstalk with pathologically reactivated embryological pathways like WNT[20], Sonic Hedgehog[21,22], and Notch[23], resulting in a pro-fibrotic feedback loop[13].

Alongside these events, the immune system reacts (e.g. innate and adaptative immune cells) altering their function, and depending on the context, by promoting repair and wound healing, or by sending aberrant signals to other immune cells and structural cells, thereby contributing to the progression of fibrosis [13,24]. The immune system's role in IPF will be discussed in depth later.

1.1.4 Diagnosis and clinical phenotypes

IPF is frequently misdiagnosed since many of the initial symptoms and signs are ambiguous and attributed to aging or other comorbidities (e.g. cardiovascular disease). Hence, multidisciplinary team management must be established in the event of suspicion [10,13]. Due to that, there is an average of 2.2 between the onset of symptoms and diagnosis [25].

Exertional dyspnea is the most common reason for a consultation, which may or may not be accompanied by a dry cough. Spirometry is used to assess lung function, and it will reveal a restrictive pattern (decrease in total lung capacity TLC) associated with aberrant gas

exchange[13]. Other findings can include digital clubbing (one-third of patients), scalene hypertrophy, and fine bibasilar inspiratory crackles (velcro-like sounds)[10]. When IPF is suspected, it is critical to do a thorough examination of the patient's personal pathological history (e.g. connective tissue illnesses, chronic hypersensitivity pneumonitis, etc.), as well as exposure to environmental and pharmacological therapies [10,13].

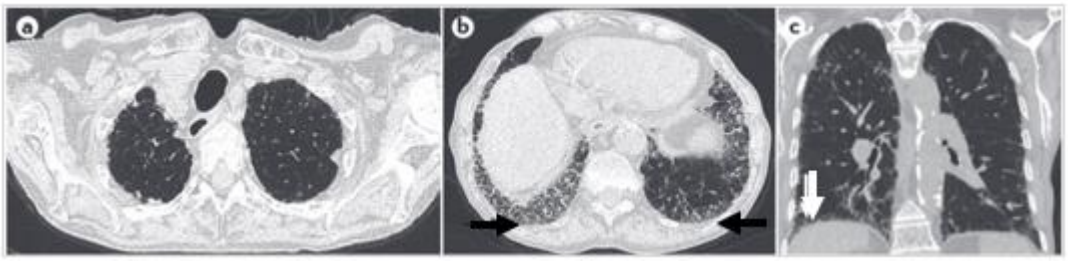

Figure 3. HRCT images from a patient with IPF. High-resolution CT (HRCT) images collected from a woman with progressive cough and dyspnea, showing her upper lung zones (panel **a**), lower lung zones (panel **b**), and the sagittal plane of the lungs (panel **c**). These images show lower lobe-predominant peripheral honeycomb change (panels **b** and **c**, arrows), a typical UIP pattern. (Modified from Martinez et al. 2017)

After excluding other probable causes, high-resolution computed tomography (HRCT) is used to identify the so-called usual interstitial pneumonia (UIP) pattern, which is defined by a honeycombing pattern that predominates in the periphery (Figure 3)[13].

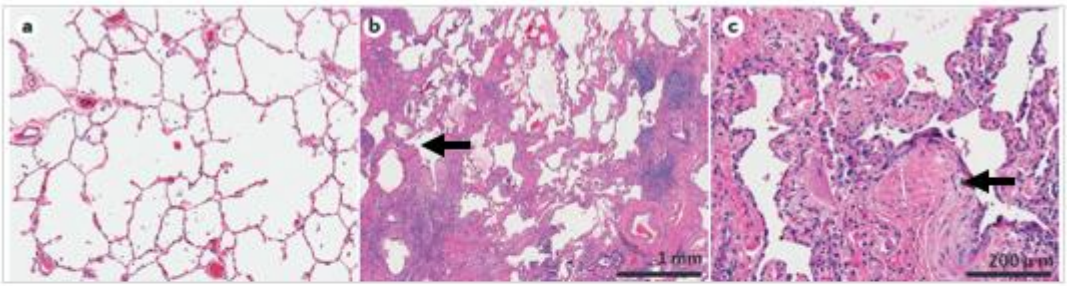

Figure 4. Honeycombing typical in IPF. Honeycombing is the feature of the usual interstitial pneumonia (UIP). **a)** Normal lung histology, **b)** Low-power H&E-stained biopsy section obtained from a patient with UIP, revealing, micro-honeycombing pattern (arrow). **c)** High-power H&E-stained (from biopsy **b**) with fibroblastic foci (arrow), with aggregates of proliferating fibroblasts and myofibroblasts that represent areas of active IPF disease. (Modified from Martinez et al. 2017)

When clinical and imaging evidence alone are inconclusive, a lung biopsy is required [5,13]. In this scenario, it is imperative to consider that this procedure could increase mortality, as well as to consider if the outcome would influence the patient's therapeutic approach [5,13].

In histologic examinations, the characteristic feature of a UIP pattern is the presence of so-called "fibroblast foci" (proliferating fibroblasts and myofibroblasts) that disturb the architecture of the lung parenchyma, giving it a heterogeneous appearance and accompanied by microscopic honeycombing and traction bronchiectasis (Figure 4). If the pathologic diagnosis is uncertain, the outcome is classed as probable, possible, or non-UIP [8,13]. Once a diagnosis is established, knowing the precise prognosis is difficult due to the presence of several clinical phenotypes that cannot be predictable. “Slow progressors” have a sluggish clinical course (with or without stability periods) and seek medical attention months or years after the onset of symptoms [26,27]. A subset of this group, with poor forced vital capacity (FVC) and sometimes a low diffusing capacity for carbon monoxide (DLco)[28], may undergo “acute exacerbations” that frequently herald the disease's fatal phase (50% mortality rate)[10]. On the other hand, due to their rapid deterioration, so-called “rapid progressors” (often male smokers) are examined by a physician within the first six months of symptom onset; these patients often have a shorter survival [5,26]. (Figure 5)

Risk evaluation tools are commonly utilized by physicians to predict the clinical trajectory of patients who have just been diagnosed with IPF. Among these tools, the GAP index stands out as a method for assessing the average mortality risk of IPF patients, which is determined by their disease stage. This staging system incorporates four key variables namely: gender **(G)**, age **(A)**, and two pulmonary physiological parameters **(P)** that are: percentage predicted forced vital capacity (FVC [%]), and percentage predicted diffusion capacity of the lungs for carbon monoxide (DL_{CO} [%]). The staging system is categorized as follows: Stage I (GAP score 0-3), Stage II (GAP score 4 and 5), and Stage III (GAP score 6-8), each corresponding to 3-year survival rates of 16.3%, 42.1%, and 76.8%, respectively)[29]. In spite of recent progress, the widespread adoption of biomarkers derived from peripheral blood,

airways, and parenchymal compartments for purposes such diagnosis, prognosis, the assessment of disease severity, and monitoring progression, is limited within the framework of IPF [30,31].

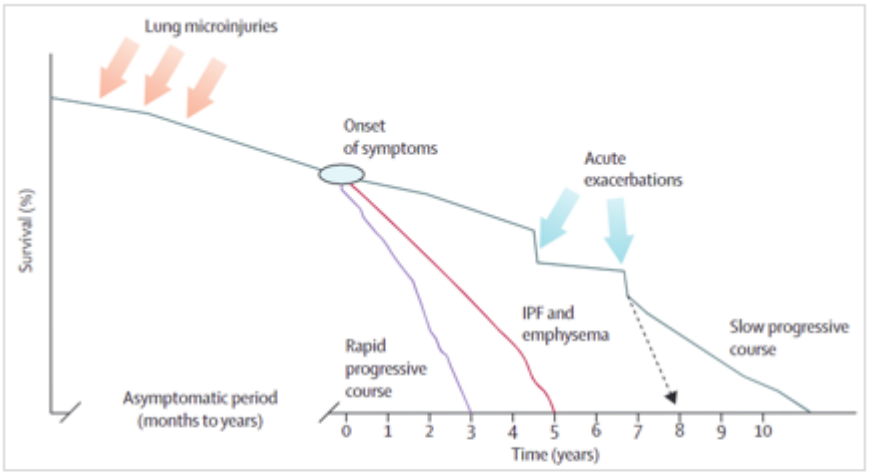

Figure 5. Clinical phenotypes in IPF. The heterogeneous natural history pattern in IPF patients. Most of the patients are "slow progressors" and about 10% of these patients can present episodes of acute clinical deterioration, so-called "acute exacerbations". A few patients have short duration illness with a rapidly progressive clinical course, so-called "rapid progressors". (Modified from King et al. 2011)

1.1.5 Treatment

Despite extensive research, there is no pharmaceutical cure for IPF. Current schemes focus on slowing the progression of lung function loss, which improves survival. Nintedanib and Pirfenidone are the two drugs currently approved by global guidelines [10,32].

In the INPULSIS-1, INPULSIS-2, and INPULSIS-ON clinical trials (phase 3), the tyrosine kinase inhibitor Nintenadib, demonstrated efficacy in delaying the rate of FVC decline and lowering the probability of a first acute exacerbation compared to placebo [33,34]. Long-term follow-ups revealed a similar safety profile [30] with diarrhea (60.1% -71.2% percent), weight loss, and bleeding (8.4%) as the most common side effects [10,33].

The mechanism of action of Pirfenidone is unknown, but it has been shown in animal models to have antifibrotic and anti-inflammatory properties (e.g. regulating TGF-ß and TNF-α action and inhibiting collagen synthesis and fibroblast proliferation)[5,35]. Furthermore, findings from the third phase of the CAPACITY and ASCEND clinical trials demonstrated its ability to also reduce FVC decline [35,36], lessen the likelihood of respiratory hospitalization [37], and slower disease progression [38]. Concurrently, the PASSPORT[39] and EMPIRE[40] (European MultiPartner IPF registry) observational investigations and other retrospective studies[41] discovered that patients who received antifibrotic therapy had longer survival. The most reported side effects were skin rash, photosensitivity, and gastrointestinal issues[42]. Combined use of Pirfenidone and Nintedanib showed less decline in FVC than Nintedanib monotherapy, but more research is required [43].

Non-pharmacological treatments such as pulmonary rehabilitation and long-term oxygen therapy are recommended by international guidelines[10,32], as they have been shown to improve 6-minute walking distance, exercise capacity, and relieve dyspnea in IPF patients [44,45]. Smoking cessation support is a high priority in this population.

However, because none of the preceding treatments are curative, therefore lung transplantation should be considered in patients with moderate to severe illness, with a 6-year median survival [13,46].

1.2 Role of the immune system in IPF

Multiple studies have demonstrated that inflammation plays a significant role in the onset and development of IPF, nevertheless, anti-inflammatory therapies (e.g., steroids) have failed or even had detrimental effects in IPF clinical trials [47]. Yet, it is evident that there is crucial immunomodulation that may be either beneficial or harmful, and a deeper understanding of the role of the innate and adaptive immune system is critical for the development of novel therapeutic approaches.

As the first line of defense, the innate immune system plays a variable role in IPF depending on the cell type. While some studies have shown that neutrophils promote tissue remodeling and fibrosis [48–50], others have found a protective effect [51], and their depletion in murine models has not improved fibrosis [52]. Activated macrophages have been widely studied for their role in fibrosis promotion [53–55], whereas M1 macrophages have more of a protective role [56]. In contrast, monocytes have a significant function in the process of fibrogenesis. This function is not limited to the production of pro-fibrotic cytokines, but also involves their role as progenitors for pro-fibrotic cells such as M2 macrophages and fibrocytes[47,57,58]. These circulating bone marrow-derived mesenchymal progenitor cells migrate to lung tissue and undergo differentiation into fibroblasts and myofibroblasts, further contributing to the fibrotic process[47,57,58]. Myeloid-derived suppressor cells (MDSCs) have also been linked to IPF, and their increased number is associated with poor prognosis [1]. Finally, although mast cells and innate lymphoid cell type 2 (ILC2) are present in IPF patients, the majority of studies show that they play a modulatory role rather than contributing to disease progression [47].

On the other hand, in the adaptive immune system, the role of the T cell is controversial and relies on the cell subtype and stage. Th2 cells[59], Th17 cells [59], and $CD8^+$T cells have demonstrated pro-fibrotic effects, whereas Th1[59], Th22, tissue-resident memory TRM $CD4^+$ T cells, and γδ-T cells have shown a protective effect. It is difficult to draw conclusions about Th9 and Tregs, which have pro-fibrotic and anti-profibrotic properties, and additional research is necessary [47,57,59,60].

1.2.1 Myeloid Cells in Lung Fibrosis

Myeloid cells emerge from common progenitors in the bone marrow and develop into the granulocytic and monocytic lineages, differing from the lymphoid lineage. Monocytes, macrophages, dendritic cells (DCs), fibrocytes, myeloid-derived suppressor cells (MDSC),

and granulocytes are all members of this category. These cells are crucial for tissue homeostasis as they initiate, suppress, or inhibit the adaptive immune response.[61,62] When tissue damage occurs danger-associated molecular patterns (DAMPs) are released and can initiate immune responses, for example in pulmonary fibrosis DAMPs are found in the ECM (nucleic acids, ATP, TLR2, uric acid; TGF-ß)[63]. In response to that, macrophages, DCs, mast cells, and other resident cells become activated, producing pro-inflammatory mediators (e.g. histamine), cytokines, and chemokines (CCl2, CXCL8), that cause the migration of other immune cells.[61,62,64] Simultaneously, the endothelial injury might result in myeloid cells infiltration (mostly neutrophils and monocytes) at the injury site, triggering an inflammatory response that attempts to prevent damage by phagocytosing debris and dead cells [65,66]. Following this inflammatory phase, ECM deposition and scarring occur as a result of myofibroblast activation by anti-inflammatory cytokines (e.g., TGF-beta, IL10) via M2-like macrophages. Following the removal of excessive ECM by e.g. metalloproteinases (MMPs), the final stage, or resolution, which is mediated by fibroblasts and macrophages, begins [62,67–69].

When there is an imbalance in this process, as is the case in IPF, repetitive injury leads to the accumulation and dysregulation of myeloid cells (e.g macrophages) and cells from the adaptive immune system (e.g., T cells) in the fibroblast foci, a structure formed by hyperproliferating fibroblast[60,70]. Moreover, fibroblasts differentiate into apoptosis-resistant myofibroblasts that generate more ECM proteins, resulting in macrophages' pro-repair polarization of (M2). These macrophages (M2) will perpetuate fibrosis by secreting CCL18, which will induce fibroblasts activation and ECM deposition[60,62].

1.2.1.1 Monocytes in IPF

Monocytes have a high degree of plasticity and have been demonstrated to play a crucial regulatory function in fibrosis[71]. Studies have shown that monocytes modulate wound healing alongside neutrophils within the first few hours after tissue injury and can phagocyte

tissue debris[69,72]. Indeed, research shows that CCL2 and fractalkine (CX3CL1) generated by the endothelium and airway epithelial cells (respectively) promote monocyte mobility in fibrotic lungs[73–75]. Furthermore, these cells not only contribute directly to the fibrotic process of IPF but also might supply populations of inflammatory macrophages and DCs that contribute in-situ to fibrosis progression[76].

Monocytes account for 10% of human circulation leukocytes and 4% of mouse circulation leukocytes. These blood cells can be categorized into three distinct types: classical, intermediate, and non-classical. In humans, the classical type is characterized by $CD14^{++}$ $CD16^{-}$ expression, while in mice, it is identified by $Ly6C^{hi}$ $CD43^{+}$ expression. The intermediate type is denoted by $CD14^{+}$ $CD16^{+}$ expression in humans and $Ly6C^{int}$ $CD43^{+}$ expression in mice. Lastly, the non-classical type is characterized by $CD14^{+}$ $CD16^{++}$ expression in humans and $Ly6C^{lo}$ $CD43^{+}$ expression in mice. Yet, the relevance of the three different subtypes in IPF is still unclear. In mouse models of pulmonary fibrosis depleting $Ly6C^{hi}$ cells, reminiscent of classical monocytes, reduced fibrosis, and adoptive transfer worsened it[77]. Intermediate monocytes can release high levels of proinflammatory cytokines (IFN-α, CCL3, CCL4), which enhance myofibroblast differentiation[47].

Interestingly, two studies suggest that monocytes from a blood differential count could be used as a biomarker for IPF. Scott and colleagues discovered a correlation between high absolute monocyte counts ($>0.95 \times 10^9$/L) and poor IPF outcomes in 7000 individuals across five cohorts. A retrospective pooled study of 2067 patients from the randomized double-blind phase 3 studies ASCEND, CAPACITY, and INSPIRE corroborated these findings (detailed in 3.1.5). Higher counts of 0.60-0.95 and $>0.95 \times 10^9$/L were associated with worse prognosis, risk of hospitalization, and high mortality after a year[78,79]. However, because the blood differential count cannot distinguish between phenotypically similar cells, we cannot be certain whether this count represents solely monocytes or monocyte-like cells, such as immature forms of monocytes and myeloid-derived suppressor cells (MDSCs). This distinction is critical because immature phenotypes, such as MDSCs[70], have been linked to

a worse prognosis in IPF, making it crucial to evaluate if these cells are contributing to increased monocyte counts. Yet, the involvement of monocytes and monocyte-like cells in the pathogenesis and natural history of IPF should be further investigated[80].

1.2.1.2 Myeloid-derived suppressor cells (MDSCs)

1.2.1.2.1 Definition, origin, features and subsets

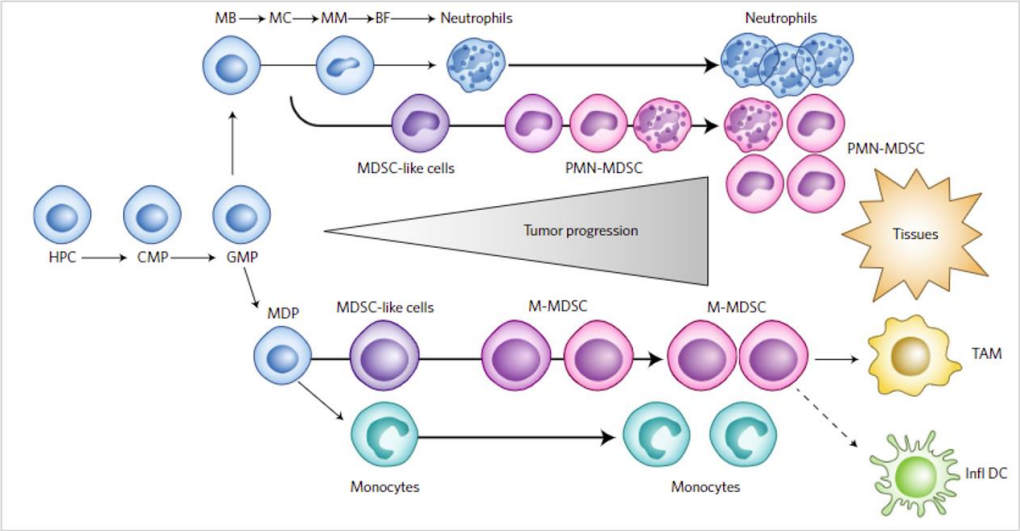

Figure 6. MDSCs differentiation and accumulation. Neutrophils and monocytes are differentiated in bone marrow from hematopoietic progenitor cells (HPCs) via common myeloid progenitors (CMPs) and granulocyte-macrophage progenitors (GMPs). Neutrophil and monocytes differentiation progresses through several progenitor and precursor stages. Under pathologic conditions like cancer, populations of immature myeloid cells are expanded and converted to immunosuppressive MDSCs and accumulate in tissue. In tumors, M-MDSCs rapidly differentiate in tumor-associated macrophages (TAMs) and inflammatory dendritic cells (infl DCs). (Modified from Veglia, F et al. 2018)

Myeloid-derived suppressor cells (MDSCs) are a heterogeneous group of immature cells derived from bone marrow hematopoietic progenitor cells that modulate the immune response through their strong immunosuppressive capacity and pathological activation program. Their increased presence has been linked to several types of cancer, autoimmune disorders, lung transplantation, and infections, among other acute and chronic conditions[81,82].

The classification of MDSCs as a cell type has been highly debated due to a lack of precise phenotyping and reliable methodologies addressing its immunomodulatory function. Although categorizing them as a cell type has helped to define "atypical behaviors" of a subset of myeloid lineage cells in various pathologies, identifying whether they are a cell type, or an undifferentiated state of myeloid cells remains challenging[83].

In both humans and mice, MDSCs can be categorized into two primary groups: granulocytic MDSCs (G-MDSCs) and monocytic MDSCs (M-MDSCs). These categories are based on their origin from either the granulocyte or monocytic myeloid cell lineages, respectively (as shown in Figure 6)[79]. The differentiation of these immature subsets during myelopoiesis is influenced by various factors, including granulocyte/macrophage colony-stimulating factor (GM-CSF), interleukin IL-6, IL-10, IL-12, cycloxygenase-2 (COX-2), prostaglandin E2 (PGE2), and vascular endothelial growth factor (VEGF)[83-86], yet the main regulators have not been identified.

Characterization of MDSCs remains difficult; in fact, a wide range of cells with properties similar to MDSCs have been seen in chronic diseases, making conclusive identification problematic. However, MDSCs in humans have traditionally been identified by the negative expression of different myeloid origin cell markers such as CD3, CD16, CD19, CD20, and CD56 (lineage negative)[87-89]. M-MDSCs are Lin^{neg} HLA-DR^{-} $CD33^{+}$ $CD11b^{+}$ $CD14^{+}$ cells and the lack or low expression of HLA-DR distinguishes them phenotypically from blood monocytes. PMN-MDSCs are Lin^{neg} HLA-DR^{-} $CD33^{+}$ $CD11b^{+}$ $CD66b^{+}$ cells, and their isolation in a low-density gradient (FICOL 1.077g/ml) helps to differentiate them from neutrophils[84,87,90]. However, the characterization of MDSCs remains difficult; in fact, a wide range of cells with similar properties have been described in chronic diseases, making a conclusive identification problematic. Nowadays, single-cell assays have the potential to shed light on this problem because they allow for more specific genetic annotations that allow for a better characterization of MDSCs and, when combined with other methods, allow us to identify different parameters that help us clarify their function and describe the networks involved

in their suppressive cascade[83]. Figure 7 depicts the newly suggested markers for more comprehensive phenotyping[91].

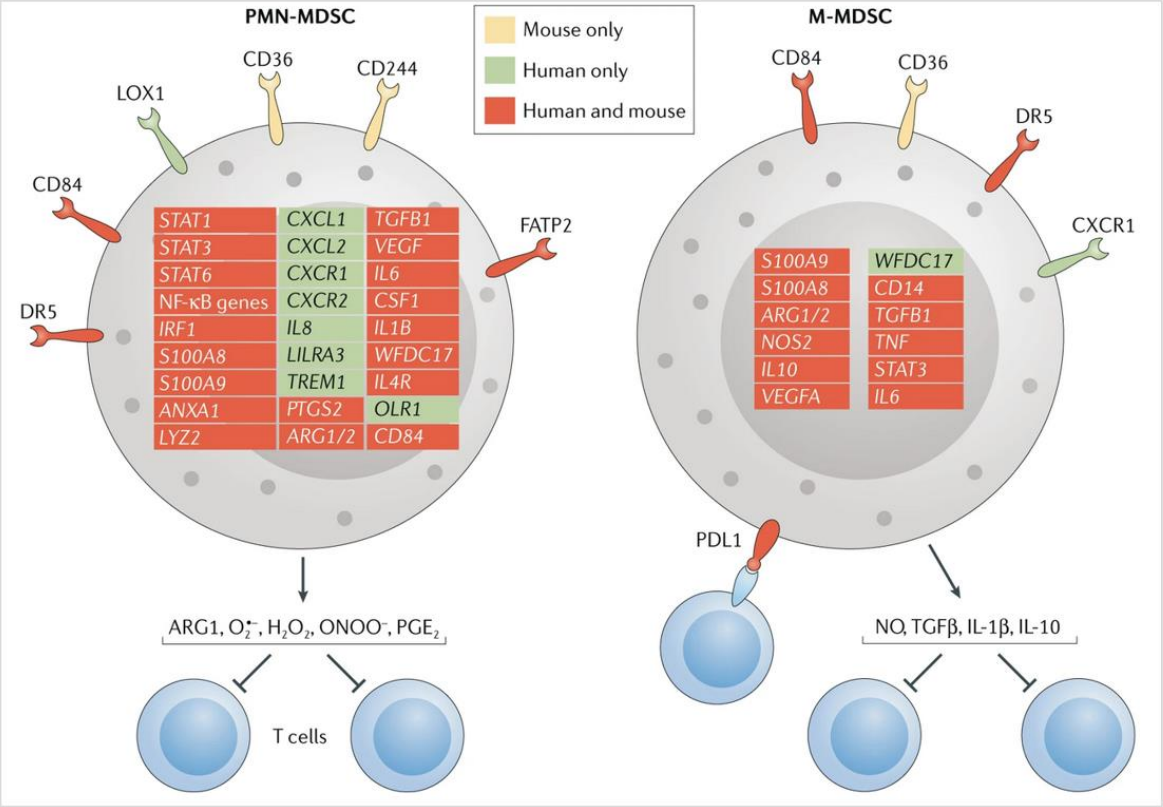

Figure 7. Distinguishing MDSCs from classical neutrophils and monocytes. The figure depicts the genes (depicted inside the cell) and surface molecules that can be used to distinguish PMN- MDSCs and M- MDSCs from classical neutrophils and monocytes. Factors are depicted in yellow, green and red based on whether they are useful markers in mice only, humans only, or both mice and humans, respectively. The figure also illustrates the main immunosuppressive mechanism used by MDSCs. Please note that this information was obtained from studies of MDSCs in cancer. CXCR1, CXC- chemokine receptor 1; FATP2, fatty acid transport protein 2; LOX1, lectin- type oxidized LDL receptor 1; NO, nitric oxide; PGE2, prostaglandin E2. (Modified from Veglia et al, 2021)

Surface molecules Gr1 and CD11b are found in mice MDSCs. Gr1 is constituted of the Ly6C and Ly6G markers. The phenotype of mouse PMN-MDSCs are $CD11b^+Ly6G^+$ and M-MDSCs is $CD11b^+Ly6C^+Ly6G^{-/low}$, which do not distinguish them from neutrophils and monocytes, respectively; thus, they are identified based on their ability to suppress other immune cells[84,90]. However, new research has identified surface markers and genes that may aid in the identification of these cells in mice, as illustrated in Figure 7.

1.2.1.2.2 MDSCs immunosuppressive mechanisms

MDSCs exert an immunoinhibitory role by either boosting immunosuppression or suppressing pro-inflammatory cells; MDSCs mediate T cell suppression primarily via increased arginase 1 (ARG1), nitrogen-oxygen synthase 2 (iNOS), and reactive oxygen species (ROS). Cell-to-cell contact is not required for ARG1-induced suppression, whereas iNOS- and ROS-mediated inhibition require T cells and MDSCs to be in close proximity[92]. The frequency of a specific immunosuppressive mechanism relies on the MDSCs subtypes and disease, as it may fluctuate in response to local inflammatory stimuli. M-MDSCs immunosuppressive activities, which limit both antigen-specific and non-specific T-cell responses, are mostly dependent on nitric oxide (NO) and cytokines such as IL-10 and TGF-ß. G-MDSCs, on the other hand, suppress antigen-specific T-cell responses by upregulating ARG1, PGE2, ROS, and reactive nitrogen species (RNS)[85,90,93]. Interestingly, active MDSCs expressed immune checkpoint proteins, including programmed death-ligand 1 (PD-L1), which may bind to the PD-1 receptor on T cells and thereby induce T cell suppression[94,95].

We have emphasized the immunosuppressive effect of MDSCs on T cells, but it is equally important to understand how the metabolic pathways of the tumor microenvironment (TEM) influence MDSCs' suppressive effects. Cells in the TEM recruit MDSCs by secreting G-CSF and GM-CSF factors[96]. Hypoxia-inducible factor 1 (HIF-1) -mediated chronic hypoxia in the TEM causes an increase in aerobic glycolysis, the so-called “Warburg effect” (a shift from oxidative phosphorylation to glycolysis), and therefore acidosis, and lactate production[96]. These events enhance the immunosuppressive effect of MDSCs by producing checkpoint immune ligands (e.g., PDL1), secreting cytokines (e.g., IL-6), or releasing growth factors (e.g., VEGF)[96,97]. ROS generated by mitochondrial oxidative phosphorylation, on the other hand, enhances PDL1 expression on the surface of MDSCs, causing immunosuppression when they engage with T cells[96].

The immunosuppressive effect of MDSCs has also been demonstrated to be influenced by TME's amino acids like glutamine and cysteine. MDSCs require glutamine to perform their immunosuppressive activity. According to some research, reducing the synthesis of this amino acid could be a target for anti-tumor therapy by inhibiting its immunosuppressive ability[96]. Furthermore, MDSCs inhibit T cell function by sequestering cysteine, an amino acid necessary for optimum T cell function, within their cytoplasm, limiting its availability and hence dampening T cell anti-inflammatory effect [96].

MDSCs suppressor capacity can be diminished by blocking some lipid and cholesterol metabolism processes, such as lipid transport, fatty acid oxidation (FAO), and lipolysis. This has been observed, for example, in G-MDSCs, where the fatty acid transport protein 2 (FATP2) plays an important role in immunosuppressive activity. In murine models, eliminating the gene encoding this protein promotes tumor rejection[96].

Finally, MDSCs secrete Wnt5a and employ autocrine signaling to exert their suppressive function. In a murine model, myeloid-specific Wnt5a suppression lowered tumor formation as well as MDSCs and Treg infiltration[96].

1.2.1.2.3 MDSCs Crosstalk with other immune cells

The immunosuppression that MDSCs exert on conventional lymphocytes T is not limited to the mechanisms described above (1.2.1.2.2); these cells interact in additional ways. Interferon gamma (IFN-γ), IL-3, and IL-10, which are produced by $CD8^+$ and $CD4^+$ T cells, can be integrated into MDSCs, activating them, and enhancing their immunosuppressive function, which has a detrimental effect on the adaptive immune system[98,99].

Natural killer cells (NK), DCs, neutrophils, tumor-associated macrophages (TAMs), and B cells are also suppressed by MDSCs. Cell-cell interaction between MDSCs and NK diminishes NK activity and blocks IFN-γ release, while NO produced by MDSCs suppresses NK cytotoxicity[81,100]. Because G-MDSCs share phenotypic features with neutrophils, it has been

postulated that they constitute neutrophils at a different stage of maturation, and that activated neutrophils might become "MDSC-like" cells with inhibitory activities[81,101,102]. M-MDSCs can also impair B cells' ability to inhibit humoral immune responses via ARG-1, ROS, iNOS, TGF-ß, PGE2, and NO suppressive mediators[103,104]. Intriguingly, MDSCs boosted PD-L1 expression on B cells, transforming them into regulatory B cells (B regs) with enhanced T-cell inhibitory capabilities[105]. G-MDSCs have also been observed to prevent DC antigen cross-presentation. Furthermore, due to their superior antigen presentation and T-cell activation properties, DCs are utilized as cancer vaccines, and one study revealed that a high number of M-MDSCs in the starting culture of monocytes when developing the vaccines could inhibit DCs maturation and reduce the quality of monocyte-derived DCs vaccines[85,106].

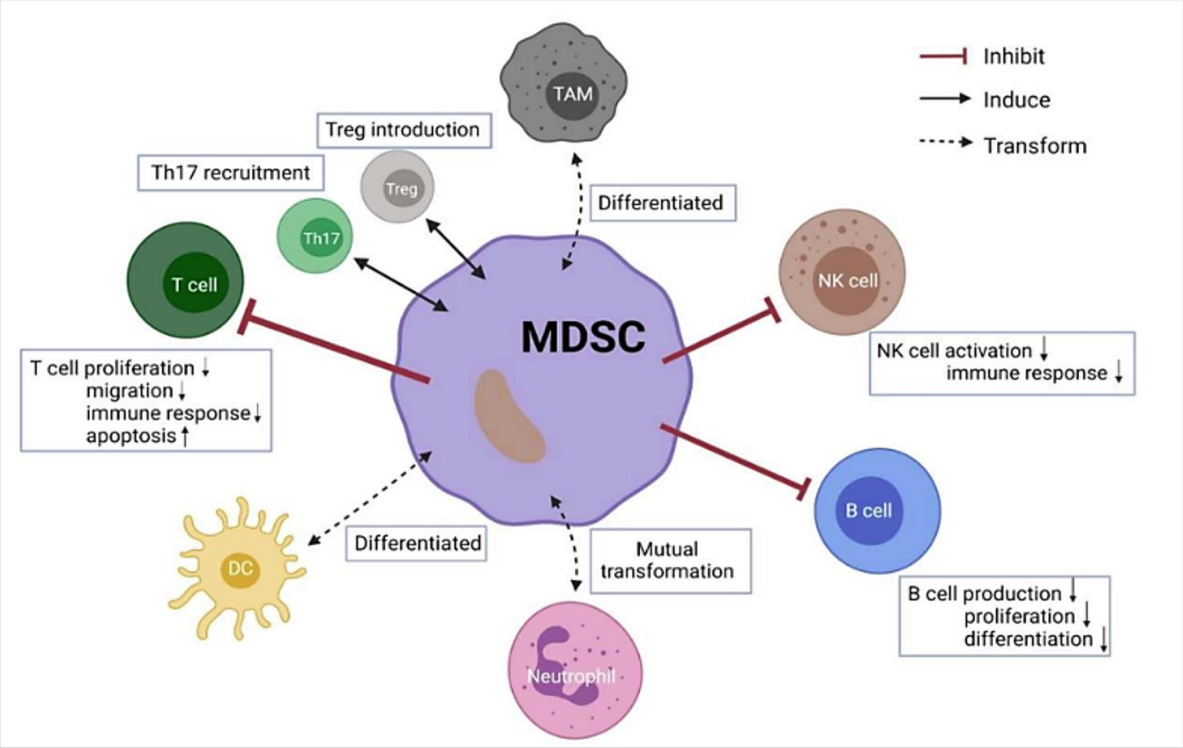

Figure 8. Crosstalk between MDSCs and other immune cells. Up arrows mean increased, and the down arrows mean decreased. (Modified from Ma T. et al. 2022)

To facilitate immunosuppression, MDSCs can stimulate other immune inhibitory cells such as Tregs and TAMs. MDSCs-Macrophages interaction prompts the differentiation of $CD4^+$ T cells (Th2), a decrease in NK, and the formation of Tregs via IL-10[107]. Moreover, ROS increase

or signal transducer and activator of transcription 3 (STAT3) inhibition can cause MDSCs to differentiate in TAMs[108]. MDSCs also induce the formation of Tregs by either cell-to-cell interaction[109,110] or secretion of soluble factors like IL-10 and TGF-β[111], thereby exerting immunosuppression. Tregs, on the other hand, can limit MDSCs proliferation and immunosuppressive potential[112].

1.2.1.2.4 MDSCs in cancer and other pathologies

MDSCs have garnered significant interest in the field of cancer research in recent years. Activated MDSCs assume a pivotal role in various facets of tumor development, encompassing immune evasion, angiogenesis, the formation of pre-metastatic niches, and the induction of epithelial-mesenchymal transition (EMT)[93,112]. A substantial body of evidence suggests a strong association between the presence of total MDSCs in peripheral blood and unfavorable prognoses across several cancer types such as pancreatic cancer, esophageal squamous cell carcinoma, gastric cancer, colon-rectal cancer, hepatocellular carcinoma, breast cancer, NK/T lymphoma, and melanoma[113,114]. Recent research has highlighted a significant increase in myeloid-derived suppressor cells (MDSCs) among patients diagnosed with both early and advanced-stage malignancies. Moreover, these elevated levels of MDSCs are positively correlated with the clinical cancer stage and the presence of metastatic disease [115]. Furthermore, ongoing research is exploring innovative therapeutic strategies that specifically target these cells, as they have shown potential for improving tumor control when combined with traditional therapy methods [116].

MDSCs have a contentious role in infections. In infections caused by Staphylococcus aureus, Mycobacterium tuberculosis, hepatitis C virus, and HIV-1, MDSCs have been linked to a poor prognosis and disease progression. They are also associated with sepsis worsening but not remission. However, they have been shown to be protective against C. albicans infection, sepsis aeruginosa infection, and Klebsiella pneumoniae infection[82]. Intriguingly, during the COVID-19 pandemic, MDSCs have been associated with infection severity[117].

MDSCs are engaged in a variety of autoimmune disorders, and although their role during pathological autoimmune reactions is not entirely known, they may be related to a protective mechanism that limits the autoimmune response to some extent. Multiple sclerosis, type 1 diabetes, rheumatoid arthritis, inflammatory bowel disease (IBD), and autoimmune hepatitis have all been associated with an increase in MDSCs. However, the expansion of MDSCs populations in autoimmune disease states is less dramatic than in cancer and infectious disorders[82,90,118].

1.2.1.2.5 Roles of MDSCs in fibrosis

MDSCs are widely recognized for their role in cancer, but they have also been connected to other processes such as fibrosis at the organ level.

In the lung, MDSCs accumulation in mice bleomycin-induced pulmonary fibrosis has been described[119,120]. Furthermore, mice treated with silica or CNT (carbon Nanotubes) exhibited a strong correlation between the accumulation of MDSCs and lung fibrosis[121,122]. MDSCs from silica-treated mice produce transforming growth factor beta 1 (TGF-ß1), which stimulates lung fibroblasts to secrete tissue inhibitors of metalloproteinase (TIMP)-1, blocking collagen degradation and promoting lung fibrosis[121]. Another possible phenomenon present during tissue repair is the differentiation of MDSCs into fibrocytes. MDSCs can evolve not only into fibrocytes, which stimulate fibroblast proliferation, migration, and collagen formation but also into myofibroblasts[123,124]. Finally, our group showed for the first time, that the MDSCs count in IPF patients was higher than in the healthy control group, and that there was an inverse correlation between lung function and circulating MDSCs counts[1].

MDSCs, particularly M-MDSCs, have been demonstrated to protect against liver fibrosis. Animal studies have shown that MDSCs, by releasing IL-10, block the profibrotic activity of activated hepatic stellate cells, which are responsible for liver fibrosis in mice. Moreover, MDSCs depletion enhanced fibrosis markers[125,126].

G-MDSCs were found in the kidneys of mice with chronic renal inflammation and fibrosis, where they regulate the excessive proliferation of effector T cells, DCs, and macrophages. In addition, MDSCs depletion in the kidney enhances fibrosis markers, implying that MDSCs play a fibrosis-protective role[126].

In contrast, G-MDSCs accumulated significantly higher than monocytic M-MDSCs in the hearts of old mice. The researchers discovered that G-MDSCs induce cardiac fibrosis by releasing S100A8/A9[127].

1.2.1.2.6 Other Roles of MDSCs

Obesity has been associated with chronic inflammation[128]. Chronic inflammation increases MDSCs in obese individuals, increasing insulin sensitivity; nevertheless, because MDSCs suppress T cells, these patients are more vulnerable to infection. Furthermore, elevated MDSCs levels raise the risk of cancer and hasten the progression of early-stage malignancies to the metastatic phase[82].

Emerging data show that MDSCs have essential roles in shaping the immune response in some physiological contexts, such as pregnancy and the early weeks of life[129]. MDSCs populations are expanded during pregnancy. MDSCs suppress T cells in pregnant women, preserving maternal-fetal tolerance. Moreover, MDSCs populations are expanded in cord blood and neonates, thereby protecting newborns against infection and inflammation[82].

Engagingly, MDSCs are rapidly being recognized as having a critical role in transplant tolerance by modulating adaptive immune responses by inhibiting allogeneic T-cell proliferation and inducing Treg formation. In a rat model, increasing MDSCs levels promote kidney transplant tolerance by suppressing T cell proliferation. Furthermore, co-transplantation with MDSCs effectively protected mouse islet allografts without the use of immunosuppressive agents, which was associated with a decrease in $CD8^+$T cells and

significant proliferation of Tregs in grafts [129]. More research is required in this context, as relevant clinical studies have yet to be published.

1.2.2 Lymphocytes T in IPF

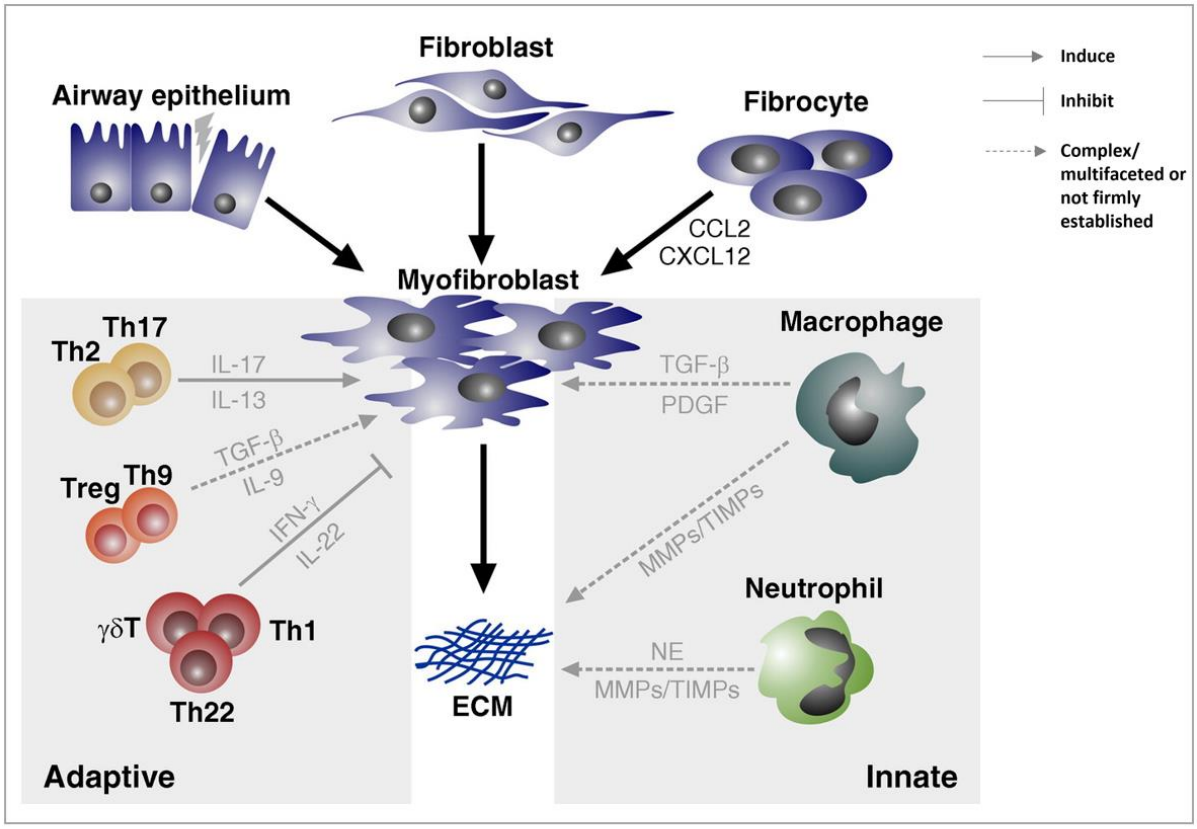

Figure 9. Effect of immune cells on myofibroblasts and fibrogenesis. Airway epithelial cell injury/epithelial-mesenchymal transition and fibroblast trans differentiation and/or chemokine (CC chemokine ligand [CCL] 2, CXC chemokine ligand [CXCL] 12)-mediated fibrocyte recruitment contribute to the generation of myofibroblasts, which represent the major producers of extracellular matrix (ECM) components. Both adaptive (T cells, left box) and innate (macrophages and neutrophils, right box) immune cells modulate fibrogenesis through various mechanisms. (Modified from Kolahian S. et al. 2016)

There has been ongoing debate regarding the involvement of adaptive immune cells in the onset and progress of pulmonary fibrosis. The roles of different T cell subtypes could be influenced by the secretion of chemokines[59], as depicted in Figure 9. Furthermore, while several studies have reported an increase in $CD4^+$ and $CD8^+$ T cells within the lungs and bronchoalveolar lavage (BAL) of IPF patients, it is unclear whether this increase holds

functional significance, as it does not consistently represent lung interstitium alterations[130]. Hence, there is a need for a deeper understanding of their role in the progression of this pathological condition.

1.2.2.1 $CD8^+$ T cells in IPF

The role of $CD8^+$ T lymphocytes in pulmonary fibrosis is debatable. Recent research on IPF lung explants revealed an increase in $CD8^+$ T cells that lacked CD28 (a condition of chronic activation) and had a profibrotic and proinflammatory transcriptional profile, whereas $CD8^+$ T cells that exhibited higher PD-1 alleviated fibrosis[131]. Another study revealed $CD8^+$ T more diffusely across the lung parenchyma and alveolar wall of IPF patients' surgical biopsies, whereas $CD4^+$ T cells were closer to lymphoid follicles, suggesting that the two cell types play separate roles in IPF progression. Higher $CD8^+$ T cells in lung biopsies of IPF patients were found to correlate with reduced total lung capacity and vital capacity in the same study[132]. Moreover, $CD8^+$ T cells differentiated into IL-13-producing profibrotic cells in the bleomycin-induced lung fibrosis model[130]. Finally, a humanized mouse pulmonary fibrosis model demonstrated that $CD8^+$ T cells were essential for the induction of pulmonary fibrosis[133]

1.2.2.2 $CD8^+$ T cell exhaustion

Prolonged exposure to antigens and/or persistent inflammation, as observed in chronic viral and bacterial infections, as well as chronic diseases, can lead to the differentiation of $CD8^+$ T cells into a state known as exhaustion[3]. In this state, there is a notable reduction in their effector functions and a diminished capacity for proliferation[3].

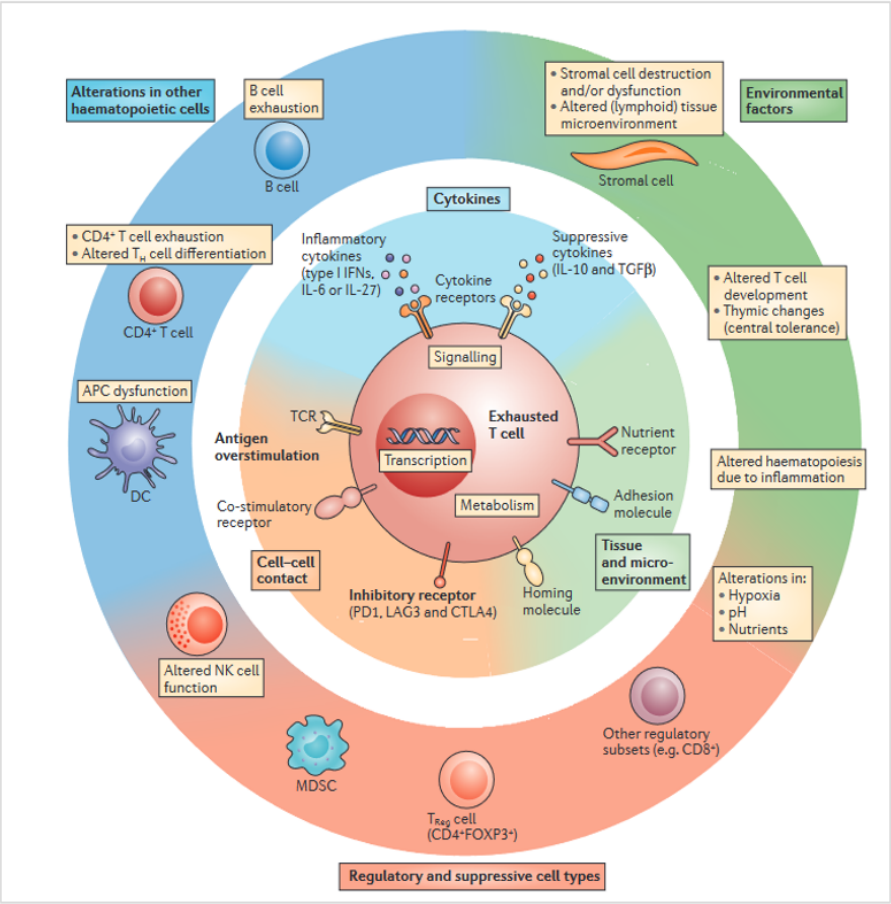

Figure 10. Overview of mechanisms of T cell exhaustion. Pathways implicated in regulating T cell exhaustion can be classified into three general categories (center and inner circle): cell-to-cell signals including prolonged T cell receptor (TCR) engagement (signal 1) and co-stimulatory and/or co-inhibitory signals (signal 2); soluble factors such as excessive levels of inflammatory cytokines (IFNs) and suppressive cytokines (IL-10, TGF-ß); and tissue and microenvironmental influences driven by changes in the expression levels of chemokine receptors, adhesion molecules and nutrient receptors. Other immune cell types and stromal cells could be the source of many of these changes (outer circle). (Modified from Wherry EJ et al. 2015)

T cell exhaustion is a hyporesponsive T cell state, that is characterized by decreased expression of effector cytokines (e.g IL-2, INF-γ, TNF-α), increased expression of co-inhibitory immune checkpoint receptors (e.g PD-1, TIM-3, LAG-3, TIGIT, and CTLA) and transcription genes changes (e.g EOMES, T-bet, TOX, TCF-1), which collectively contribute to inhibitory signaling and a decrease in T cell cytotoxicity[3,131,134,135]. T cell exhaustion is not

solely reliant on the expression of a single co-inhibitory receptor; rather, it is determined by the concurrent expression of multiple co-inhibitory receptors [3].

T cell exhaustion is caused by a variety of pathways, which may be divided into three broad categories (see Figure 10): a) cell-to-cell signals (including prolonged TCR engagement and co-stimulatory and/or co-inhibitory signals), b) soluble factors such as high levels of inflammatory and suppressive cytokines (e.g., interferons, IL-10, TFG-ß), and c) tissue and micro environmental influences via changes in the expression levels of chemokine receptors, adhesion molecules, and nutrient receptors. Other immune and stromal cell types (e.g., APCs, $CD4^+$ T cells, NK, B cells), as well as regulatory cells (e.g., MDSCs and TReg), may be responsible for these changes within this final group[3].

Although $CD8^+$ T cells have been the most well-documented in terms of exhaustion, dysfunctional states caused by chronic antigen stimulation have also been observed in $CD4^+$ T cells[135,136].

1.2.2.3 T cell exhaustion in IPF

Despite some studies have linked T cell biology with poor prognosis in IPF[136–138], the involvement of T cell checkpoint receptors in the disease's progression is unclear. The majority of research has focused on co-stimulatory (activation) receptors, rather than the co-inhibitory receptors linked to T cell exhaustion. In a recent study, $CD4^+$ $PD1^{+,}$ circulating cells were found to be increased in IPF patients compared to controls, and they were able to induce collagen I production when co-cultured with human fibroblasts. The same group discovered that using PD-1 null mice or an antibody against programmed cell death ligand 1 (PD-L1) dramatically decreased fibrosis compared to controls in a bleomycin mouse model of lung fibrosis[139].

2 Objectives

In recent years, immune dysregulation has emerged as a driver of IPF[130]. Among the regulators of immune responses, MDSCs stand out for their role in preserving immune balance. However, in chronic conditions, the expansion of MDSCs can have dual effects, either exacerbating disease progression or suppressing the host immune defense. Previous studies by our group have shown that an increase in circulating MDSCs correlates with IPF disease progression and a worse prognosis[1]. Yet, the precise function of MDSCs and their effect on lung fibrosis remain poorly understood.

This thesis is based on our research group's preliminary findings. The primary aims of this study are as follows: 1) To understand the immunomodulatory role of MDSCs; and 2) To elucidate the interactions between MDSCs and structural cells within the lung in IPF. The results may contribute to a better understanding of the molecular and cellular processes underlying the onset and progression of IPF, thereby facilitating the development of immune-based therapeutic interventions that may improve clinical outcomes.

3 Materials and Methods

3.1 Materials

3.1.1 Human samples

The study was conducted in compliance with approved protocols from the Ludwig-Maximilians Universität München and CPC BioArchive ethics review board (Ethikkommission numbers 180-14 and 454-12). Human samples, including whole blood, lung tissue, and primary human fibroblast (phFbs), were sourced from the CPC bioarchive in Munich, Germany. Prior to participating in the research study and molecular testing, all subjects provided informed written consent.

3.1.2 Antibodies

3.1.2.1 Primary Antibodies

The primary antibodies are described in Table 1.

Table 1. Primary Antibodies

ANTIGEN	CLON	PRODUCT NUMBER	HOST	APPLICATION	DILUTION	MANUFACTURER
CD33	Polyclonal	HPA035832	Rabbit	Multiplex IHC IHC Cytospin	1:500	Atlas Antibodies AB
CD11b	EPR1344	Ab133357	Rabbit	Multiplex IHC	1:8000	Abcam
CD3	SP7	RBK024	Rabbit	Multiplex IHC	1:100	Zytomed
CD274 (PDL-1)	E1L3N	13684 S	Rabbit	Multiplex IHC	1:200	Cell Signaling
CD279 (PD1)	EH33	43248 S	Mouse	Multiplex IHC	1:100	Cell Signaling
CD274 (PDL1)	MIH1	14-5983-82	Mouse	Cytospin	1:100	eBioscience™

CD8	C8/144B	372902	Mouse	IHC	1:50	Biolegend
PD1	EPR4877	ab137132	Rabbit	IHC	1:250	Abcam
CD14	-	BAF383	Sheep	IHC	1:20	R&D
L1CAM	2C2	ab24345	Mouse	IHC	1:300	Abcam
CD3	SP7	ab169669	Rabbit	IHC	1:150	Abcam
α-SMA	1A4	C6198	N/A	IHC	1:1000	Sigma-Aldrich®
CD3	OKT3	16-0037-85	Mouse	T cell Exhaustion	1:1000	Invitrogen

3.1.2.2 Secondary Antibodies

The secondary antibodies are described in Table 2.

Table 2. Secondary Antibodies

FLUOROPHORE	PRODUCT NUMBER	HOST	APPLICATION	DILUTION	MANUFACTURER
OPAL 520	OP-001001	N/A	Multiplex IHC	1:150	AKOYA
OPAL 570	OP-001003	N/A	Multiplex IHC	1:150	AKOYA
OPAL 620	OP-001004	N/A	Multiplex IHC	1:150	AKOYA
OPAL 690	OP-001006	N/A	Multiplex IHC	1:150	AKOYA
OPAL 780	OP-001008	N/A	Multiplex IHC	1:25	AKOYA
OPAL TSA-DIG	OP-001007	N/A	Multiplex IHC	1:1000	AKOYA
Alexa Fluor 488	A-21202	Donkey	Cytospin IHC	1:250	Thermo Fisher
Alexa Fluor 568	A-10042	Donkey	Cytospin IHC	1:250	Thermo Fisher
Alexa Fluor 568	A-21099	Donkey	IHC	1:250	Thermo Fisher
Alexa Fluor 488	A-21206	Donkey	IHC	1:250	Thermo Fisher
Alexa Fluor 568	A-10037	Donkey	IHC	1:250	Thermo Fisher
Alexa Fluor 647	A21448	Donkey	IHC	1:250	Thermo Fisher

Alexa Fluor 647	A31573	Donkey	IHC	1:250	Thermo Fisher

3.1.2.3 Flow Cytometry Antibodies

Table 3 describes the flow cytometry antibodies and their respective isotypes.

Table 3. Flow cytometry antibodies and isotypes

ANTIGEN	CLON	FLUOROPHORE	PANEL	ISOTYPE	MANUFACTURER
CD33	WM53	BV 421	Human MDSC	Mouse IgG1	Biolegend (USA)
CD56	HCD56	FITC	Human MDSC	Mouse IgG1	Biolegend (USA)
CD20	2H7	FITC	Human MDSCs	Mouse IgG2b	Biolegend (USA)
CD19	HIB19	FITC	Human MDSCs	Mouse IgG1	Biolegend (USA)
CD16	3G8	FITC	Human MDSCs	Mouse IgG1	Biolegend (USA)
CD3	UCHT1	FITC	Human MDSCs	Mouse IgG1	Biolegend (USA)
CD66b	G10F5	PE	Human MDSCs	Mouse IgM	Biolegend (USA)
CD11b	ICRF44	PerCP Cy5.5	Human MDSCs	Mouse IgG1	Biolegend (USA)
HLA-DR	L243	PE Cy7	Human MDSCs	Mouse IgG2a	Biolegend (USA)
CD236	DJR3	APC	Human MDSCs	Mouse IgG1	Biolegend (USA)
CD14	HCD14	APC Cy7	Human MDSCs	Mouse IgG1	Biolegend (USA)
CD304 (Neuropilin-1)	CD304	BV 510	Human MDSCs	Mouse IgG2a	Biolegend (USA)
CD276 (B7H3)	B7H3	APC	Human MDSCs	Mouse IgG1	Biolegend (USA)
CD195 (CCR5)	J418F1	BV 510	Human MDSCs	Rat IgG2b	Biolegend (USA)
CD274 (PDL1)	MIH1	Alexa Fluor700	Human MDSCs	Mouse IgG1	Invitrogen™ (USA)
CD4	RPA-T4	PE	Human T_{ex}	Mouse IgG1	Biolegend (USA)
CD8a	HIT8a	PE Cy7	Human T_{ex}	Mouse IgG1	Biolegend (USA)
CD3	HIT3a	AF 700	Human T_{ex}	Mouse IgG2a	Biolegend (USA)

CD279 (PD1)	EH12.2H7	BV 510	Human T_{ex}	Mouse IgG1	Biolegend (USA)
CD223 (LAG3)	11C3C65	PerCpCy5.5	Human T_{ex}	Mouse IgG1	Biolegend (USA)
CD366 (TIM3)	F38-2E2	APC Cy7	Human T_{ex}	Mouse IgG1	Biolegend (USA)
TFC1	C63D9	AF 488	Human T_{ex}	Rabbit IgG	Cell Signaling (
Ly6G	1A8	BV 421	Mouse MDSCs	Rat IgG2a	Biolegend (USA)
CD11c	N418	FITC	Mouse MDSCs	Arm Hams IgG	Biolegend (USA)
CD171	555	PE	Mouse MDSCs	Rat IgG2a	Biolegend (USA)
Ly6C	AL-21	PerCP Cy5.5	Mouse MDSCs	Rat IgM	Biolegend (USA)
CD11b	M1/70	PE Cy7	Mouse MDSCs	Rat IgG2b	Biolegend (USA)
CD304	3E12	APC	Mouse MDSCs	Rat IgG2a	Biolegend (USA)
INF-γ	4S.B3	APC	Cytokine production	Mouse IgG1	Biolegend (USA)
TNF-α	Mab11	Pacific Blue	Cytokine production	Mouse IgG1	Biolegend (USA)

3.1.3 Reagents and Chemicals

The chemicals and reagents used in the multiple experiments are listed in table 4.

Table 4. Reagents and Chemicals

PRODUCT	PRODUCT NUMBER	APPLICATION	MANUFACTURER
AR6 Buffer	AR600	Multiplex IHC	AKOYA Biosciences (USA)
ProLong™ Gold antifade	P36930	Multiplex IHC	Invitrogen (USA)
Opal Antibody Diluent/Block	ARD1001EA	Multiplex IHC	AKOYA Biosciences (USA)
Opal Polymer HRP Mouses + Rabbit	ARH1001EA	Multiplex IHC	AKOYA Biosciences (USA)
1X Plus Amplification Diluent	FP1498	Multiplex IHC	AKOYA Biosciences (USA)
ZytoChem Plus HPR Polymer System	POLHRP-100	Multiplex IHC	Zytomed Systems (Germany)
Antibody Diluent	ZUC025-500	Multiplex IHC/IHC	Zytomed Systems (Germany)

Lymphoprep™	07861	PBMC isolation	STEMCELL Technologies (Germany)
PAP Pen Mini	LP0002	Multiplex IHC	Zytomed Systems (Germany)
Recombinant Human IL-2	554603	T cell experiments	BD Pharmigen™ (USA)
Ethanol	A3678	Various	AppliChem (Germany)
Dimethyl sulfoxide (DMSO)	67-68-5	Various	AppliChem (Germany)
Fluorescence mounting medium	S3023	IHC	Dako (Germany)
Penicillin-Streptomycin (10,000 U/ml)	15140148	Cell culture	Gibco™ (USA)
Phalloidin	A12379	IHC	Invitrogen™ (USA)
CD3 Monoclonal Antibody (OKT3), Functional Grade	16-0037-85	T cell experiments	eBioscience™ (USA)
autoMACS® Running Buffer - MACS® Separation Buffer	130-091-221	Immune cell isolation	Miltenyi Biotec (Germany)
Citrate Buffer, pH 6.0, 10X, Antigen Retriever	C9999-1000ML	IHC	Sigma-Aldrich® (USA)
Tris-Buffered Saline, pH 7.6	S1968	IHC	Agilent (USA)
Trypsin-EDTA (0,25%), phenolrot	11560626	Cell Culture	Gibco™ (USA)
autoMACS Pro Washing Solution	130-092-987	Immune cell isolation	Miltenyi Biotec (Germany)
TGF-ß (Recombinant Human)	240-B002	MDSC-phFbs co-culture	R&D Systems (USA)
Collagen G gel	L7213	Collagen gel	Sigma-Aldrich (Germany)
Cell tracker red CMTPX dye	C34552	Collagen gel	Life Technologies (Germany)
Methanol	106018	MDSC-phFbs co-culture IHC	Merck (Germany)
0.1% Triton 10X	9002-93-1	MDSC-phFbs co-culture IHC	AppliChem (Germany)
Spectral DAPI	FP1490	Multiplex IHC	AKOYA Biosciences (USA)
Hoechst	62249	IHC	Thermo Scientific™ (Germany)
DAPI	D9542	IHC	Sigma-Aldrich (Germany)
Paraformaldehyde (PFA) 4%	J61899-AK	IHC	Thermo Scientific™ (Germany)
Hydrogen peroxide (H_2O_2)	231-765-0	Multiplex IHC	AppliChem (Germany)
1× Tris- Buffered Saline - Tween20 (TBS-T)	99975	Multiplex IHC	Cell Signaling Technology® (USA)
TSA plus reaction buffer	NEL749	Multiplex IHC	PerkinElmer (USA)

Fixable Viability Dye - Zombie UV	423107	Flow Cytometry intracellular staining	BioLegend (USA)
Ionomycin	I0634	Cytokine production	Sigma-Aldrich (Germany)
Phorbol-12-myristate-13-acetate 8	P1585	Cytokine production	Sigma-Aldrich (Germany)
Brefeldin A	B7651	Cytokine production	Sigma-Aldrich (Germany)
FACSFlow Sheath Fluid, 20 Liter	5001131	Flow Cytometry	BD Becton, Dickinson (Germany)
MitoTracker Green	M7514	Flow Cytometry Mitochondrial Mass	Invitrogen™ (USA)
Phosphate-buffered saline (PBS)	14190-094	Various	Gibco™ (USA)
Collagenase type II	C2-BIOC	FACS in lung tissue	Merck (Germany)
Triptan Blue	T8154	Various	Sigma-Aldrich (Germany)

3.1.4 Microbeads and Kit systems

Table 5 lists the kits and microbeads used in the various settings of the experiments.

Table 5. Microbeads and kits

NAME	PRODUCT NUMBER	APPLICATION	SPECIES	MANUFACTURER
Anti-PE MicroBeads	130-105-639	PE positive selection	Human	Miltenyi Biotec (Germany)
Pan Monocyte Isolation Kit	130-096-537	Monocyte isolation	Human	Miltenyi Biotec (Germany)
CD33 MicroBeads	130-045-501	CD33 positive selection	Human	Miltenyi Biotec (Germany)
REAlease® CD8 MicroBead Kit	130-117-036	CD8 positive isolation	Human	Miltenyi Biotec (Germany)
CellTrace™ CFSE Cell Proliferation Kit	C34554	Cell Proliferation for Flow Cytometry	N/A	Invitrogen™ (USA)
Essential Immune Response Panel LEGENDplex™	740930	Cytokines production	Human	BioLegend (USA)
nCounter Human Fibrosis V2 Panel	XT-CSO-HFIB2-12	Gene expression	Human	NanoString (USA)
Pan T Cell Isolation Kit	130-096-535	Pan T cell isolation	Human	Miltenyi Biotec (Germany)
FP, Lysing Kit,300 T	6603152	Blood lysis	N/A	Beckman Coulter (Germany)

CD45 MicroBeads	130-045-801	Lung suspension/ Myeloid lung cells isolation	Human	Miltenyi Biotec (Germany)
Vibrant CFDA SE green cell tracer kit	V12883	Invasion Assay	N/A	Invitrogen™ (USA)
Viability/Cytotoxicity Assay Kit for Animal Live & Dead Cells	30002	3D Gel	N/A	Biotum (USA)
FoxP3 Fixation/permeabilization	5523-00	Flow Cytometry	N/A	eBioscience™ (USA)

3.1.5 Cell Culture Media and Buffers

The composition of some of the cell media and buffers used in cell culture are described in Table 6.

Table 6. Cell culture media and buffers

CELL TYPE/ EXPERIMENT	CELL CULTURE MEDIUM /BUFFERS	PRODUCT NUMBER	MANUFACTURER
phFbs medium	DMEM F-12 Medium 20 % Fetal bovine serum 1% Penicillin/Streptomycin	11320033 P30-3702 15140122	Gibco™ (USA) PAN Biotech™ (Germany) Gibco™ (USA)
T Cell Media	TexMACS™ Medium 1% Penicillin/Streptomycin	130-097-196 15140122	Gibco™ (USA) Gibco™ (USA)
Deprivation Media	RPMI 1640 Medium 0,5 % Human serum 1% Penicillin/Streptomycin	11875101 P30-2901 15140122	Gibco™ (USA) PAN Biotech™ (Germany) Gibco™ (USA)
Complete immune cell medium	RPMI 1640 Medium 10% Human serum 1% Penicillin/Streptomycin	11875101 P30-2901 15140122	Gibco™ (USA) PAN Biotech™ (Germany) Gibco™ (USA)
MACS Buffer	autoMACS Running Buffer 2 % Fetal bovine medium	130-091-221	Miltenyi Biotec (Germany)

3.1.6 Laboratory Equipment

The types of equipment used for the different experiments are listed in Table 7.

Table 7. Laboratory equipment

LABORATORY EQUIPMENT	MANUFACTURER
Digital orbital shaker (SHO-1D)	Witeg Labortechnik (Wertheim,Germany)
Microwave "The Genius" (NN-CD87KS)	Panasonic (Lueneburg, Germany)
-20˚C freezer Mediline LGex 410	Liebherr (Biberach, Germany)
-80˚C Freezer U570 HEF	New Brunswick (Hamburg, Germany)
Analytical scale XS20S Dual Range	Mettler Toledo (Gießen, Germany)
Autoclave DX-45	Systec (Wettenberg, Germany)
Autoclave VX-120	Systec (Wettenberg, Germany)
Axiovert 40C microscope	Zeiss (Jena, Germany)
Cell culture workbench herasafe KS180	Thermo Fisher Scientific (Darmstadt, Germany)
Centrifuge MiniSpin Plus	Eppendorf (Hamburg, Germany)
Centrifuge Rotina 420R	Hettich (Tuttlingen, Germany)
Centrifuge with cooling, Micro200R	Hettich (Tuttlingen, Germany)
CO_2 cell Incubator BBD6620	Thermo Fisher Scientific (Darmstadt, Germany)
Confocal microscope LSM 710	Zeiss (Jena, Germany)
Corning® LSE™ Mini Microcentrifuge, 120V	Corning (Wiesbaden, Germany)
Demineralisation Milli-Q®	Thermo Fisher Scientific (Darmstadt, Germany)
Dry ice container Forma 8600 Series, 8701	Thermo Fisher Scientific (Darmstadt, Germany)
Electronic pipette filler	Eppendorf (Hamburg, Germany)
Fisher Science Education™ Microtube Racks	Thermo Fisher Scientific (Darmstadt, Germany)
Fridge MediLine LKv 3912	Liebherr (Biberach, Germany)
Ice machine ZBE 110-35	Ziegra (Hannover, Germany)
Light cycler LC480II	Roche Diagnostic (Mannheim, Germany)
Liquid nitrogen cell tank BioSafe 420SC	Cryotherm (Kirchen/Sieg, Germany)

Magnetic stirrer KMO 2 basic	IKA (Staufen, Germany)
Mastercycler Nexus	Eppendorf (Hamburg, Germany)
Microm HMS740 Robot-Stainer	Thermo Fisher Scientific (Darmstadt, Germany)
Multipette stream	Eppendorf (Hamburg, Germany)
Nalgene® Freezing Container (Mr. Frosty)	Omnilab, Munich, Germany
NanoDrop 1000	PeqLab (Erlangen, Germany)
pH meter InoLab pH 720	WTW (Weilheim, Germany)
Pipettes Research Plus	Eppendorf (Hamburg, Germany)
Plate centrifuge 5430	Eppendorf (Hamburg, Germany)
Scale XS400 2S	Mettler Toledo (Gießen, Germany)
Shaker Duomax 1030	Heidolph (Schwabach, Germany)
Thermomixer compact	Eppendorf (Hamburg, Germany)
Ultra-pure water supply MilliQ Advantage A10	Merck Millipore (Darmstadt, Germany)
Vibratome	Hyrax V55, Zeiss (Jena, Germany)
Vortex mixer	IKA (Staufen, Germany)
Water bath Aqua Line AL 12	Lauda (Lauda-Königshofen, Germany)
BD LSRII flow cytometer	Becton Dickinson (Heidelberg, Germany)
Coulter MT Q-Prep working station	Beckman Coulture (California, USA)
Pressure chamber 2100 retrieval	Aptum Biologics (Hants, UK)
Shandon Cytofunnel®	Thermo Scientific (Darmstadt, Germany)
Cytospin® 4 Cytocentrifuge	Thermo Scientific (Darmstadt, Germany)
autoMACS®	Milteny Biotec (Bergisch Gladbach, Germany)
LCI microscope	Zeiss (Jena, Germany)
Vectra Polaris Automated Quantitative Pathology Imaging System	PerkinElmer, Inc (Waltham, USA)

3.1.7 Disposable Materials

Table 8 below lists all of the disposable materials that were used.

Table 8. Disposable material

NAME	MANUFACTURER
EDTA Blood Vacutainer Tubes Monovette®	Sarstedt (Germany)
epT.I.P.S - Standard®	Eppendorf (Germany)
Eppendorf tubes® 5.0 mL	Eppendorf (Germany)
MS Columns	Miltenyi Biotec (Germany)
96-well black imaging plates, Falcon®	Corning (Germany)
Trucount absolute counting tubes IVD	BD Becton, Dickinson (Germany)
Pre-Separation filters (30 µM)	Miltenyi Biotec (Germany)
V-Bottom plate for LEGENDplex™ Assay	BioLegend (USA)
Cell culture dishes	Corning (Germany)
Cell culture multi-well plates	TTP (Switzerland)
Combitips Advanced®	Eppendorf (Germany)
Cryovials 1.5 ml	Greiner Bio-One (Germany)
Falcon™ tube (15 ml, 50 ml)	BD Bioscience (Germany)
Filter tips	Biozym Scientific (Germany)
Glas pasteur pipettes	VWR International (Germany)
Microscope slides	Thermo Fisher Scientific (Germany)
Reaction tubes (0.5 ml, 1.5 ml, 2 ml)	Eppendorf (Germany)
Corning® Costar® reagent reservoirs	Corning (USA)
Sealing foils for 96-well plates	Kisker Biotech (Germany)
70 M nylon filters	BD Falcon (Germany)
FACS Tubes	BD Falcon (Germany)

3.1.8 Software

The software used for this thesis is listed below (Table 9)

Table 9. Software

SOFTWARE	MANUFACTURER
Axio Vision	Zeiss (Germany)
GraphPad Prism 9	GraphPad Software (USA)
Zen Digital imaging for light microscopy software	Zeiss (Germany)
Microsoft Office Professional	Microsoft® (USA)
FlowJo Software	TreeStart Inc (USA)
LEGENDPlex V.8.0 Data	BioLegend® (USA)
Imaris 9.0 Software	Bitplane (Switzerland)
inForm® with MOTiF™ V 2.6.0	AKOYA Biosciences (USA)
Phenoptic™	AKOYA Biosciences (USA)
Phenochart™ 1.0	PelkinElmer, Inc (USA)

3.2 Methods

3.2.1 Patients and donors

IPF patients and healthy donors were recruited at the Klinikum der Universität München Großhadern and the Comprehensive Pneumology Center between 2018 and 2022. This study involved 41 IPF and 12 healthy donors. To evaluate the T cell exhaustion features, IPF and healthy donors were included (23 and 13, respectively).

IPF was diagnosed following the international American Thoracic Society (ATS) consensus[32,140]. At the time of sampling, healthy donors were free of infections, pulmonary or autoimmune diseases. Eligible healthy donors were over the age of 50.

The research was conducted in compliance with protocols approved by the Ethics review board from the Ludwig-Maximilians-Universität München (Ethical approval number: 80-14 and 454-12). All participants provided written informed consent for the research project.

3.2.1.1 Human immune cells isolation

3.2.1.1.1 Peripheral blood mononuclear cell (PBMC) isolation

Human whole peripheral venous blood from healthy donors and IPF patients was taken in EDTA- tubes (Table 8) and processed within two hours after the blood collection; PBMCs were isolated using density gradient centrifugation. After dilution of 15 ml of blood with 10 ml of phosphate buffer saline (PBS) (Table 4), 12 ml of Lymphoprep TM (Table 4) was gently added and centrifuged for 20 minutes at 450x g, room temperature (RT), minimum acceleration (2), no break (0). Then, the PBMC cloud was collected and washed with MACS buffer (Table 6) to separate the different immune cell subsets.

3.2.1.1.2 MDSCs subsets magnetic bead isolation

After PBMC separation, we performed a positive CD66b G-MDSCs isolation following previous protocols[1]. Briefly, cells were rinsed with MACS buffer (centrifuged 450g x 5 minutes RT) and incubated with CD66b PE (Table 3) antibody for 15 minutes at room temperature. The pellet was resuspended in 100µl of PBS, then anti-PE microbeads (Table 5) were added and incubated at 4 °C for 15 minutes. After washing the cells, autoMACS® (Table 7) positive bead isolation was performed. The positive fraction (G-MDSCs) was preserved at 4°C for future use.

In order to isolate M-MDSCS using magnetic microbeads, the following protocol was established (see Appendix Figure A1 and A2 for details). The negative fraction from CD66b$^+$ was collected (see above) and incubated using the pan monocyte isolation kit's instructions (Table 5). The protocol was modified by adding an HLA-DR biotin antibody together with the pan monocyte biotin-antibody cocktail for positive selection. Using autoMACS®, the remaining steps were carried out under the company's recommendations. The negatively selected fraction from the preceding stage was then stained with CD33 microbeads (Table 5), incubated for 15 minutes at room temperature, rinsed, and centrifuged (450g for 5 minutes at 4°C). The cells were then magnetically isolated using autoMACS®, with the resulting positive fraction (CD33$^+$) being HLA-DR negative monocytes, therefore phenotypically M-MDSCs. This fraction was kept at 4°C until further experimentation.

In the 3D gel invasion assay, MDSCs were previously frozen and cryopreserved in freezing media (90% FBS mixed with 10% DMSO) kept at -80°C and thawed for the experiment. Moreover, when experiments refer to Total MDSCs, it indicates that the two subtypes were combined at a 1:1 ratio.

3.2.1.1.3 CD8$^+$ T bead magnetic cell isolation

To obtain microbead-free CD8$^+$ T cells, the human REAlease® CD8 MicroBead Kit (Table 5) was used. To identify specific cell surface markers, the REAlease technology employs antibody fragments with low epitope affinity. However, when fragments are multimerized in the REAlease CD8-Biotin complex, they bind to epitopes with a high degree of avidity. The REAlease Technology regulates the multimer/monomer state of antibody fragments. This method enables the generation of bead- and label-free cells in which monomerized antibody fragments dissociate off the cell surface[141] (Figure 11).

The CD8$^+$ T isolation for the studies included in this thesis was done according to the company's methodology until the REAlease complex was removed (available online).

Magnetic separation was manually performed using MS columns (Table 8). The $CD8^+$ T fraction was kept at 4°C till the following application.

Autologous cells were used in the experiments wherein $CD8^+$ T cells were co-cultured with MDSCs. In these scenarios, PMBCs were initially employed to isolate $CD8^+$ T cells. Subsequently, the negative fraction resulting from this process was utilized to isolate MDSCs.

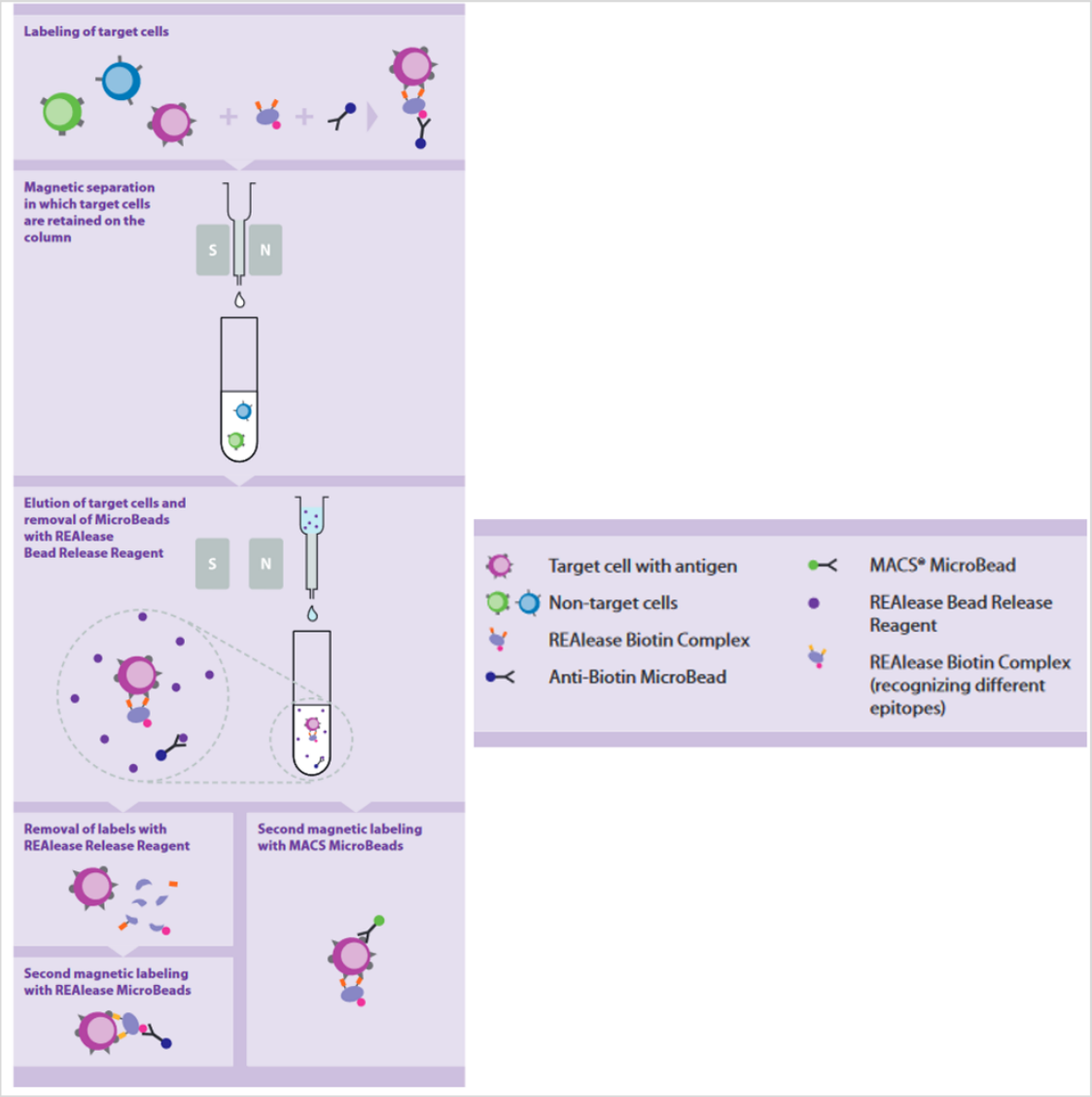

Figure 11. REAlease® CD8 MicroBead Kit. Protocol Overview (Modified from product data sheet)

3.2.2 Primary human lung fibroblast (phFbs) culture and cryopreservation

The primary human lung fibroblasts (phFbs) used in this study were obtained from the CPC-M Bioarchive located in Munich, Germany. For the fibroblast culture, we initiated thawing by immersing the cryovials containing phFbs in a 37°C water bath for a period of 2 to 3 minutes or until complete defrosting was achieved. Following, the cell suspension was transferred to a 50 ml falcon containing phFbs media (Table 6) and centrifuged at 500g for 5 minutes, after which the supernatant was discarded. The resulting cell pellet was reconstituted in fresh phFbs media and was subsequently transferred to a sterile 10 cm cell culture dish and grown at 37°C under conventional cell culture conditions.

The medium was replaced every 48 hours, and the cells were split when they reached 80 to 90% confluence. To split the confluent dishes, the cells were rinsed with fresh 1X PBS, before being incubated for 5 minutes with 1 ml of 0.25 % Trypsin-EDTA (Table 4) at 37 °C. Following the incubation, the cell suspension was transferred to a Falcon with 10 ml phFbs media and centrifuged at 500g for 5 minutes. The supernatant was then removed, and the cell pellet was immediately suspended in phFbs media. During this study, phFbs from passages 3 to 7 were used.

If the phFbs were not used at the time, they were suspended in freezing medium (90% FBS with 10% DMSO), transferred to cryovials, and kept in liquid nitrogen at -195°C for long-term storage.

3.2.3 3D Collagen gel-based assays

3.2.3.1 Collagen gel preparation

Previous research has employed collagen G (Table 4) from calfskin to create 3D collagen gels[142]. This gel was prepared as follows: In a 1:1 ratio, filtered 1 (M) HEPES buffer (Table 10) and 0.7 (M) NaOH were combined to make Solution A. Solution B was created by

combining solution A with 20% FBS in 10X PBS (pH = 7.4) in a 1:1 ratio. For the final gelation, collagen G and solution B were mixed in a 4:1 ratio to obtain solution C (Table 10). All reactions were held on ice to achieve a homogeneous gel and avoid Collagen G solidification at RT.

Table 10. Collagen gel components

SOLUTION	COMPONENTS	RATIO
Solution A	0.7(M) NaOH + 1(M) HEPES	1:1
Solution B	Solution A + 20% FBS in 10X PBS	1:1
Solution C	Solution B + Collagen G	1:4

3.2.3.2 MDSCs collagen gel invasion assay

To allow polymerization, 50 µl of the collagen G solution (solution C) was pipetted into each well of a 96-well plate and incubated at 37°C for 4-6 hours prior to the invasion assay. To enhance reproducibility, an electronic Multipette (Eppendorf) was used to properly distribute the viscous collagen solution in the cell culture dishes.

Meanwhile, as previously described (3.2.1.1.2), MDSCs subsets were isolated and dyed differently in order to differentiate them. Cell tracker red CMTPX (Table 4) was used to stain M-MDSCs c at a dilution of 1:1000. This was accomplished by mixing 1µl of CMTPX dye into 999ml of RPMI 1640. In 1 ml of this solution, the cells were suspended and incubated at 37°C for 30 minutes. Following that, the reaction was stopped by washing for 5 minutes at room temperature with 1 ml of PBS containing 2% fetal bovine serum (FBS) at 450g. The pellet was then resuspended in RPMI 1640 medium with 10% human serum and 1% penicillin/streptomycin.

G-MDSCs, on the other hand, were stained for 10 minutes at 37°C using a 1ml pre-dilution of Vybrant CFDA SE green tracer reagent (1µl CFDA in 5,625ml PBS) (Table 5). After stopping

the reaction with 4 ml of FBS for 2 minutes, the cells were washed with 6 ml of pure RMPI 1640 at 450g for 5 minutes. The pellet was then reconstituted in RPMI 1640 medium containing 10% human serum and 1% penicillin/streptomycin. The following steps including the data acquisition and analysis were kindly performed by Arunima Sengupta (Helmholtz Zentrum Munich).

Upon the solidification of the gel, we seeded $2x10^4$ cells per well on top and allowed to invade/infiltrate the collagen matrix over a period of 48 hours, while being maintained under conventional cell culture conditions (37°C and 5% CO_2). Following that, the wells were washed with 1X PBS and fixed with 4 % PFA for 30 minutes at RT. Following this fixation step, we employed an LSM 710 confocal microscope to capture images of each well containing 3D collagen matrix-embedded cells (as illustrated in Figure 12).

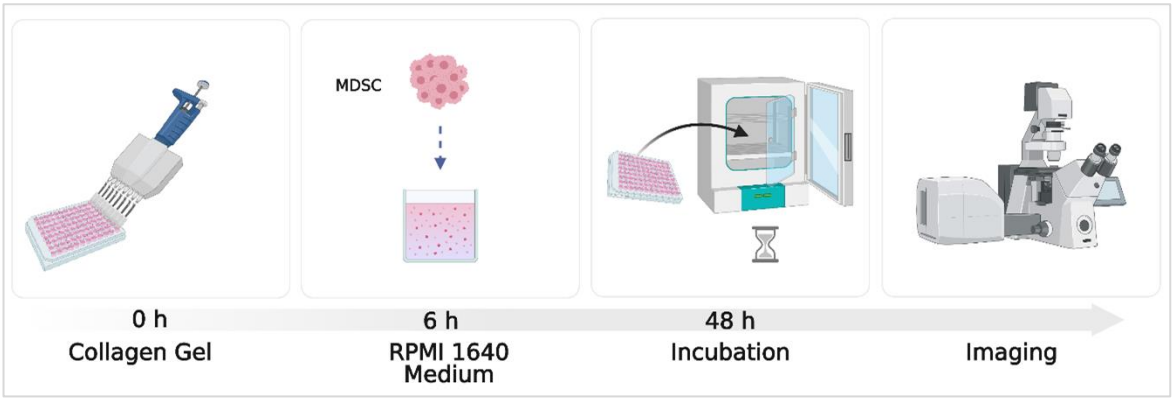

Figure 12. Schematic representation of MDSC collagen gel invasion assay. Created with BioRender.com

This study included myeloid-derived suppressor cells (MDSCs) derived from three patients diagnosed with IPF and three healthy donors. The gathered imaging datasets were imported into Imaris 9.0 software (as detailed in Table 9), and a 3D projection of the image was generated. Subsequently, a spot-detection algorithm was applied to associate one spot with each red or green fluorescent cell. The total number of spots was further refined by considering their z-position, with a threshold set at the lowest point within the collagen gel. Next, the statistical analysis tool was employed to ascertain the quantity of spots or

cells that had infiltrated the collagen gel, alongside the complete count of spots. GraphPad Prism 9 (Table 9) was used to generate graphs and statistical analyses.

3.2.3.3 MDSCs and Fibroblast 3D gel co-cultures

The MDSCs subsets were isolated as previously described (3.2.1.1.2) and stained with the Viability/Cytotoxicity Assay Kit for Animal Live & Dead Cells according to the manufacturer's protocol (Table 5). This assay differentiates between viable (green) and dead cells (red color). This kit includes two components. Calcein AM is a non-fluorescent esterase substrate that enters the living cells' cytoplasm and is cleaved by esterases to produce the green, fluorescent dye calcein. Calcein is retained in the cytoplasm of viable cells with intact plasma membranes because it is negatively charged and impermeable to cell membranes. Ethidium homodimer III (EthD-III) is an impermeable DNA dye to the plasma membrane and is therefore rejected by viable cells. Until it binds to DNA, EthD-III is nearly non-fluorescent. EthD-III enters dead cells with compromised plasma membranes and emits a brilliant red fluorescence from the nucleus.

After staining, total MDSCs (3.2.1.1.2) were combined in a 1:1 ratio with phFbs and cultured as described above (3.2.2). This mixture was divided into aliquots of $20x10^4$ cells and centrifuged at 450g for 5 minutes at RT.

The pellet was then resuspended in 50µl of freshly prepared non-polymerized collagen gel after the supernatant was removed. Aliquots of collagen-resuspended ($20x10^4$ cells) were incubated for one hour under standard cell culture conditions to allow the gel to partially polymerize. Then, RPMI 1640 supplemented with 10% FBS and 1% penicillin/streptomycin was added on top, and it was immediately taken for live imaging for 72 hours (37°C and 5% CO2) in an LCI microscope (Table 7). Here, the aim was to determine whether MDSCs tend to be in close proximity to fibroblasts. For the video recordings, ZEN digital imaging software (Table 9) was used (Figure 13).

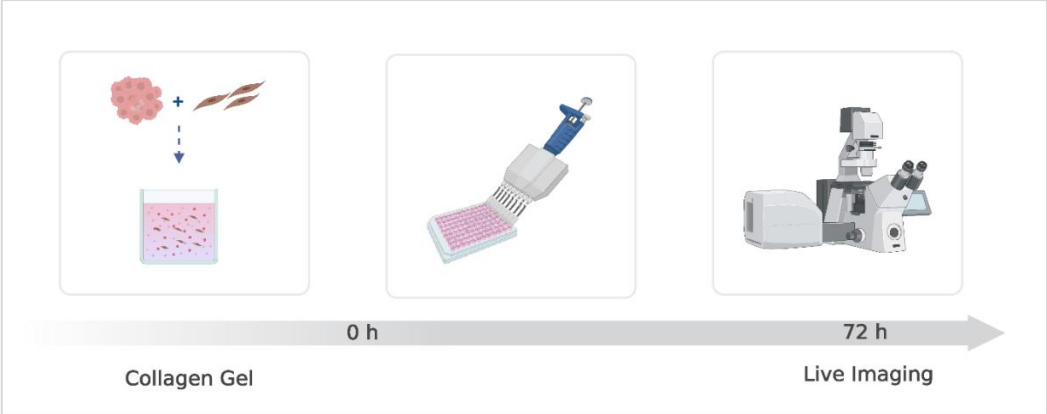

Figure 13. Schematic representation of MDSC - Fibroblats 3D Collagen Gel. Created with BioRender.com

3.2.4 CD8⁺ T cell Exhaustion experiments

3.2.4.1 CD8⁺ T lymphocytes exhaustion

The CD8⁺ T lymphocyte exhaustion experiments were performed in accordance with previously published methods[143]. Briefly, freshly isolated CD8⁺ T lymphocytes (3.2.1.1.3) from IPF patients and healthy donors were incubated with 0.5 µl/ml of IL-2 (Table 4) and 1µl/ml of CD3 (Table 1) in T cell medium (Table 6), seeded at a cell density of 1 x 10^6 per well on a 6-well-plate, and incubated for 48 hours under standard conditions (37°C and 5% CO_2). This day is referred to as day zero in the experimental design.

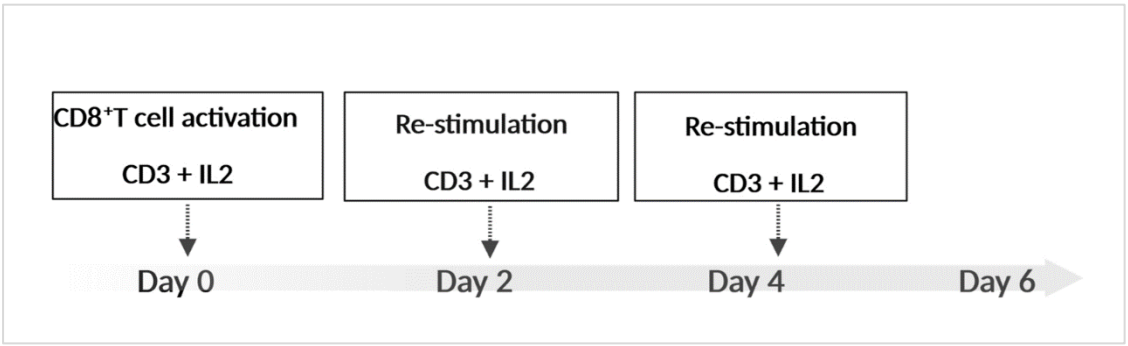

Figure 14. Schematic representation of *in vitro* CD8⁺ T cell exhaustion. Created with BioRender.co

Afterward, $CD8^+$ T cells were centrifuged and resuspended in a fresh T cell media containing IL-2 and CD3 (same concentrations as day 0) and seeded into new wells every 48 hours for 6 days (Figure 14). An aliquot of $CD8^+$ T cells was collected on day 0 (before activation) and day 6, for flow cytometry (FACS) analysis to assess T cell exhaustion markers (Panel in 3.2.6.3) and mitochondrial mass (Refer to 3.2.6.5).

3.2.4.2 MDSC and exhausted $CD8^+$ T lymphocyte co-culture

The next section provides a comprehensive description of the two versions of the experiment that were conducted.

3.2.4.2.1 Re-stimulation with IL-2 and CD3 every 48 hours

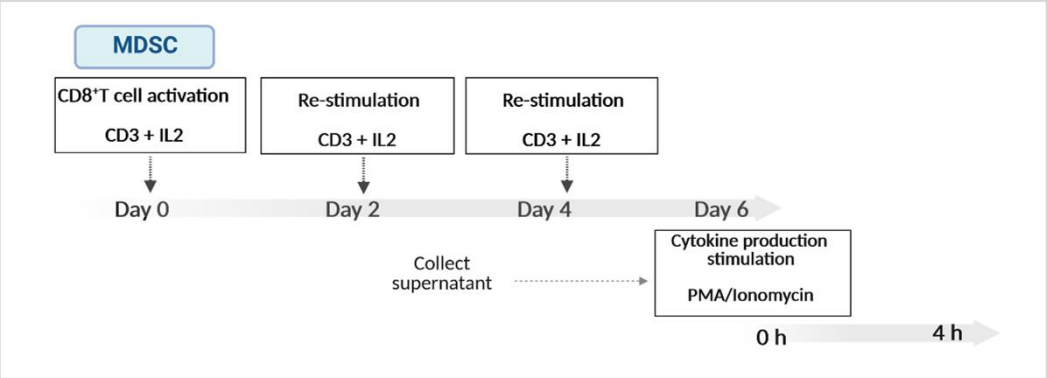

Figure 15. Schematic representation of *in vitro* $CD8^+$ T cell exhaustion in co-culture with MDSC (variant 3.2.4.2.1). Created with BioRender.com

Isolated $CD8^+$ T lymphocytes from IPF patients and healthy donors (3.2.1.1.3) were co-cultured (ratio 2:1) with autologous total MDSCs (3.2.1.1.2) and activated with 0.5 µl/ml of IL-2 and (Table 4) 1µl/ml of CD3 (Table 1) in T cell medium (Table 6), seeded at a cell density of 5x 10^5 per well on a 24-well-plate and incubated under standard conditions (37°C and 5% CO_2) for 48 hours. The co-cultures were then centrifuged and resuspended in a fresh T cell media containing IL-2 and CD3 (same concentrations as day 0) before being seeded

into new wells every 48 hours for 6 days. In addition, negative control was conducted under identical conditions but without total MDSCs. An aliquot of $CD8^+$ T cells was collected on day 0 and day 6 for flow cytometric analysis to detect T cell exhaustion markers (3.2.6.3). The remaining cells on day 6 were used for stimulation of cytokine production (3.2.4.3)

3.2.4.2.2 No IL-2 and non CD3 re-stimulation every 48 hours

On day 0 of this experiment, $CD8^+$ T cells from IPF patients and healthy donors were co-cultured (ratio 2:1) with autologous total MDSCs and activated with 0.5 µl/ml of IL-2 (Table 4) and 1µl/ml of CD3 (Table 1) in T cell medium (Table 6), seeded at a cell density of 5x 10^5 per well in a 24-well-plate and placed in the incubator (37°C and 5% CO_2) for 48 hours. After that, the cells were replaced every 48 hours till day 6 using only T cell media (without IL-2 and CD3). Additionally, there was a setting in which CD8 T cells were re-stimulated with IL-2 and CD3 every 48 hours.

On days 0 and 6, T cells were collected for flow cytometric analysis of T cell exhaustion markers (3.2.6.3). Here, cytokine production was also stimulated for further analysis. (3.2.4.3)

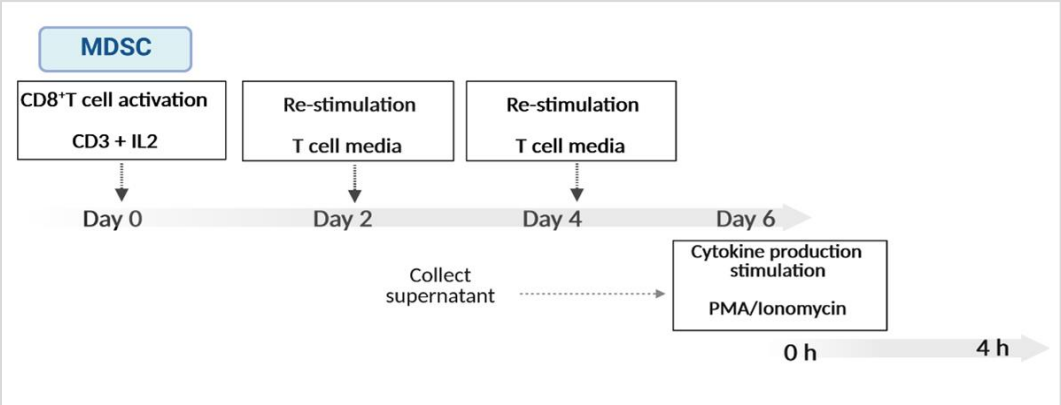

Figure 16. Schematic representation of *in vitro* CD8+ T cell exhaustion in co-culture with MDSC (variant 3.2.4.2.2). Created with BioRender.com

3.2.4.3 Cytokines production

Following $CD8^+$ T cell exhaustion on day 6, the cells were stimulated to release cytokines by switching to a fresh T cell media containing 20ng/ml phorbol 12-myristate 13-acetate (PMA) (Table 4) and 1g/ml Ionomycin (Table 4) and incubating for 4 hours under normal conditions. After collecting the supernatants, they were centrifuged at 450g for 5 minutes, transferred to a new Eppi, and spun down at maximum speed for 5 minutes. The supernatants were collected, snap-frozen in liquid nitrogen, and stored at -80°C for further measurement (3.2.4.3.1)

3.2.4.3.1 Cytokines production quantification (Supernatants)

Quantification of IFN-γ and TNF-α from the $CD8^+$ T cell exhaustion experiment, as well as TGF-ß from the MDSCs–fibroblast co-culture supernatants were performed using a customized BioLegend's LEGENDplex™ bead-based immunoassay (Table 5). This assay, like the sandwich Enzyme-Linked Immunosorbent Assay (ELISA), captures a soluble analyte between two antibodies. The assay kit comprises two sets of beads, each with distinct levels of APC fluorescence and differing in size, allowing for clear differentiation between them. These bead sets are designed to serve as capture beads for specific analytes, as they are each coupled with a unique antibody on their surface. When these capture beads are mixed and exposed to a sample containing target analytes, each analyte selectively binds to its corresponding capture bead. Following the addition of biotinylated detection antibodies, each detection antibody forms bonds with its specific analyte that is tethered to the capture beads. This leads to the formation of sandwiched structures consisting of the captured bead, analyte, and detection antibody. The subsequent step involves the addition of streptavidin-phycoerythrin (SA-PE), which attaches to the biotinylated detection antibodies and generates a fluorescent signal that is directly proportional to the amount of bound analyte[144]. Figure 17 provides a visual representation of the described concept.

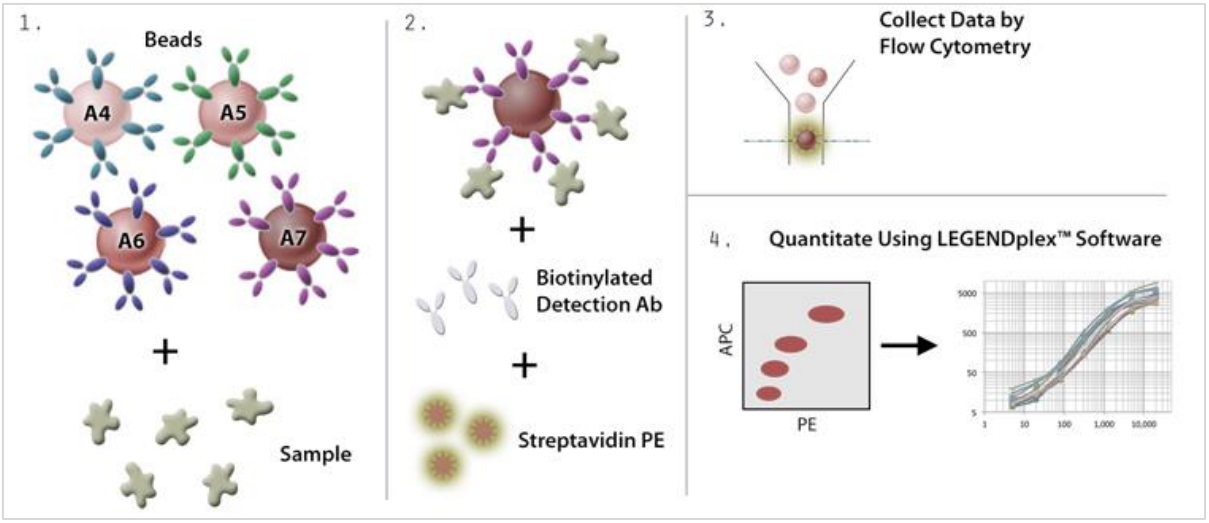

Figure 17. Schematic representation of BioLegend's LEGENDplex™ bead-based immunoassay[52]

In this experiment, supernatants that had previously been collected and stored at -80°C were thawed on the ice at RT and used undiluted. The company's protocol was then followed step by step and the PE signal fluorescence intensity of each bead population (TGF-ß, IFN-γ, and TNF-α) was assessed by flow cytometry on a BD LSRII flow cytometer the same day (Table 7). The concentration analysis of each cytokine was determined based on a known standard curve using the LEGENDplex v.8.0 data (Biolegend, http:// www. vigenetech. com/). Figures and statistical analysis were performed in GraphPad Prism 9 (Table 9).

3.2.5 Immunohistochemistry and Immunofluorescence experiments

3.2.5.1 MDSC- Fibroblast Co-culture immunohistochemistry

In this experiment, phFbs cultured in vitro were subjected to trypsinization and washing procedures as previously outlined. They were then seeded onto a 96-well imaging plate at a concentration of $2x10^4$ per well, using DMEM-F12 suplemented with 20% FBS and 10% penicillin/streptomycin. The plate was then placed in an incubator set at 37°C with 5% CO2 for 24 hours, allowing the cells to attain 80% confluence. Following this initial culture

period, the medium was replaced with deprivation media composed of RPMI 1640, 0.5% human serum, and 1% penicillin/streptomycin. The plate was then incubated for an additional 6 hours under the same conditions (37°C and 5% CO2). During this incubation, MDSC subsets were isolated following established protocols.

After 6 hours, the culture medium for the fibroblasts was aspirated, and MDSCs in the deprivation media were introduced into each well at a concentration of $1x10^4$ cells/well, maintaining a 2:1 ratio of fibroblasts to MDSCs. The plate was promptly returned to the incubator (37°C and 5% CO2) for a 48-hour incubation period. This experimental setup encompassed three distinct conditions: fibroblasts cultured in isolation (serving as the negative control), fibroblasts co-cultured with MDSCs (comprising M-MDSCs, G-MDSCs, or Total MDSCs), and fibroblasts treated with TGF-B at a concentration of 2 ng/ml, as specified in Table 4 (serving as the positive control).

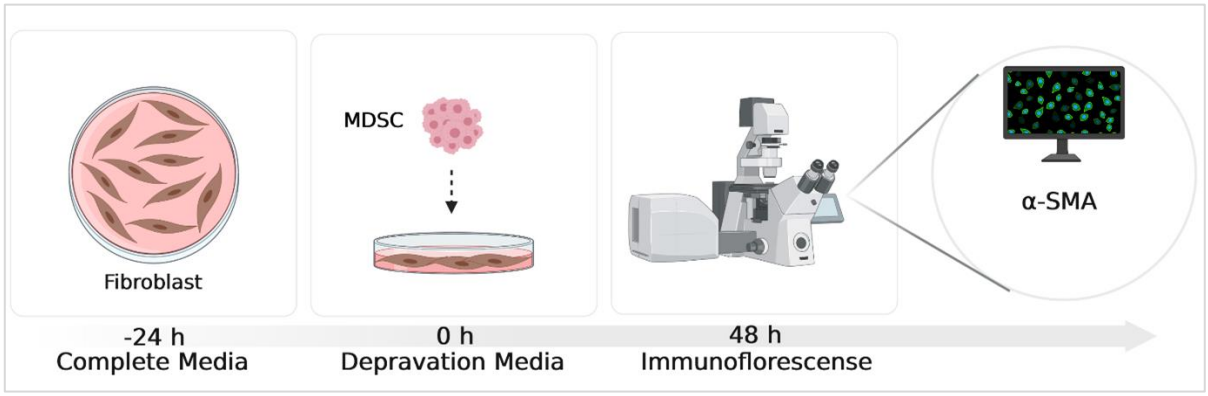

Figure 18. Schematic representation of MDSCs - Fibroblasts Co-culture Created with BioRender.com

After 48 hours of culture, the supernatants were collected for TGF-β measurement (the wells were washed twice with PBS (using the Integra Multi Pipette) and fixed with ice-cold Methanol (MeOH) 1% (Table 4) at -20°C for two minutes. The MeOH was subsequently removed, and the wells were washed twice with PBS before being treated for 10 minutes with cold 0.1 % Triton 10X (dilution 1:1000 in MiliQ water) to induce permeabilization. After rinsing with PBS, the cells were subjected to a staining procedure using α-SMA antibody

(1:1000) (Table 1) and Hoechst (1:100) diluted in a deprivation medium (Table 6) at 37°C for 3 hours. The LSM 710 confocal microscope (Table 7) was used for imaging. The quantification of α-SMA was performed using median fluorescence intensity (MFI) and subsequently normalized to the number of DAPI-positive cells in three IPF patients.

3.2.5.2 Conventional immunohistochemistry (IHC) of paraffin-embedded lung tissue sections

Initially, Formalin-fixed paraffin-embedded (FFPE) lung tissue sections from control (tumor-free tissue areas) and IPF patients were incubated overnight at 60°C for conventional immunohistochemistry (IHC). The next day, the tissue was deparaffinized using the following cycles on the Microm Robot-Stainer:

Table 11. Deparaffinization cycles

REAGENT	CYCLE	TIME
Xylene (100%)	2X	5 min
Ethanol (100%)	2X	2 min
Ethanol (90%)	1X	1 min
Ethanol (80%)	1X	1 min
Ethanol (70%)	1X	1 min
dH_2O	1X	30 seconds

Following that, the slides were immersed in a citrate buffer solution with a pH of 6.0 (Table 4), in order to enhance the retrieval of antigens. Subsequently, the slides were quickly placed within a Decloaking Chamber for an interval of 30 minutes and subjected to a carefully regulated heating procedure, encompassing temperatures of 125°C for a period of 30 seconds, succeeded by 90°C for a duration of 10 seconds. The slides were then gradually

allowed to cool until reaching room temperature. To prevent nonspecific binding, the slides underwent a thorough triple wash in Tris buffer and were subsequently subjected to a one-hour blocking step in a solution consisting of 5% BSA and Tris buffer. Primary antibodies were applied to the slides, and they were then incubated overnight at 4°C within a dark, humid chamber. On the following day, the slides underwent three rounds of rinsing with Tris buffer. Subsequently, they were incubated with a 1:250 dilution of each fluorescently labeled secondary antibody (diluted with antibody diluent)(Table 2). Additionally, DAPI (Table 4) was used at a 1:2000 dilution. This incubation took place for one hour at room temperature in darkness and under humid conditions. Following this incubation, the slides were once again washed with Tris buffer and then coated with Fluorescence Mounting Medium (Table 4).

The following primary and secondary anti-human antibodies were employed to detect M-MDSCs and $CD8^+$ T cells in IPF and control lung tissue slides. Table 12 provides the dilutions and other details. Axiovert II (Table 7) was used for microscopy, and pictures were processed with ZEN 2010 software (Carl Zeiss AG).

Table 12. Antibodies panel for IHC

Cell Type	Primary Ab	Secondary Ab
MDSCs	CD33 (1:150) CD14 (1:20) L1CAM (1:300)	Alexa Fluor 488 Alexa Fluor 647 Alexa Fluor 568
$CD8^+$ T cell	CD3 (1:100) CD8 (1:50) PD1 (1:250)	Alexa Fluor 647 Alexa Fluor 488 Alexa Fluor 568

3.2.5.3 Immunocytochemistry in MDSCs Cytospins

A total of $3x10^4$ freshly isolated M-MDSCs and G-MDSCs obtained through magnetic bead isolation from IPF patients, were suspended in 200 µl of MACS buffer. These cell suspensions

were then transferred to Shandon Cytofunnels® (Table 7). Centrifugation was then performed at a speed of 300rpm for a duration of 10 minutes at RT. Subsequently, cytospin slides were left to air-dry overnight at room temperature after the centrifugation process. Following the air-drying step, the cells were fixed with 4% PFA for 10 minutes at RT, followed by a gentle wash with PBS. The cells were then permeabilized for 15 minutes in PBS containing 0.1% Triton X-100 (Table 4) and then washed with PBS. A blocking solution, consisting of 5% BSA, was added and allowed to incubate at room temperature for one hour.

Next, PDL-1 anti-human (Table 1) and CD33 anti-human antibodies (Table 1) were added to a diluent solution and incubated overnight at 4°C in a humid, dark environment. The following day, the slides were washed three times with PBS for three minutes before being stained with 1:250 secondary antibodies AF488 donkey anti-rabbit and AF568 donkey anti-mouse, diluted, and counterstained with DAPI (1:2000) for 30 minutes in a damp, dark chamber at room temperature. Isotype-labeled control rat IgG and mouse IgG1 were also used.

After completing the staining procedure, the slides underwent three additional washes with PBS and were subsequently mounted using mounting media (Table 4). For imaging, Axiovert II was used, and ZEN 2010 was utilized for image processing.

3.2.5.4 Multiplexed immunohistochemistry (mIHC) of paraffin-embedded lung tissue sections

During a short stay in the laboratory of Dr. Sebastian Marwitz at the pathology department of the Research Center Borstel/Leibniz Lung Center, lung tissue slides from IPF patients (n=5) and non-IPF ILD (n=5) were subjected to multiplexed immunohistochemistry (mIHC). This space biology technique permits the simultaneous detection of several markers on a single tissue segment, thereby offering a comprehensive view of the spatial distribution of markers and tissue composition.

To apply this technique, the FFPP lung tissue segment slides (tumor-free tissue portions), were deparaffinized as follows:

Table 13. Deparaffinization cycles in Multiplex IHC

REAGENT	CYCLE	TIME
Xylene (100%)	2X	10 min
Ethanol (100%)	2X	2 min
Ethanol (90%)	1X	2 min
Ethanol (80%)	1X	2 min
Ethanol (70%)	1X	2 min
dH_2O	1X	30 seconds

We adhered to the previously published protocol[145] for our procedure. To initiate the process, the slides were positioned within a cuvette containing AR6 antigen-retrieval buffer (Table 4). Subsequently, the slides were microwaved for 1 minute at high power (1000 W) followed by 10 minutes at low power (100 W) to retrieve antigens with heat. Afterward, the slides were cooled with tap water, and this process was repeated twice. To prevent background staining, the slides were soaked in a 3% hydrogen peroxide (H2O2) solution for 10 minutes, which inhibits the activity of endogenous peroxidases.

Next, the slides were immersed in 1X Tris- Buffered Saline with Tween20 (TBS-T, Table 4). All incubations were meticulously carried out within a dark and humid chamber employing an orbital shaker at a rate of 300 rpm, at RT. After each incubation, the slides were thoroughly washed with TBS-T. The mIHC protocol included a single heat-induced antigen-retrieval step (as previously explained), a 10-minute blocking step using Opal Antibody Diluent/Block (Table 4), and incubation with the primary antibodies (Table 1) as per the previously published protocol.

The primary antibodies rabbit anti-CD33, rabbit anti-CD11b, rabbit anti-CD3, mouse anti-PD1, and rabbit anti-PDL-1 were were thinned down in 1X Plus Amplification Diluent (Table 4). Then the slides were incubated with the diluted primary antibodies for for 45 minutes (or 60 minutes for PDL-1) and then incubated with either anti-mouse/anti-rabbit HRP polymer (Table 4) or the ZytoChem Plus HPR Polymer System (for PDL-1, as found in Table 1) for 10 minutes. To to better visualize the primary antibodies, we conducted a Tyramide-signal amplification (TSA) reaction using OPAL fluorochromes, diluted at a ratio of 1:150 in TSA + reaction buffer for 10 minutes. This was followed by a washing step with 1 TBS-T. For Opal 780 (PDL-1), an extra step was necessary. After the HRP incubation and rinsing, the slides were incubated with Opal TSA-Dig reagent for 10 minutes. Subsequently, a brief antigen-retrieval process was carried out using a microwave: first for 1 minute at 1000 W and then for 5 minutes at 100 W, both in AR6 antigen-retrieval buffer. Following this, spectral DAPI (diluted at a 1:500 ratio in phosphate-buffered saline) was applied and left for 5 minutes. Afterward, the slides underwent three washes with TBS-T and one wash with Milli-Q grade water. Finally, coverslips were manually affixed using ProLong Diamond Antifade Mountant (Table 4) and allowed to set before the scanning procedure.

The fluorochromes' positions and combination in the multiplex panel were as follows:

Table 14. Fluorochromes positions and combination in the multiplex-panel

POSITION	PRIMARY ANTIBODY	OPAL FLUOROPHORE
1	CD33	OPAL 570
2	CD11b	OPAL 690
3	CD3	OPAL 520
4	PD1	OPAL 620
5	PD-L1	OPAL 780

The capture of images consisted of scanning mIHC stained slides using Vectra Polaris Automated Imaging System (Table 7) using the 20 objective lenses with saturation protection scanned as a whole-slide overview. The resulting files were saved in a.qptiff format, with a pixel resolution of 0.5m. Phenochart software's (Table 9) stamped fields feature was used to annotate immune cell clusters. Throughout the experiments, a spectral library was employed to evaluate all mIHC panels.

The staining of each marker in a multiplex panel was previously validated in the Laboratory of Dr. Sebastian Marwitz (Research Center Borstel, Leibniz Lung Center) with IF monoplex stains to result in comparable staining patterns (data not shown).

3.2.5.4.1 Image selection and analysis

Following image analysis, we used InForm V.2.6.0 (Table 9), Multiband V.0.8.65, and the PhenoptR R (Part of Phenoptics™, see Table 9). The slides were additionally incorporated into the same inForm project. Multiple representatives .im3 photos were chosen for training within the inForm program.

3.2.5.4.2 Cell segmentation

For cell segmentation, the inForm software V.2.6.0's adaptive cell segmentation or object-based method was employed.

3.2.5.4.3 Phenotyping

Iterative user-guided phenotyping training was performed if batch analysis of the complete dataset for each panel resulted in false negative/false positive cellular phenotypes. After achieving adequate accuracy in cell segmentation and phenotyping, the approach was locked down and subsequently applied for batch analysis across all images. Machine learning-based categorization and counting of cellular phenotypes on cell lineage markers

(CD3, CD33, CD11b, PD1, and PDL-1) were performed using the inform software, resulting in a single positive event. To choose common cellular phenotypes, a meticulous process of manual annotation of each segmented cell within inForm software was performed, including numerous images from different samples. The PhenoptR R program, which is a part of Phenoptics™ (refer to Table 9) was used to identify and establish the threshold for the intensity of each marker. The PhenoptR R program employed individual intensity threshold values as cut-off points for calculating marker combinations through the phenotypic rules function. The 'count inside batch' tool was used to count all potential phenotypes in each sample.

3.2.5.4.4 Spatial analysis of mIHC

We employed the PhenoptR R program to examine spatial correlations among various cellular phenotypes included within the 'cell_seg_data' files in inForms software. To achieve this, we utilized the 'count_within_batch' function. Multiple pairings were organized into a list. The term 'radii' was employed to define the area in micrometers (µm) around a specific phenotype, where the mean number of another phenotype was to be assessed[145]. In this case, using the argument 'base cell (e.g., CD33, CD11b, PD1)', 'target cell (e.g., CD3, PD1)' as a 'pair' enabled us to determine the mean number of $CD3^+$ $PD1^+$ cells within a given distance around one $CD33^+CD11b^+PDL1^+$.

3.2.6 Flow cytometry

3.2.6.1 MDSCs Immunophenotyping in human blood and tissue

For flow cytometric MDSCs detection, one aliquot of whole blood (100µl) and one aliquot of PBMC (300 000 cells) from IPF patients and healthy donors were stained for 20 minutes at 4°C in the dark with the following anti-human antibody cocktails. After staining,

erythrocytes in whole blood were lysed using a Coulter Q-Prep working station (Table 7). Several multicolor panels were used, described below in detail:

- Cocktail 1: Lineage (CD56, CD20, CD19, CD16, and CD3), HLA-DR, CD33, CD11b, CD14, CD66b, CD236 and Neuropilin-1 (see Table 3)
- Cocktail 2: Lineage (CD56, CD20, CD19, CD16, and CD3), HLA-DR, CD33, CD11b, CD14, CD66b, B7H3, CCR5 and PDL-1 (see Table 3)

For MDSCs characterization, blood cells were gated as lineage^{neg}/HLA-DR^{neg}/CD33^{+}/CD11b^{+}, and findings were reported as a percentage of gated HLA-DR negative cells. M-MDSCS were defined as lineage^{neg}/HLA-DR^{neg}/CD33^{++}/CD11b^{+}/CD14^{+}, whereas G-MDSC were defined as lineage^{neg}/HLA-DR^{neg}/CD33^{++}/CD11b^{+}/CD66b^{+}. Following that, the expression of unique markers such as CD236, Neuropilin-1, B7H3, CCR5, and PDL-1 was afterward analyzed in the total MDSCs, M-MDSCs, and G-MDSCs populations and presented as median fluorescence intensity (MFI) and percentage of total MDSCs or each subset.

Flow cytometry was also used to investigate the presence of MDSCs in whole lung cell suspension. In DMEM media containing 10% fetal bovine serum (FBS) 1-3 mm^2 pieces of human explanted lungs or biopsies were minced and treated for 2 hours at 37°C on a roller with 0.2% type II collagenase (Table 4). Lung fragments were then sieved using a 400-500 m filter followed by a 100 m filter. The cells were centrifuged at 450g for 5 minutes at room temperature. After resuspending the pellet, the number of cells was determined using trypan blue staining and a Neubauer chamber. Myeloid lung cells were isolated and stained with antibody cocktail 1 using CD45 MicroBeads (Table 5). The tissue gating strategy was identical to the blood strategy.

The flow cytometry data acquisition was performed in a BD LSRII flow cytometer (Table 7). Data were analyzed using the FlowJo software (Table 9). Negative thresholds and isotype-labeled controls were employed to set the gates.

3.2.6.2 Whole blood and PBMC cell surface T exhaustion markers panel

An aliquot of blood and PBMC were stained with the human antibody cocktail CD4, CD8a, CD3, PD1, LAG3, and TIM3 for the identification of T cells and the expression of exhaustion markers, just like MDSCs. T cells ($CD3^+$), T-helper ($CD3^+CD4^+$), and T-cytotoxic ($CD3^+CD8^+$) lymphocytes were gated. Expression of the exhaustion markers PD1, TIM3, and LAG3 was analyzed in the cytotoxic and helper cells and reported as MFI.

The flow cytometry data was collected using a BD LSRII flow cytometer (Table 7). Data were analyzed using the FlowJo software (Table 9). Negative thresholds and isotype-labeled controls were employed to set the gates.

3.2.6.3 $CD8^+$ T cell surface and intracellular exhaustion markers panel

$CD8^+$ T lymphocytes (3.2.1.1.3), were incubated for 10 minutes at RT with Fixable Viability Dye - Zombie UV (Table 4) at a dilution of 1:200. After CD8a, TIM3, and LAG3 anti-human antibodies were added and incubated for 20 minutes at 4°C. Following that, cells were washed at 450g for 5 minutes with MACS buffer, the supernatant was discarded, and 0.5ml of FoxP3 Fixation/permeabilization working solution (diluted according to kit instructions) was added, vortexed, and incubated at 4°C for 15 minutes under light-protective conditions. The supernatant was discarded after adding 1ml of 1X Permeabilization Buffer (previously diluted in dH_2O) and centrifuging at 400g for 5 minutes. The TCF1 antibody (Table 3) was then added directly and incubated for 30 minutes at RT while being kept dark. The cells were then rinsed at 400g for 5 minutes with 2 ml of 1X Permeabilization Buffer, and the supernatant was discarded. The pellet was resuspended in 300µl MACS buffer before flow cytometry assessment.

The expression of PD1, LAG3, TIM3, and TCF1 exhaustion markers was examined in alive ($Zombie\ UV^{neg}$) previously isolated $CD8^+$ T cytotoxic cells. Flow cytometry acquisition was

performed using a BD LSRII flow cytometer (Table 7). FlowJo software was used to analyze the data (Table 9). To configure the gates, isotype-labeled controls were used.

3.2.6.4 Cytokines production (Intracellular)

$CD8^+$ T lymphocytes collected after 4 hours of cytokines production stimulation (3.2.4.3), were incubated with Fixable Viability Dye - Zombie UV (Table 4) at a dilution of 1:200 for 10 minutes at RT to assess INF-γ and TNF-α intracellular production. After, CD8a anti-human antibody (Table 1) was added and incubated at 4°C for 20 minutes. Following that, cells were washed at 450g for 5 minutes with MACS buffer (Table 6), the supernatant was discarded, and 0.5ml of FoxP3 Fixation/permeabilization working solution (diluted according to kit instructions) was added (Table 5), vortexed, and incubated at 4°C for 15 minutes under light-protective conditions. After adding 1ml of 1X Permeabilization Buffer (previously diluted in dH_2O) and centrifuging at 400g for 5 minutes, the supernatant was discarded. INF-γ and TNF-α anti-human antibodies (Table 3) were then added directly and incubated at RT for 30 minutes while being protected from light. Next, cells were washed at 400g for 5 minutes with 2 ml of 1X Permeabilization Buffer, and the supernatant was discarded. The pellet was resuspended in 300µl MACS buffer before flow cytometry assessment.

The quantification of INF-γ and TNF-α was performed in alive $CD8^+$ T cytotoxic cells (Zombie UV^{neg}). Flow cytometry acquisition was performed using a BD LSRII flow cytometer (Table 7). FlowJo software was used to analyze the data (Table 9). To configure the gates, isotype-labeled controls were used.

3.2.6.5 Mitochondrial Mass measurement

Mitochondrial mass was measured in $CD8^+$ T lymphocytes at two-time points: before (day 0) and after (day 6) in vitro exhaustion stimulation using CD3 and IL-2 (as described in section

3.2.4.1). In this experiment, 1 µl of Mitotracker green (Table 4) was diluted according to the manufacturer's procedure and subsequently further diluted in 496 µl of PBS. To this solution, a volume of 2.5 µl of Zombie UV (1:200) was incorporated (Table 4). Subsequently, a $CD8^+$ T lymphocytes aliquot (50 000 cells) was stained using the previously described staining solution for 15 minutes at RT. Subsequently, the cells were washed with 1 ml of MACS buffer at 450g for 4 minutes. The supernatant was discarded, and the cells were rinsed once more. Following, the pellet was reconstituted in 300 µl of MACS buffer and transferred into a FACS tube. The fluorescence intensity was quantified using FACS. Unstained $CD8^+$ T cells aliquot stained solely with Zoombie was used as a negative control.

3.2.7 Statistical analysis

GraphPad Prism v9.0 (Table 9) was used for statistical analysis. Applying unpaired and paired t-tests (two-tailed) or One-way ANOVA with Dunnett's multiple comparison test, statistical analysis was conducted. Linear regression and Pearson correlation were used to establish relationships between variables. The significance threshold for statistical analysis and significance was established at $p < 0.05$. The results are displayed as vertical box-and-whiskers graphs with a mean standard deviation.

4 Results

4.1 Part I: Circulating MDSCs Characterization in IPF

MDSCs are found in chronic diseases, such as cancer and have been linked to poor prognosis; however, their precise role in IPF is not fully understood. Our group performed a characterization of MDSCs in both the peripheral blood and lung tissue of IPF patients and described for the first time that disease progression is correlated with an increase in circulating MDSCs[1]. This section aims to quantify the abundance of MDSCs in a newly recruited cohort of IPF patients.

4.1.1 Patients' demographics for MDSCs characterization

The cohort of subjects in the MDSCs characterization consisted of patients with IPF and controls. As a control, participants with chronic illnesses, infections, or immunomodulatory therapy were excluded (Table 15).

Table 15. MDSCs characterization of patients' demographics

CHARACTERISTICS	CONTROL	IPF
Subjects	12	41
Age (Years)	58.25±4.62	65.27±8.19**
Gender **Female** **Male**	 3 (25 %) 9 (75 %)	 9 (21.96 %) 32 (78.05%)
Smoking Status[#, $] **Never** **Former** **Current**	 6 (50 %) 5 (41.67 %) 1 (8.33 %)	 10 (25.0 %) 27 (67.5 %) 3 (7.32 %)
Lung Function **DLCo (% predicted) §** **FVC (% predicted) ^**	 - 	 40.24±15.91 69.79±19.14

Data displayed as % along with the number of subjects. Lung function data is shown as Mean±SD and includes the diffusing capacity of the lung for carbon monoxide (DLCo) and the forced volume capacity of the lung (FVC). [#]: Subjects with history of ≥5 pack-years of cigarette smoking. **: denotes statistical significance with $p<0.01$ compared with healthy controls. [$]One IPF patient had no smoking-history information available (n=40). [§]No DLCo data available for 10 IPF patients (n=31). ^No FVC data available for 5 IPF patients (n=36)

4.1.2 MDSCs characterization in the peripheral blood

Human peripheral blood MDSCs were characterized as Lineage^{neg} HLA-DR^{-} CD33^{+} CD11b^{+} (Figure 19A). M-MDSCs were defined Lineage^{neg} ^{HLA}DR^{-} CD33^{+} CD11b^{+} CD14^{+} and G-MDSCs as Lineage^{neg} HLA-DR^{-} CD33^{+} CD11b^{+} CD66b^{+}, as previously described[1]. Isotype control was used as a threshold of positive and negative populations (Figure 19B, C).

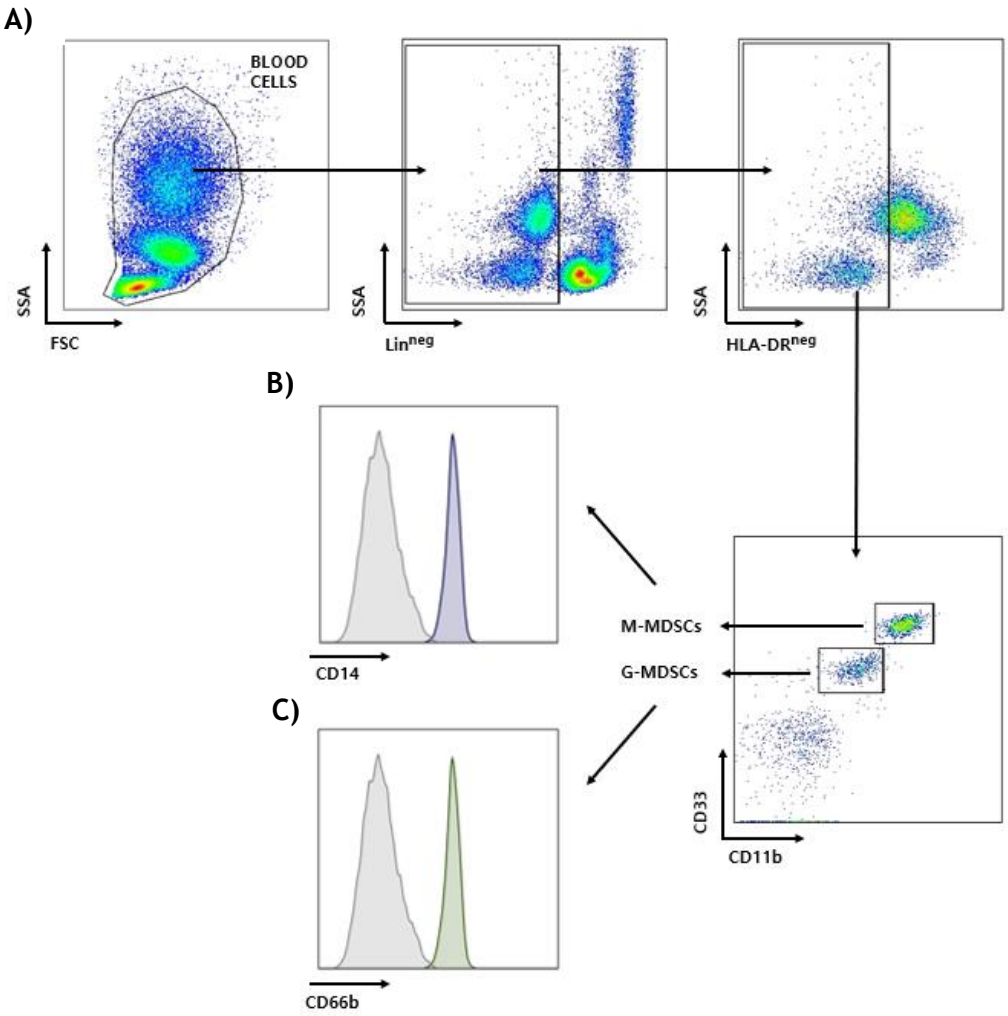

Figure 19. MDSCs immunophenotyping in peripheral blood. A) MDSCs gating strategy in flow cytometry represented by dot-plots graphs of peripheral blood. Lineage negative was used to exclude differentiated and mature cell populations; **B)** M-MDSCs (CD14^{+}) are represented in blue histograms and **C)** G-MDSCs (CD66b^{+}) in green. Isotypes are represented in gray.

4.1.3 MDSCs are increased in peripheral blood of IPF patients

Our group has previously reported an increase in MDSCs in IPF patients' circulation[1]. We investigated the amount of circulating MDSCs (as cells/µl gated in HLA-DR^{neg}) in a new cohort of IPF patients and found that IPF patients had a greater number of MDSCs (50.20±118.2 cells/µl, p<0.01) than controls (13.09±11.06 cells/µl), thereby confirming and bolstering the prior findings (Figure 20A).

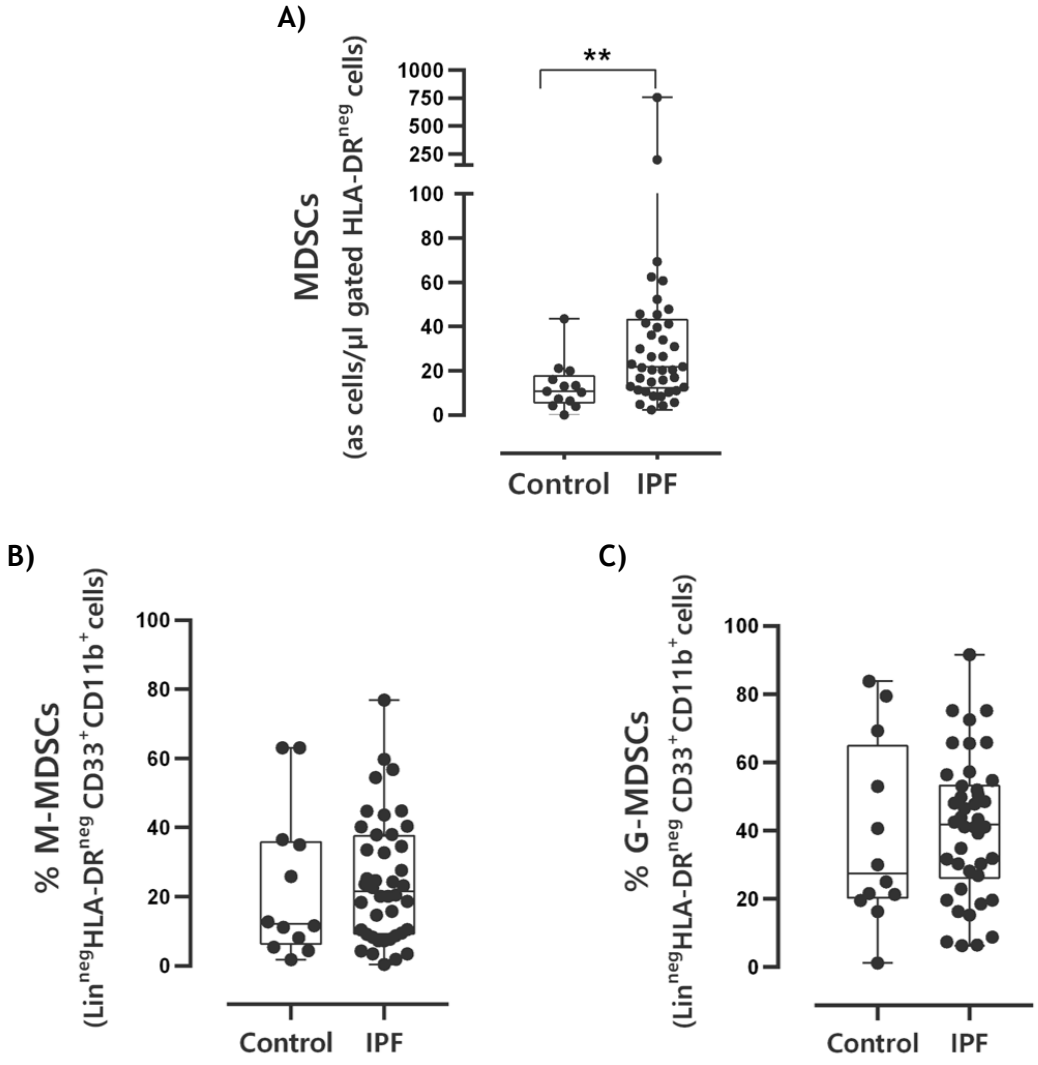

Figure 20. MDSCs abundance in peripheral blood. A) Scatter dot plots depict MDSCs in cells/µl (gated in HLA-DR^{neg}). Healthy donors n= 12, IPF n= 41; **B) %** M-MDSCs (gated in Lin^{neg}HLA-DR^{neg} CD33^{+}CD11b^{+} cells). Healthy donors n=12, IPF n= 41; **D)** % G-MDSCs (gated in Lin^{neg}HLA-DR^{neg} CD33^{+}CD11b^{+} cells). Control n=12, IPF n=41. Statistical analysis between two groups was performed using, non-parametric two-tailed Mann-Whitney U test. **p<0.01 when compared with control.

Next, to determine which MDSCs subset was predominant in IPF patients, we measured the percentage of M-MDSCs (gated in $Lin^{neg}HLA\text{-}DR^{neg}CD33^{+}CD11b^{+}$ cells) and G-MDSCs (gated in $Lin^{neg}HLA\text{-}DR^{neg}CD33^{+}CD11b^{+}$ cells). We observed no statistically significant difference between the two subsets (data not shown). In addition, we investigated if the prevalence of these subtypes differed from that of healthy donors. When comparing IPF versus control in both M-MDSCs (24.5417.93 vs 23.23, p=NS) (Figure 20B) and G-MDSCS (41.0820.62 vs 38.45, p=NS), no significant differences were identified (Figure 20C).

4.2 Part II: MDSCs immunomodulation

MDSCs have been widely studied in cancer, particularly for their capacity to regulate the tumor microenvironment through interacting with other immune cells, particularly T lymphocytes (described in 1.2.1.2). Intriguingly, a recent study revealed that MDSCs metabolically modify $CD8^{+}$ T cells via the transfer of cytoplasmic components and reduce their effector activity when in proximity[146], suggesting a stronger connection between these two cell types.

Based on the aforementioned findings, the purpose of this chapter was to characterize the interaction between MDSCs – $CD8^{+}$ T cells in IPF and its potential pro-fibrotic role.

4.2.1 $CD8^{+}$ $PD1^{+}$ T cell exhausted phenotype is present and increased in IPF lung tissue

Our lab previously published data proving that IPF MDSCs have the ability to suppress the proliferation of autologous $CD8^{+}$ T cells, confirming MDSCs' suppressive functions[1] (Figure 21).

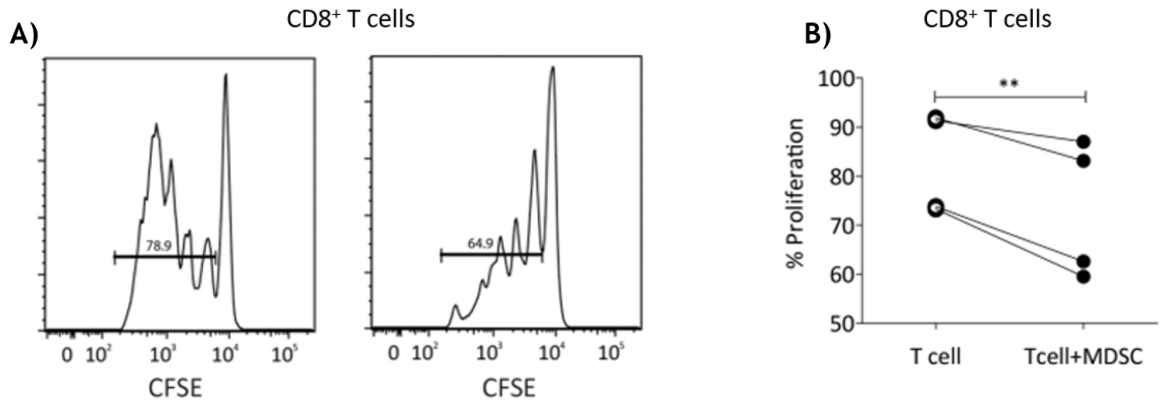

Figure 21. Myeloid-derived suppressor cells (MDSCs) suppress autologous CD8⁺ lymphocytes proliferation in IPF. **A)** Representative histogram of CD8⁺ T cell proliferation, assessed by carboxyfluorescein succinimidyl ester (CFSE) incorporation and measured by flow cytometry, with medium only (left-hand panel) and co-cultured with autologous MDSCs (right-hand panel); **B)** Quantification of % proliferation of CD8⁺ T cells alone or in co-culture with autologous MDSCs in IPF patients (n=4). For statistical analysis paired t-tests were used. ** $p<0.01$. (Modified from Fernandez I.E., 2016)

Interestingly, the reduction of T lymphocyte proliferative capacity is one of the features of CD8⁺ T cell exhaustion; hence, we sought to investigate if IPF patients' lungs exhibit a CD8⁺ T cell exhaustion phenotype by web-based data-mining. To do this, we used the IPF cell atlas (ipfcellatlas.com), a recent multi-institutional cooperation that contains a single-cell RNA database of 312,928 cells from 32 IPF and 29 healthy control lungs[147]. In this Atlas among the immune cell populations in IPF lungs, CD8⁺ T cells exhibit exhaustion markers such as PD1, LAG3, and TIM3, with PD1 being the highest expressed (Figure 22A). Moreover, the PD1 gene expression was higher IPF than in control lung tissue (Figure 22B).

Next, since the IPF atlas revealed that PD1 is the most expressed marker among all, we decided to verify its presence by immunofluorescence staining in lung tissue slides from explanted lungs. We found that CD8⁺PD1⁺ cells were present in IPF lungs (Figure 22C).

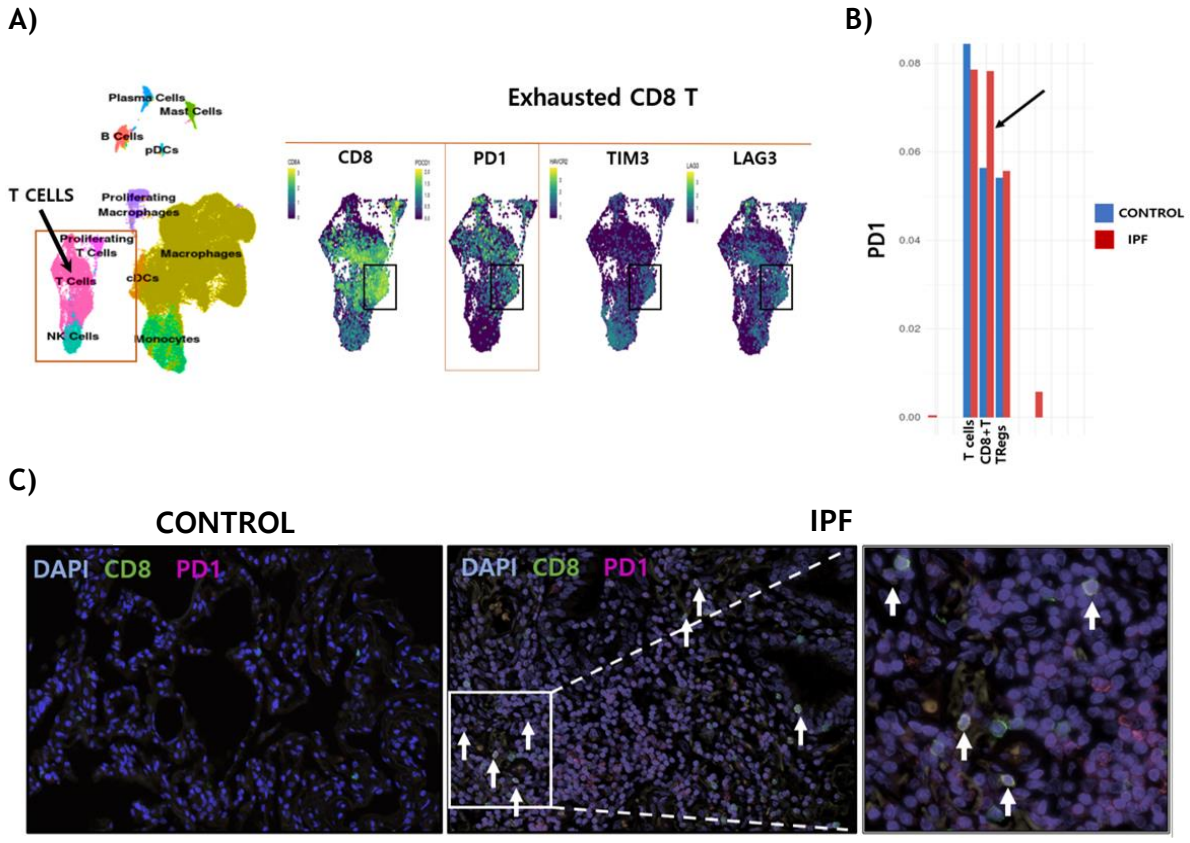

Figure 22. CD8⁺PD1⁺ T are present in IPF lung tissue. A) UMAP analysis illustrates the distribution of immune cell populations in IPF lung tissue. Black squares highlight the presence of CD8, PD1, TIM3 and LAG3. The UMAP color scheme indicates varying marker expression levels, with yellow representing high expression and purple indicating low expression (data sourced from IPFcellatlas.com); **B)** Bar plot displays the proportion of of PD1 distribution in control (blue) and IPF (red) lung tissue (data obtained from IPFcellatlas.com); **C)** Representative immunofluorescence images despict control and IPF lung FFPE sections co-stained for CD8 (green) and PD1 (magenta). Nuclei are counterstained with DAPI (blue). Cells that are double positive for CD8 and PD1 are marked with arrows. The two initial images represent lower magnifications at 10X (scale bar=50µm), while the white square represents higher magnification view (scale bar= 20µm). Sections are representative samples stains of three IPF patients and three controls subjects.

4.2.2 PDL1, the PD1 ligand is more expressed in M-MDSCs

Based on our findings, we observed that CD8⁺ PD1⁺ cells are present in IPF lung tissue, thus we sought to investigate whether IPF MDSCs expressed PDL1, one of the PD1 ligands. We analyzed data from the IPF atlas that also contained lung tissue of ILD patients and controls.

In collaboration with Meshal Ansari (Ph.D. student at the Helmholtz Institute, Munich), we found that PDL1 is abundantly expressed in tissue myeloid cells of ILD patients (Figure 23A).

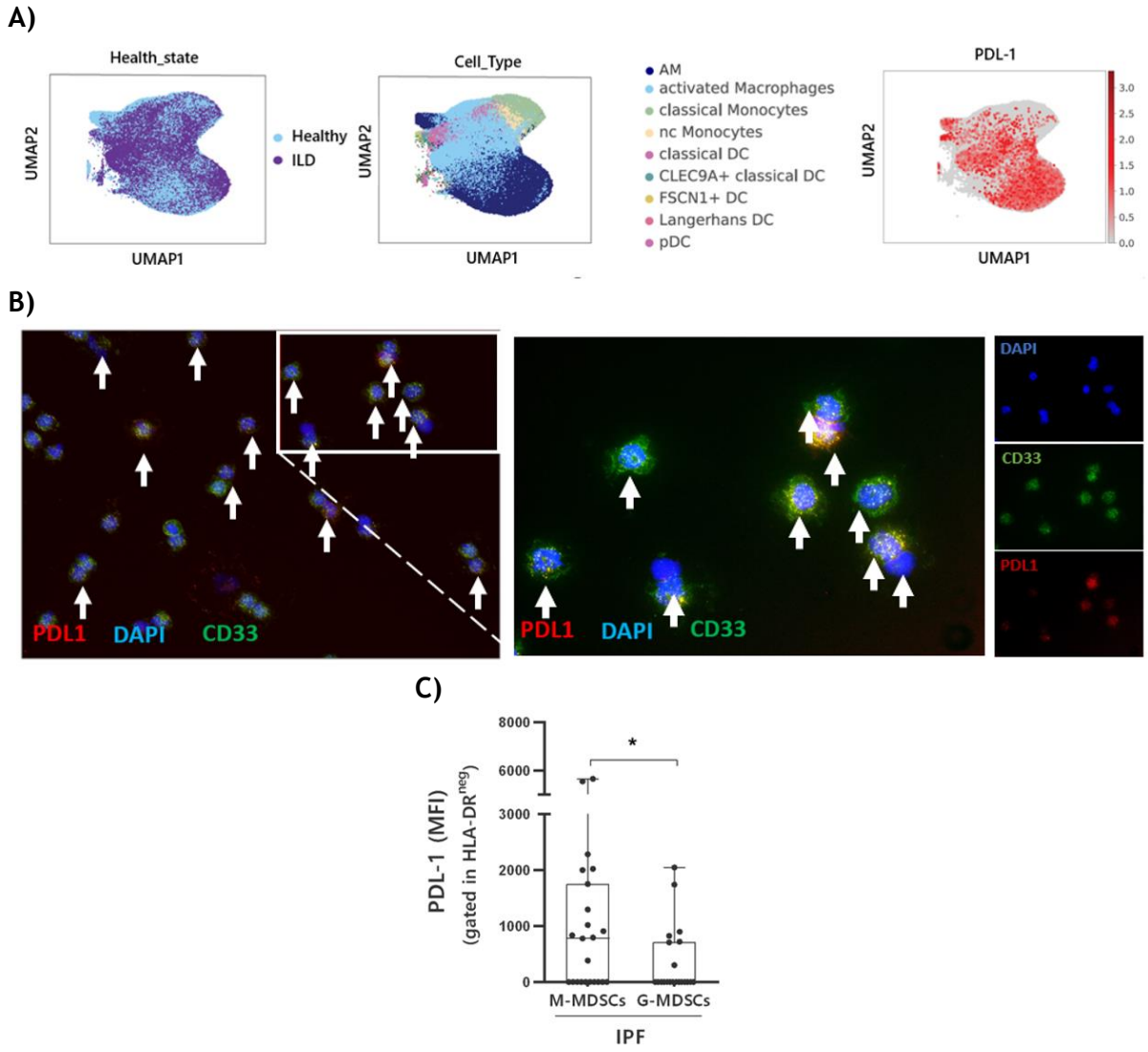

Figure 23. PDL1 expression in MDSCs. A) UMAP plots from single cell sequencing showing myeloid cells clusters in lung tissue. First plot on the left illustrates cell clusters from healthy (light blue) and IPF (purple) lungs. The second plot depicts myeloid cells clusters in different colors (see legend). Third plot shows cell clusters expressing PDL1; **B)** Representative immunofluorescence of M-MDSCs cytospins co-stained for CD33 (green) and PDL1 (red). Nuclei were counterstained with DAPI (blue). Double positive cells are indicated with arrows. Lower magnification (first image) is presented at 10X (scale bar=50µm). White square represents higher magnification (scale bar= 20µm). The three images on the right represent single staining of the high magnification picture. Pictures are representative stains of three IPF M-MDSCS cytospins. **C)** Scatter dot-plots depict the mean fluorescence intensity of PDL1 in MDSCs subsets assessed by flow cytometry in peripheral blood. IPF n=23, Control n= 9; Statistical analysis between two groups was performed using, non-parametric two-tailed Mann-Whitney U test. *p<0.06. **Note:** Single-cell RNA sequencing performed by Meshal Ansari and Dr. H.B. Schiller, Helmholtz Munich.

Next, we performed flow cytometry in peripheral blood to confirm the presence of PDL1 in IPF MDSCs and we detected a significantly increased PDL1 MFI in M-MDSCs compared to G-MDSCs in IPF (1098±1608 vs 344.6±604.5, p=<0.06) (Figure 23C). Moreover, we found the co-expression of PDL1 and CD33 in cytospins of bead-sorted M-MDSCs (Figure 23B) by immunofluorescent staining. All these findings corroborate the existence of PDL1, the ligand of PD1, in IPF MDSCs.

4.2.3 M-MDSCs expressing PDL1 are present in IPF lung tissue and close proximity to $CD3^+PD1^+$ cells

To investigate whether M-MDSCs ($CD33^+CD11b^+$ cells) expressing PDL1 were present in IPF lung tissue and located near lymphocytes T expressing PD1 ($CD3^+PD1^+$) cells, we performed a multiplexed immunohistochemistry (mIHC) of paraffin-embedded lung tissue sections (described in detail on 3.2.5.4). This approach enabled the simultaneous detection of six markers on a single segment of tissue, thereby providing a comprehensive view of the spatial distribution of the different markers. First, we found that $CD33^+CD11b^+PDL1^+$ cells were present in IPF tissue (Figure 24A, B). Quantification of $CD33^+CD11b^+PDL1^+$ cells localized in the lung parenchyma of explanted IPF subjects was significantly increased when compared to non-IPF ILD subjects (286.2±192.0 cells/mm^2 vs 57.20±29.43 cells/mm^2, p=<0.05) (Figure 24C).

Next, we confirmed the presence of $CD3^+PD1^+$ cells in the same IPF tissue slides (Figure 25A, B) with further quantification showing a significant increase in IPF when compared to non-IPD ILD (1497±553 cells/mm^2 vs 87.20±67.21 cells/mm^2, p = <0.005) (Figure 25C).

Finally, in order to better characterize the distribution of $CD3^+PD1^+$ cells and $CD33^+CD11b^+PDL1^+$ cells in IPF tissue vs non-IPF ILD tissue, we looked at how close they were to each other and we found that the two cell types were seen to be in closer proximity in

IPF than in non- IPF ILD lung explant tissue (48.05 ±27.48µm vs 113.3±41,46µm, p=<0.05) (Figure 24D), suggesting that in IPF these cells have a closer interaction.

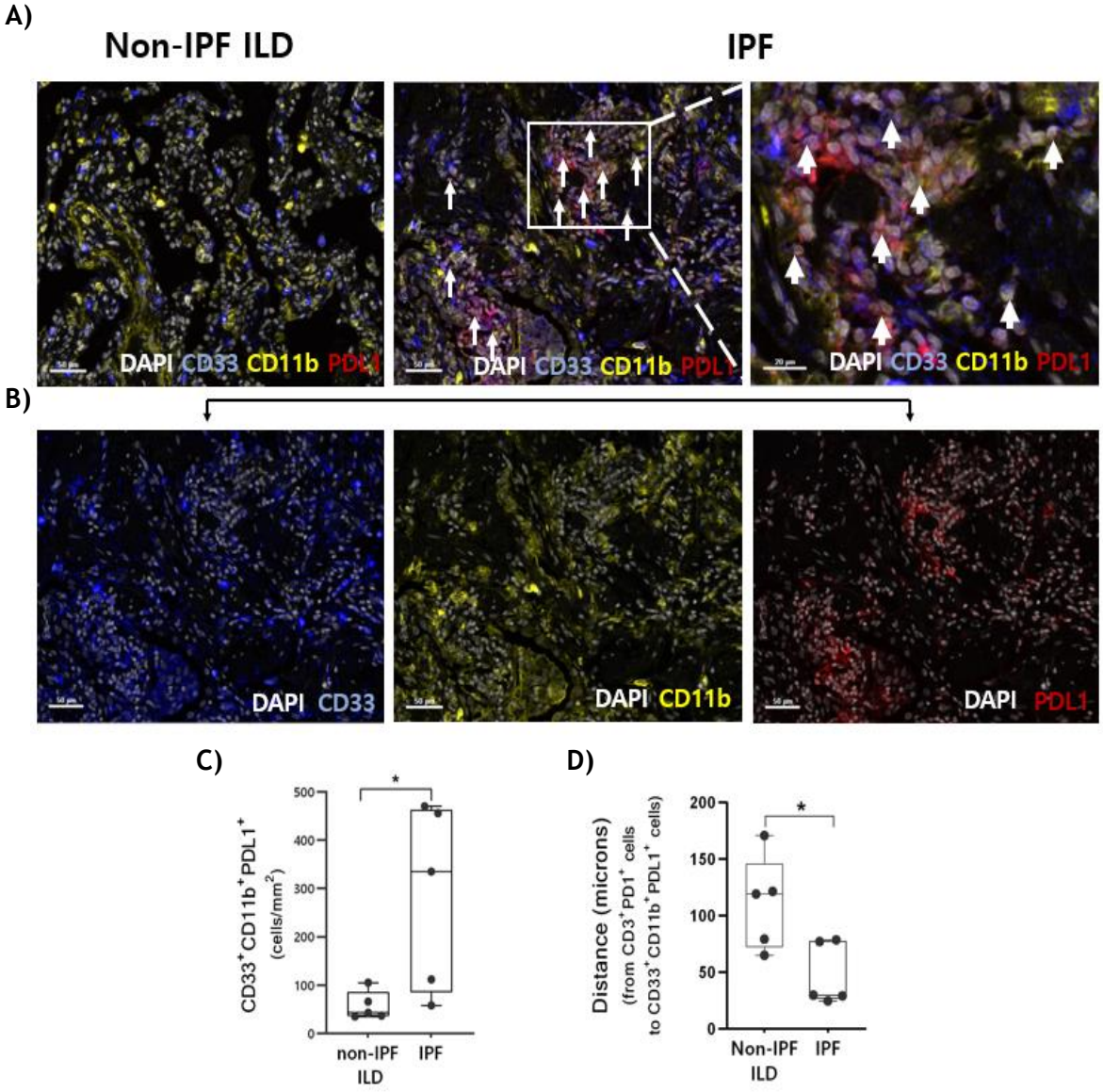

Figure 24. Multiplexed immunohistochemistry (mIHC) reveals that CD33⁺ CD11b⁺ cells (M-MDSCs) express PDL1 expression are in close proximity to CD3⁺PD1⁺ cells in IPF lung tissue. A) Representative mIHC image of IPF non-IPF ILD lung FFPE sections co-stained for CD33 (blue), CD11b (yellow) and PDL1 (red). Nuclei were counterstained with DAPI (white). Double positive cells are indicated with white arrows. Lower magnifications (two first images) are given at 10X (scale bar=50µm). White square represents greater magnification (scale bar= 20µm). Sections are representative IPF n=5 and non-IPF ILD n= 5. **B)** Single stains from IPF tissue displayed in **A** at 10X magnification (scale bar=50µm). **C)** Quantification (cells/mm^2) of CD33⁺CD11b⁺PDL1⁺ cells in IPF and non-ILD lung tissue is depicted by scatter dot-plots. IPF n=5, non-IPF ILD n= 5; **D)** Scatter dot-plots show the distance (microns) between CD3⁺PD1⁺ cells and CD33⁺CD11b⁺PDL1⁺ cells in IPF and non-ILD lung tissue. IPF n=5, non-IPF ILD n= 5

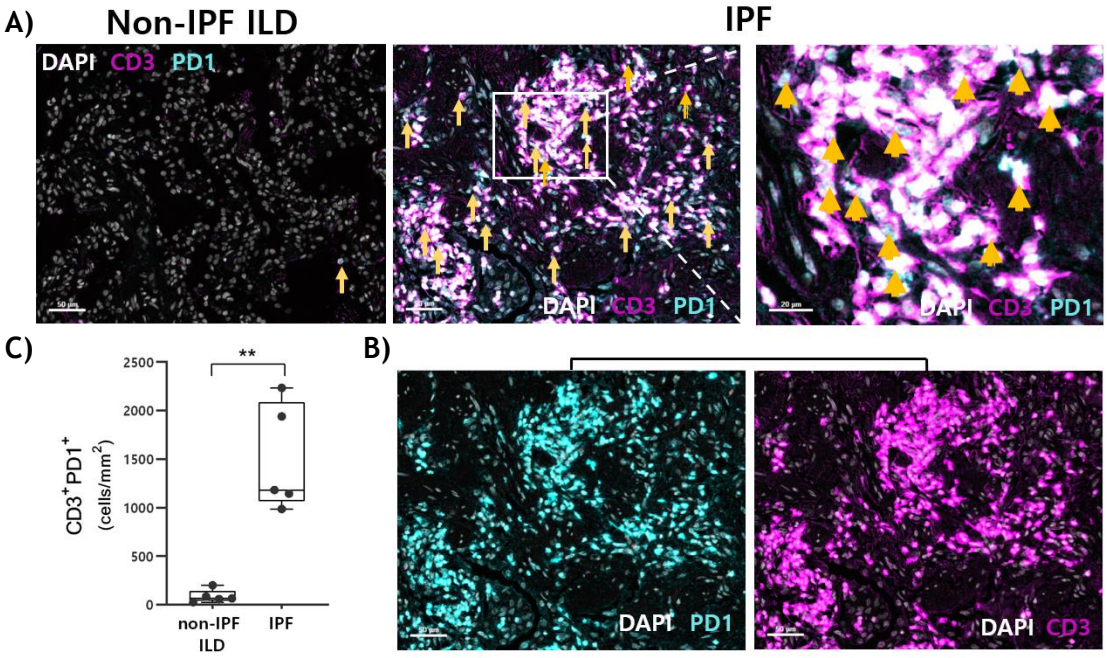

Figure 25. Multiplexed immunohistochemistry (mIHC) reveals that CD3⁺ (lymphocytes T) expressing PD1⁺ are increased in IPF lung tissue. A) Representative mIHC image of IPF non-IPF ILD lung FFPE sections co-stained for CD3 (magenta) and PD1 (turquoise). Nuclei were counterstained with DAPI (white). Double positive cells are indicated with yellow arrows. Lower magnifications (two first images) are given at 10X (scale bar=50µm). White square represents greater magnification (scale bar= 20µm). Sections are representative IPF n=5 and non-IPF ILD n= 5. **B)** Single stains from IPF tissue displayed in **A)** at 10X magnification (scale bar=50µm). **C)** Quantification (cells/mm^2) of CD3⁺ PD1⁺ cells in IPF and non-ILD lung tissue is depicted by scatter dot-plots. IPF n=5, non-IPF ILD n= 5.

4.2.4 Exhaustion markers in circulating CD8⁺ T cells

In section 4.2.2, we demonstrated the presence of an exhausted CD8⁺ T cell phenotype in IPF lung tissue. To understand if this phenotype is present already in circulation, we investigated the presence of CD8⁺ T cells by flow cytometry. Exhaustion markers PD1, LAG3, and TIM3 were measured and quantified in freshly isolated PBMCs CD3⁺CD8⁺ T cells from IPF patients and controls (Table 16).

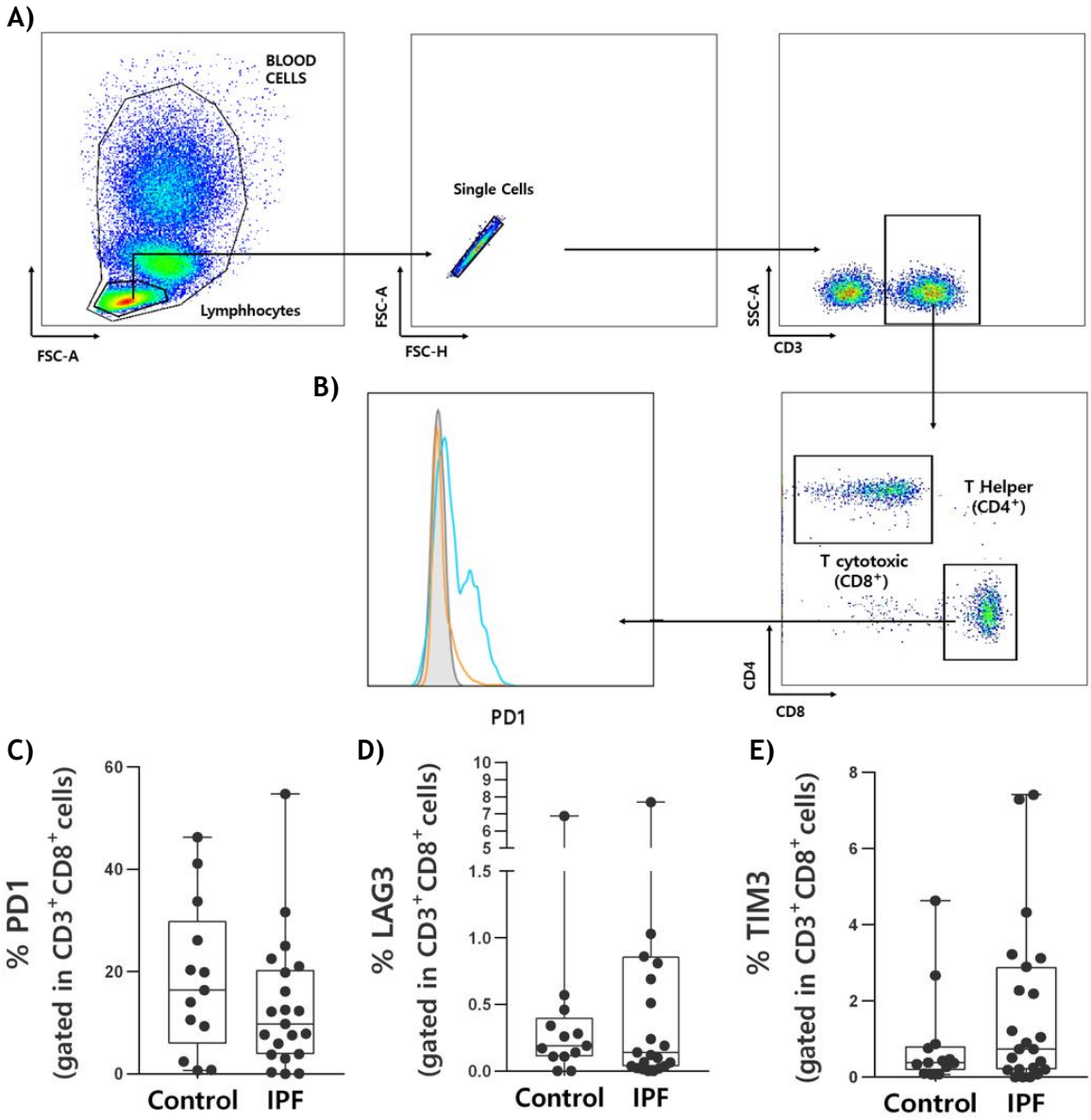

Figure 26. Exhausted phenotype in circulating CD8⁺ T cells. A) CD8+ T cells (cytotoxic) gating strategy in flow cytometry represented by dot-plots graphs of peripheral blood; **B)** Representative histogram of PD1 in IPF CD8+ T cells. Control is represented in turquoise, IPF in yellow and isotope in grey. Scatter dot-plots represent % of C**)** PD1, **D)** LAG3 and **E)** TIM3 expressed by $CD3^{+}CD8^{+}$ T cells. Control n= 13, IPF = 21. Statistical analysis between two groups was performed using non-parametric two-tailed Mann-Whitney U test.

PD1 (12.4±12.63% vs 18.59±14.83%, p= NS), LAG3 (0.95±1.79% vs 0.73±1.85%, p=NS) and TIM3 (1.70±2.16% vs 0.87±1.31%, p=NS) was not significantly regulated in $CD8^{+}$ T cells in IPF compared with control.

Table 16. CD8⁺ T cell exhaustion patients' demographics

CHARACTERISTICS	CONTROL	IPF
Subjects	13	21
Age (Years)	57.15±4.24	64.81±8.32
Gender **Female** **Male**	 6 (46.15 %) 7 (53.85 %)	 1 (4.76 %) 20 (95.24 %)
Smoking Status[#, &] **Never** **Former** **Current**	 9 (%) 2 (%) 1 (%)	 4 (21.05 %) 14 (73.68 %) 1 (5.26 %)
Lung Function **DLCo (% predicted)[§]** **FVC (% predicted)^**	 -	 35.53±14.44 67.94±15.16

Data displayed as % along with number of subjects. Lung function data is shown as Mean±SD and includes the diffusing capacity of the lung for carbon monoxide (DLCo) and the forced volume capacity of the lung (FVC). [#]: Subjects with history of ≥5 pack-years of cigarette smoking. *: $p<0.05$ denotes statistical significance compared with healthy controls. [&]Two IPF patients had no smoking-history information available (n=19). [§]No DLCo data are available for 4 IPF patients (n=17). ^ No FVC data are available for 3 IPF patients (n=18)

4.2.5 IPF CD8⁺ T cells can become exhausted *in vitro*

To investigate the exhaustion capacity of circulating CD8⁺ T cells in IPF patients, we developed an in vitro assay to induce CD8⁺ T cell exhaustion as previously published[143]. Briefly, to induce exhaustion, we isolated IPF CD8⁺ T cells and activated them with IL-2 and CD3 on day 0, followed by re-stimulation with the same cocktail every 48 hours until day 6 (described in detail in 3.4.5.1) (Figure 27A).

Exhaustion markers PD1, LAG3, and L1CAM were measured in IPF CD8⁺ T cells before (day 0) and after *in vitro* exhaustion (day 6). After 6 days of *in vitro* exhaustion, MFI of PD1 in IPF CD8⁺ T cells was significantly increased compared with day 0 (5313±2468 vs 1617±745.9, $p<0.0001$) (Figures 24B and 24E). Similarly, LAG3 and TIM3 showed a significant MFI increase in IPF CD8⁺T cells after 6 days compared to day 0 (3803±2119 vs 1228±948,1, $p<0.001$ and

18966±13713 vs 3430±5603, p<0.005 respectively) (Figures 27B and 27E). We did not find significant differences when compared with controls (data not shown).

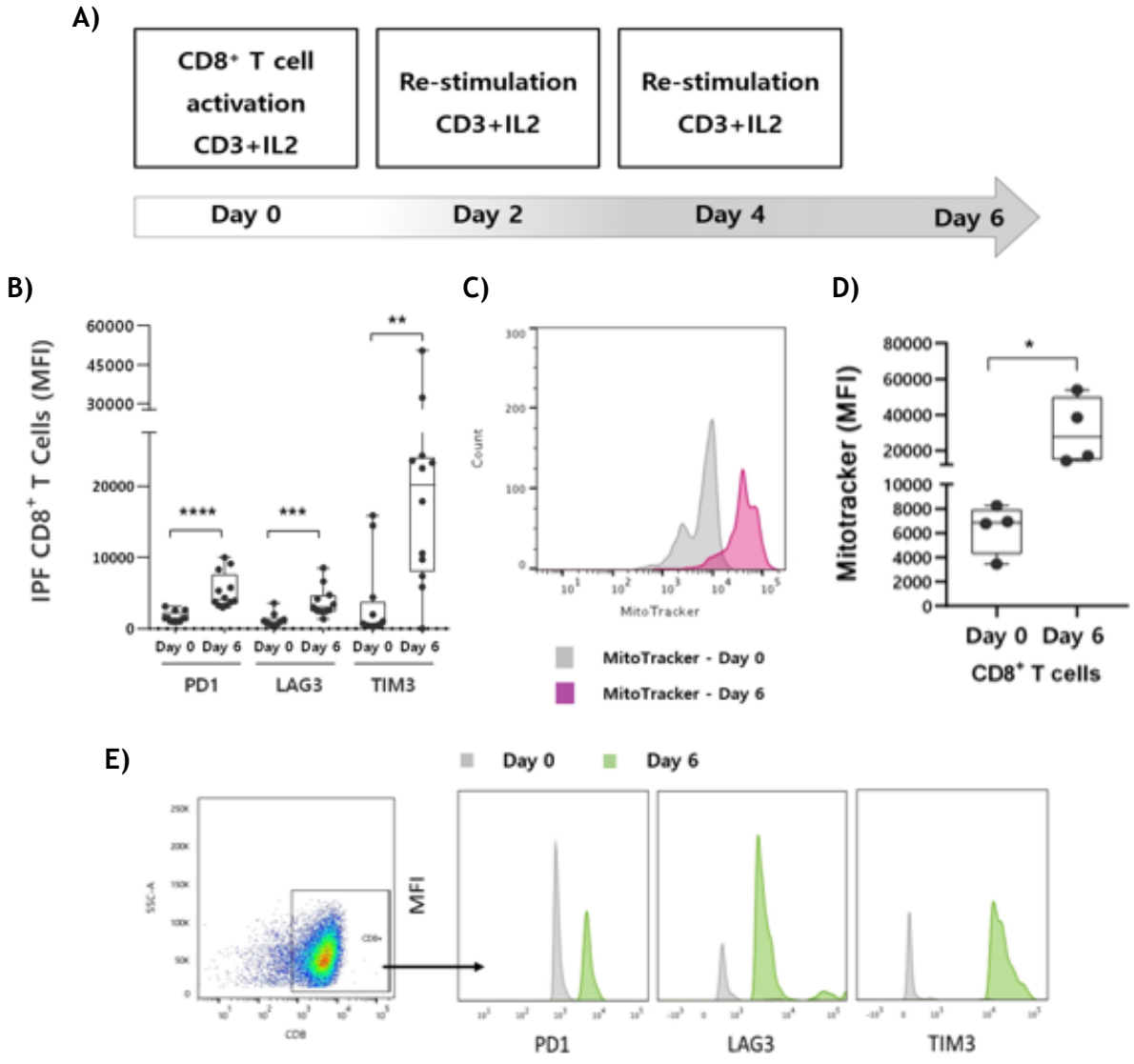

Figure 27. IPF CD8⁺ T cells get exhausted after 6 days *in vitro* stimulation. A) Schematic representation of the assay workflow; **B**) Scatter dot-plots show the mean fluorescence intensity (MFI) of PD1, LAG3 and TIM3 in isolated IPF CD8⁺ T cells on day 0 and 6. IPF n= 12; C**)** Representative histogram of mitochondrial mass in IPF CD8⁺ T cells, assessed by Mitotracker incorporation and measured by flow cytometry. Day 0 in gray and day 6 in pink; **D)** Scatter dot-plots depict the MFI of Mitotracker in isolated IPF CD8⁺ on day 0 and 6. IPF n= 4; **E)** Representative histograms of MFI of PD1, LAG3 and TIM3. Day 0 is represented in gray and day 6 in green. Statistical analysis between two groups was performed using non-parametric two-tailed Mann-Whitney U test. * represents p<0.05, **p<0.005, ***p<0.001 and ****p<0.0001 when compared with another group.

Furthermore, since increased mitochondrial mass is characteristic of T cell exhaustion[143], we used Mitotracker to quantify mitochondrial mass in IPF $CD8^+$ T cells that underwent *in vitro* exhaustion. We found an increased Mitotracker MFI in IPF $CD8^+$ T cells that were subjected to *in vitro* exhaustion for 6 days (30862±18748, $p<0.05$) compared to day 0 (6366±2041) (Figures 27C-D). Together, our results demonstrate the exhaustion capacity of $CD8^+$ T cells in IPF.

4.2.6 IPF MDSCs induce the expression of PD1 and LAG3 in $CD8^+$ T cells *in vitro*

MDSCs contribute to T cell exhaustion[3]. After inducing exhaustion *in vitro* in IPF $CD8^+$ T cells, based on the experiment above (see detailed in 3.2.4.2) we added autologous MDSCs to determine their effect on the expression of exhaustion markers on $CD8^+$ T cells after 6 days of co-culture (Figure 28A). We had the following conditions: Only $CD8^+$ T cells, $CD8^+$ T cell + MDSCs with cocktail IL2-CD3 (test condition), and $CD8^+$ T cells with cocktail IL2-CD3 (positive control).

When IPF $CD8^+$ T cells were co-cultured with MDSCs (CD3+IL2), PD1 MFI was higher than in $CD8^+$ T cells alone (2806±1090 vs. 1068±166.4, ***$p<0.001$). There was no statistically significant difference between IPF $CD8^+$ T cells + MDSCs (CD3+IL2) and the positive control condition (2806±1090 vs 4411±1907 p=ns) (Figure 28B). In control subjects, similar results were seen (data not shown). Similarly, LAG3 was significantly elevated when IPF $CD8^+$ T cells were co-cultured with MDSCs (CD3+IL2) versus only $CD8^+$ T cells (1839±536.7 vs 630.4±214, $p<0.005$). The expression of LAG3 did not differ significantly from the positive control condition (1839±536.7 vs 2659±757.1, p=ns) (Figure 28C).

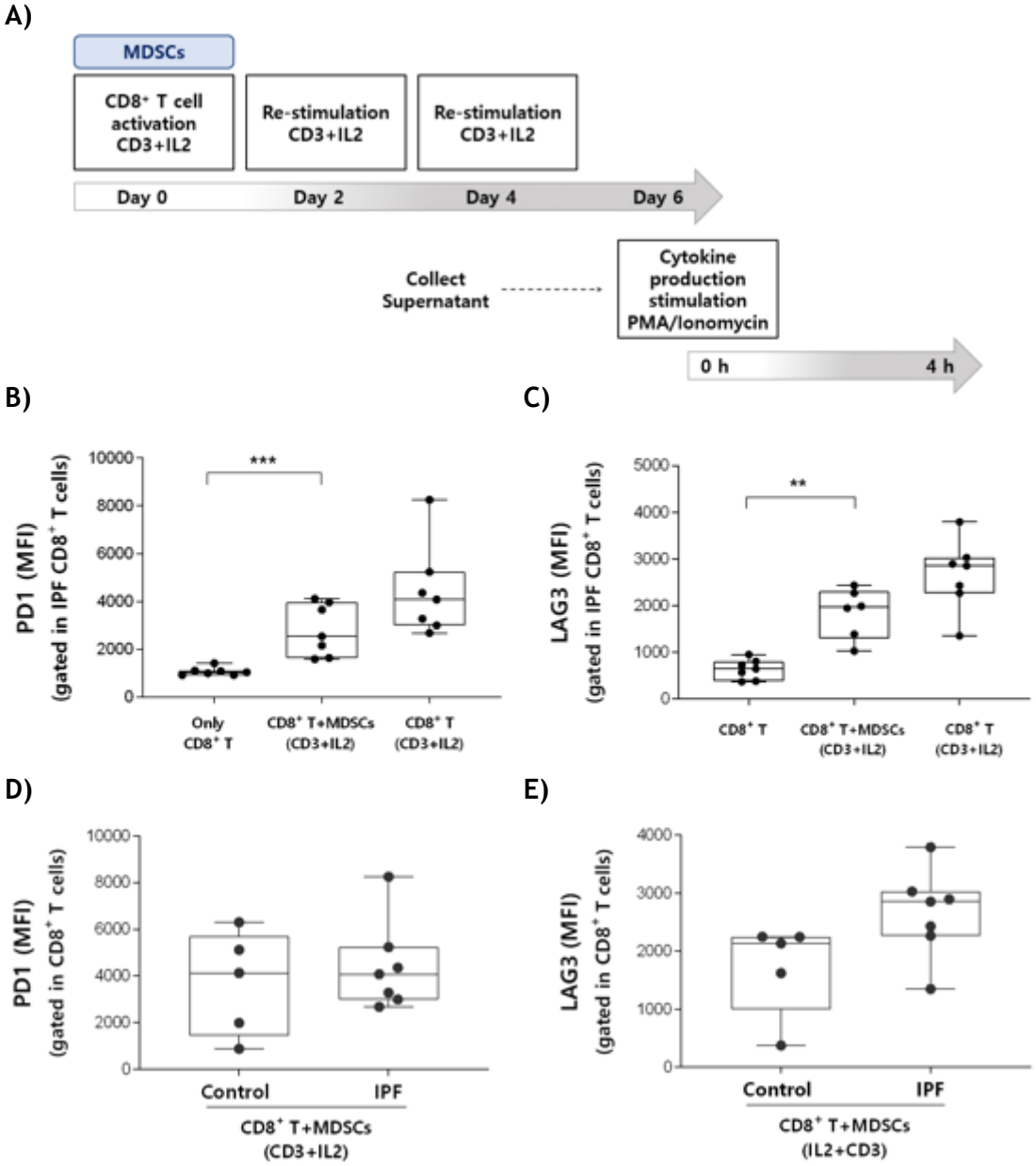

Figure 28. CD8⁺ T cells exhaustion markers expression in co-culture with autologous MDSCs *in vitro*. A) Schematic representation of the assay workflow; Scatter dot-plots show the mean fluorescence intensity (MFI) of **B)** PD1 and **C)** LAG3 in isolated IPF CD8⁺ T cells when co-cultured with MDSCs on day 0 and 6. Conditions Only CD8⁺ T cells (negative control), CD8⁺ T cell + MDSCs with cocktail CD3+IL2 (test condition) and CD8⁺ T cells with cocktail CD3+IL2 (positive control) IPF n= 7; Scatter dot-plots show the mean fluorescence intensity (MFI) of **D)** PD1 and **E)** LAG3 in isolated IPF CD8⁺ T cells when co-cultured with MDSCs from controls and IPF on day 6. IPF n= 7, Control n=5; Statistical analysis between two groups was performed using non-parametric two-tailed Mann-Whitney U test. * represents $p<0.05$, **$p<0.005$, and ***$p<0.001$ when compared with another group.

Moreover, as decreased cytokine production and secretion is another sign of T cell exhaustion, we stimulated the cells with PMA and Ionomycin to induce cytokine release on day 6, and using flow cytometry assessed INF-γ and TNF-α in supernatants of co-cultured cells (see details in 3.2.4.3) (figure 28A). There were no significant differences in cytokine production between co-cultures of $CD8^+$ T cells with or without MDSCs nor between IPF patients and healthy controls (data not shown).

4.2.7 CD3 and IL-2 may influence the effect of MDSCs on PD1 and LAG3 expression in $CD8^+$ T cells.

Next, to investigate the effect that CD3 and IL-2 might have on the expression of the PD1 and LAG3 in co-cultured IPF $CD8^+$T cells with MDSCs, we repeated the experiment without restimulation with CD3 and IL2 every 48 hours (Figure 29A). We had the following conditions: IPF $CD8^+$ T cell (negative control), $CD8^+$ T cell + MDSCs only (test condition), and $CD8^+$ T cells with cocktail CD3+IL2 (positive control). We found an increase in the MFI of PD1 and LAG3 when IPF $CD8^+$ cells were co-cultured with MDSCs compared with negative control (2774±1579 vs 942±223.8, $p<0.005$ and 11378±21511 vs 396.3±78.12, $p<0.001$ respectively) (Figure 29B-C). Similarly, elevated PD1 and LAG3 expression were seen in the positive control compared to the negative control (2865±1535 vs 942±223.8, $p<0.05$ and 1627±613,19 vs 396.3±78.12, $p<0.001$, respectively) (Figure 29B-C). In both markers, there were no significant differences between the positive control and the test condition.

In addition, we measured cytokines production (TNF-α and IFN-γ) on day 6 in the supernatants of $CD8^+$ T cell cultures. Interestingly, the MFI of TNF-α in IPF $CD8^+$ T cells co-cultured with MDSCs was significantly decreased compared to the positive control, suggesting higher induction of exhaustion (5431±6132 vs 15033±6538, $p<0.05$) (Figure 29D-E). In contrast, there were no significant differences in IFN-γ MFI in $CD8^+$ T cells when co-

cultured with MDSCs compared to the positive control (13855±19032 vs 27724±17771, p=NS) (Figures 29D and 29F)

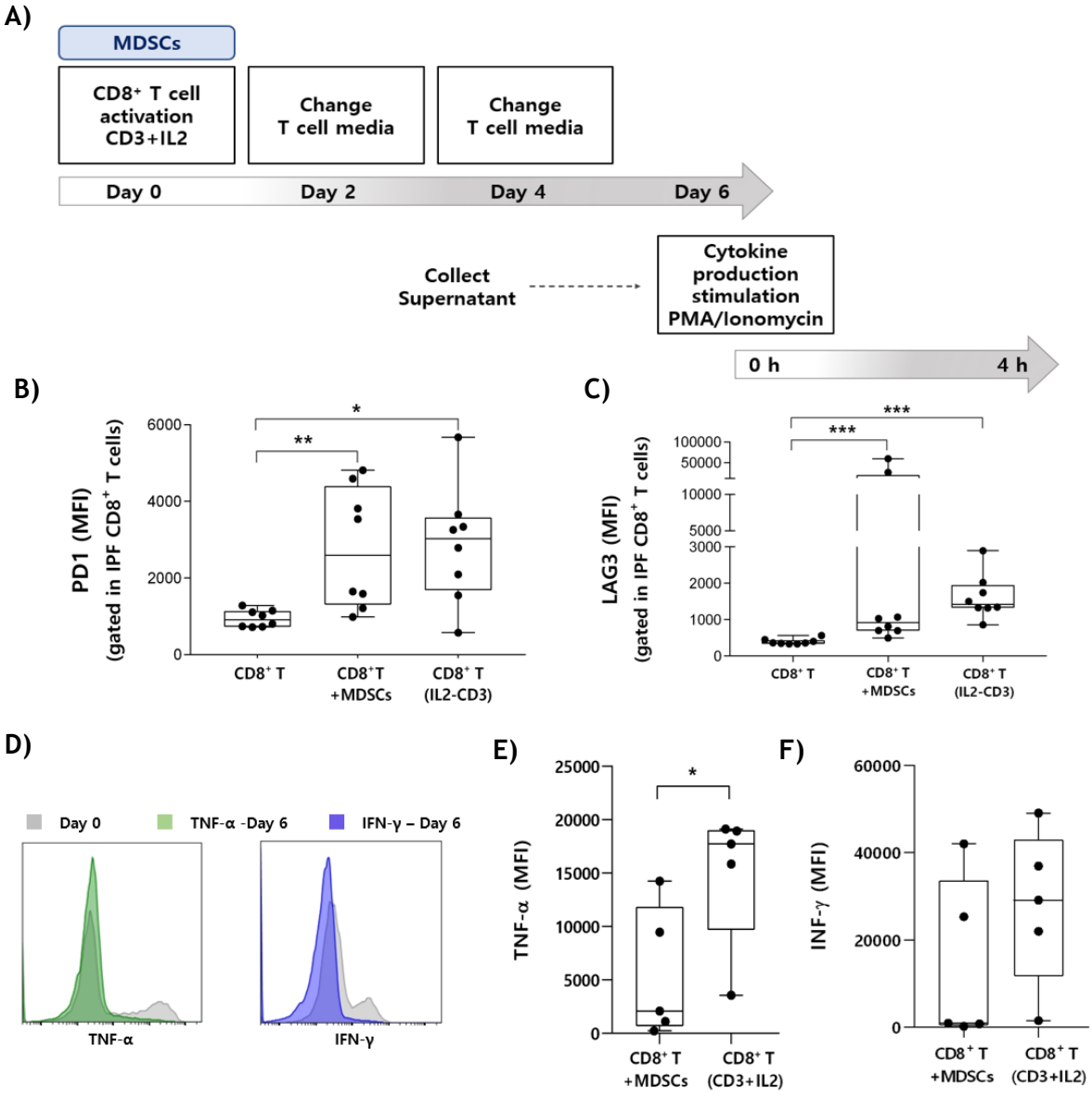

Figure 29. IPF CD8⁺ T cells exhaustion markers expression and cytokines production in co-culture with autologous MDSCs *in vitro* (without CD3+IL2) A) Schematic representation of the assay workflow; Scatter dot-plots show the mean fluorescence intensity (MFI) of **B)** PD1 and **C)** LAG3 in isolated IPF CD8⁺ T cells co-cultured with MDSCs on day 0 and 6. Only CD8⁺ T cell (negative control), CD8⁺ T cell + MDSCs (test condition) and CD8⁺ T cells with cocktail CD3+IL2 (positive control), IPF n= 8; **D)** Representative histogram plots depict the mean fluorescence intensity (MFI) of cytokines TNF-α (green) and INF-γ (blue) in supernatants of IPF CD8⁺ T cultures on day 6 following stimulation with PMA and Ionomycin; The MFI of cytokines **E)** TNF-α and **F)** INF-γ assessed by flow cytometry in supernatants of IPF CD8⁺ T cell cultures on day 6 after stimulation with PMA and Ionomycin are depicted using scatter dot-plots. IPF n=5. Statistical analysis between two groups was performed using non-parametric two-tailed Mann-Whitney U test. *Represents p<0.05, **p<0.005, and ***p<0.001 when compared with another group.

4.3 MDSCs interaction with structural cells

The contribution of myeloid cells to the fibrotic process and the importance of their interaction with structural cells remain poorly understood. The lack of MDSCs-specific markers hinders the differentiation from other myeloid cells. Identifying unique molecules expressed by MDSCs that invade lung tissue will allow us not only to properly identify these cells but also to modulate their communication with fibroblasts and epithelial cells, thereby enhancing our understanding of the dynamics of their migration to the lung and the influence they exert in situ during fibrosis.

The objective of this chapter was to discover markers solely expressed by MDSCs, investigate the migratory patterns, and evaluate their *in situ* effects on fibroblasts.

4.3.1 Circulating MDSCs and monocytes express unique markers in IPF

Our group performed mass spectrometry on autologous circulating MDSCs and monocytes from IPF patients in search of MDSC-specific markers, to further identify and differentiate MDSCs from monocytes (Figure 30A). Based on these findings, we selected and investigated markers that were specifically expressed by MDSCs (e.g. CD263, Neuropilin, and L1CAM)(Figure 30B). We assessed the expression of these markers in circulating MDSCs using FACS. We observed that the CD263 expression was significantly increased in IPF MDSCs when compared with MDSCs from controls (28.65±7.12% vs 0.816±0.46%, $p<0.001$) (Figures 30C-D). Similarly, Neuropilin was significantly increased in IPF compared to controls (1.976±0.268% vs 0.061±0.023%, $p<0.05$) (Figures 30C-D). L1CAM did not show a difference between the two groups. (Figures 30C-D).

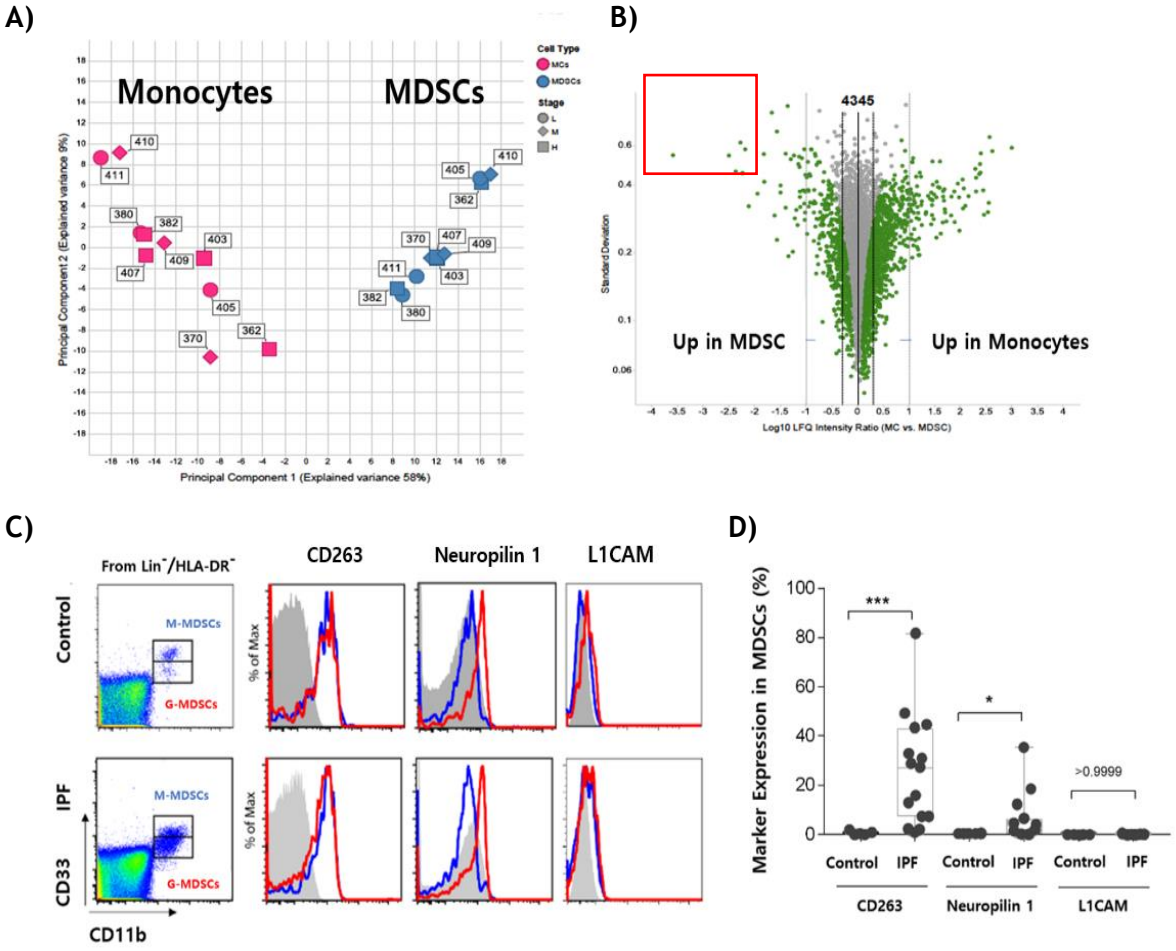

Figure 30. Exclusive expression of markers in circulating MDSCs. A) and **B)** Volcano plot analysis of exclusive proteins expressed by monocytes or MDSCs; In **B)** the red square shows the top upregulated protein in MDSCs (Including CD263, Neuropilin and L1CAM; **C)** Histogram plots of top regulated proteins CD263, Neuropilin and L1CAM in IPF and control . G-MDSCs are represented in red and M-MDSCs in blue. Isotype is represented in gray; **D)** Scatter dot-plot show % of expression of CD263, Neuropilin and L1CAM. Control n=5, IPF= 14. Statistical analysis between two groups was performed using non-parametric two-tailed Mann-Whitney U test. * represents $p<0.05$ and ***$p<0.001$ when compared with control.

4.3.2 MDSCs expressing unique markers are present in lung fibrous tissue.

To investigate if circulating MDSCs were present in lung tissue, we first quantified MDSCs in lung homogenates from ILD patients and controls. Although there were no significant differences in the abundance of MDSCs between ILD and controls (data not shown), there

was a significant increase of CD263 and L1CAM in M-MDSCs in ILD compared to controls (8.250±4.84 % vs 2.924±4.176, p<0.05, 1.355±1.689 % vs 0.095±0.189 %, p<0.05, respectively) (Figure 31A, B)

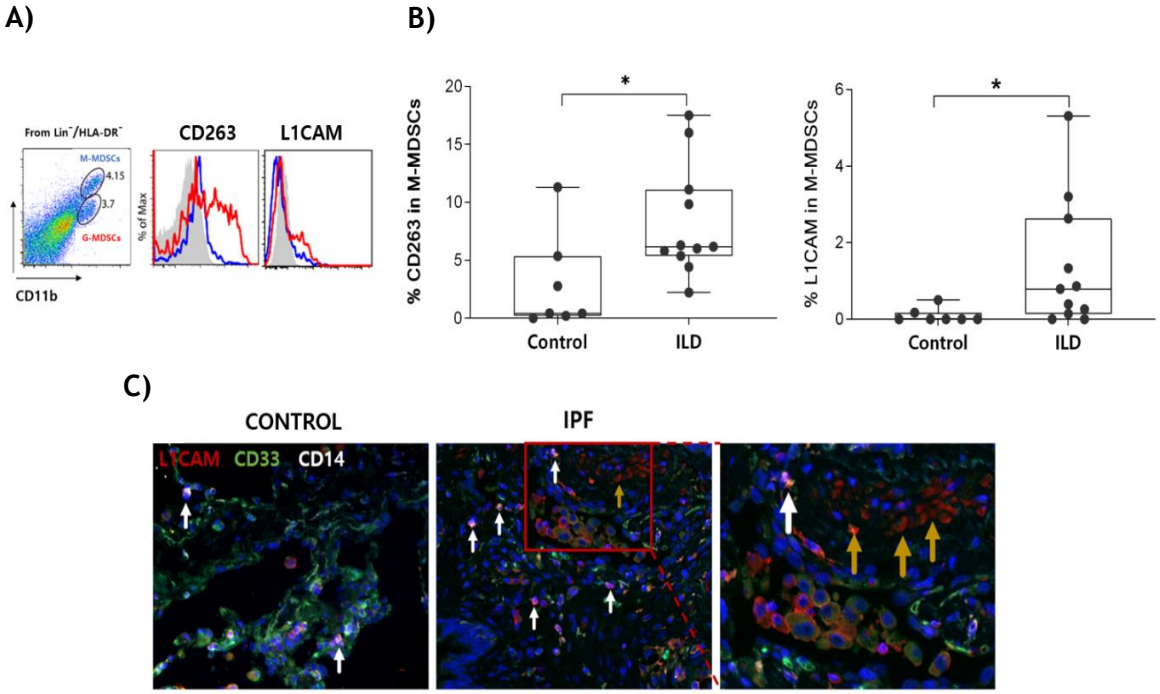

Figure 31. MDSCs are present in tissue. A) Histogram plots of top regulated proteins CD263 and L1CAM in ILD and controls. In red G-MDSCs and in blue M-MDSCs. Isotype is represented in grey; **B)** Scatter dot-plot show % of expression of CD263 and L1CAM. Control n=7, IPF= 10; **C)** Validation of tissue expression of L1CAM by immunofluorescence staining of IPF lung and healthy donor (IPF n=3, control=3). White arrows indicate triple positive cells; yellow arrows indicate L1CAM positive in niches. Scale bar 50µm and 20µm. Statistical analysis between two groups was performed using non-parametric two-tailed Mann-Whitney U test. * represents p<0.05 when compared with control.

Next, as we observed low numbers of MDSCs expressing L1CAM in circulation, we thought to determine whether these cells are present in the lung tissue of IPF patients. For this, immunofluorescent staining was performed using lung tissue slides from explanted IPF lungs. We found that $CD33^{+}CD14^{+}L1CAM^{+}$ cells, suggestive of M-MDSCs, were present in IPF lungs. In addition, L1CAM-positive cells were identified in fibrotic niches (Figure 31C).

4.3.3 IPF M-MDSCs have a higher invasive profile compared to G-MDSCs when invading a collagen gel matrix

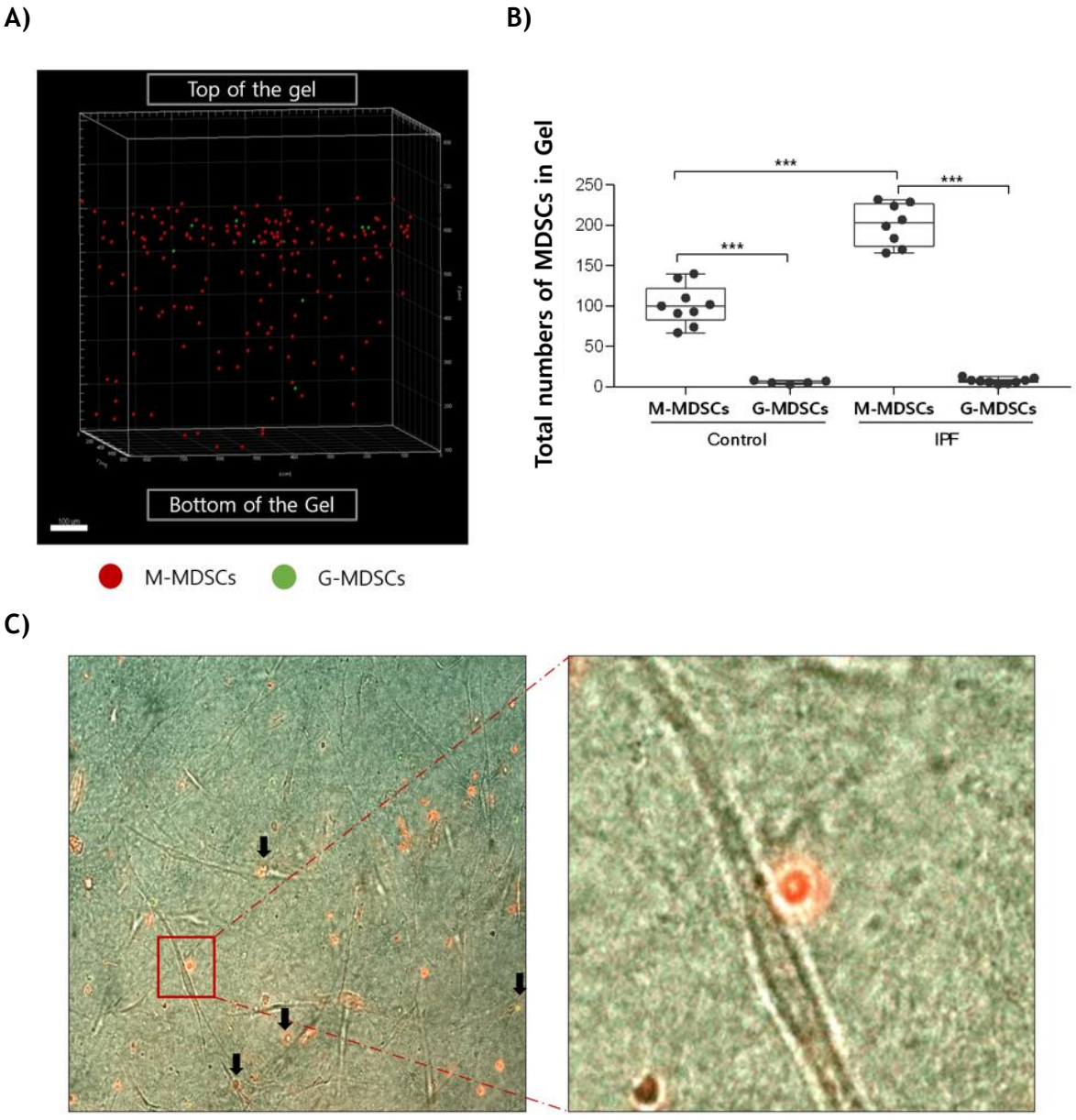

Figure 32. 3D collagen gel assays. A) Microscopy images of 3D collagen-based invasion assay. In red M-MDSCs and in green G-MDSCs; **B)** Scatter dot-plot show % of MDSCs invading the gel. Control n=3, IPF= 3; **C)** MDSCs + Fibroblast collagen gel co-culture. Black arrows indicate MDSCs in close contact with fibroblasts. Statistical analysis between groups was performed using One-way ANOVA with Dunnett's multiple comparation test. *** represents $p<0.001$ when compared with other group.

Since we investigated the presence of MDSCs in lung tissue, we thought to explore their ability to invade. To accomplish this, a 3D collagen-based invasion assay (attempting to replicate collagen buildup during IPF fibrosis) was employed (as described in section 3.2.3.2). During the experiment, previously fluorescently labeled M-MDSCs (red) and G-MDSCs (green) were used to migrate across the collagen gel (Figure 32A). After 48 hours of incubation, IPF M-MDSCs invaded significantly more than IPF G-MDSCs (201.4±26.15 cells vs 7.33±3.162 cells, $p<0.001$) (Figure 32B). Similarly, in the control group, M-MDSCs migrated considerably more than G-MDSCs (101.3±24.52 cells vs 5.60±1.949 cells, $p<0.001$). Interestingly, when comparing M-MDSCs between IPF and controls, we found that IPF MDSCs invaded more, suggesting that M-MDSCs have a more invasive profile in IPF (201.4±26.16 cells vs 101.3±24.52 cells, $p<0.001$) (Figure 32B).

Next, using a similar collagen gel-based experimental setting, we sought to determine if MDSCs and fibroblasts (phFbs) interact when co-cultured in the gel matrix. For this, a video was recorded through the 72-hour incubation period (as described in section 3.2.4.3). We observed some MDSCs in close proximity with fibroblast, suggesting a potential interaction (Figure 32C).

4.3.4 M-MDSCs modulate α-SMA deposition and TGF-B secretion in co-culture with primary human fibroblast (phFbs)

Our previous results showed the presence of MDSCs within IPF lung tissue. Furthermore, our findings in the collagen gel experiment revealed a tendency for MDSCs to localize close to fibroblasts, suggesting a potential interaction between these cell types. Therefore, we intended to determine the effect of MDSCs on fibroblasts. To accomplish this, we measured the amount of α-SMA deposition when MDSCs were co-cultured with fibroblasts (as described in section 3.2.5.1). We had four different conditions: A) Only fibroblast (negative control),

B) Fibroblast + MDSCs subset (test condition), C) Fibroblast + MDSCs subset + TGF-B (test condition), and D) Fibroblast + TGF-B (positive control).

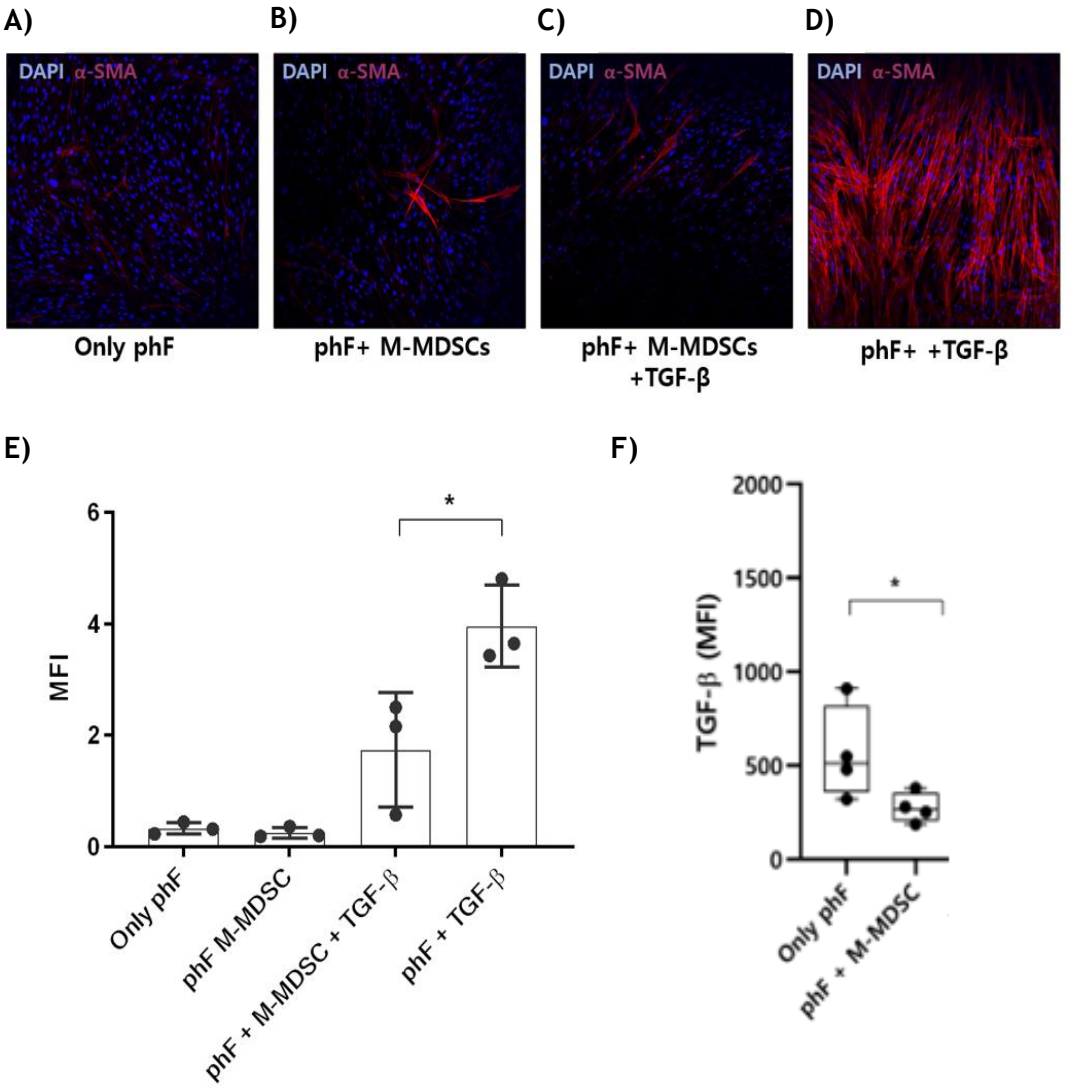

Figure 33. MDSCs co-culture with primary human fibroblasts. α-SMA immunofluorescence staining after 48 hours in MDSCs – fibroblasts co-culture in **A)** Only fibroblast (negative control), **B)** Fibroblast + MDSCs subset (test condition), **C)** Fibroblast + MDSCs subset + TGF-B (test condition) and D**)** Fibroblast + TGF-B (positive control). Cell nuclei are stained in blue (DAPI) and α-SMA in red; **E)** Scatter dot plots show the MFI quantification of α-SMA positive cells in the MDSCs -Fibroblast co-culture as mean fluorescence intensity. Control (n=3) and IPF (n=3); **F)** Scatter dot plots show the quantification of TGF-β as MFI in supernatants from MDSCs-fibroblast co-culture. Control (n=4) and IPF (n=4). Statistical analysis between two groups was performed using non-parametric two-tailed Mann-Whitney U test. * represents $p<0.05$ when compared to other group in **E** and *$p<0.06$ when compared to other group in **F.**

We found no difference in α-SMA MFI quantification when fibroblasts were co-cultured with M-MDSCs compared to the negative control (0.2510±0.096 vs 0.3310±0.105, p= >0.5) (Figures 33A, B, E). Intriguingly, when we boosted α-SMA deposition by adding TGF-B in fibroblast + M-MDSCs condition, we observed a substantial reduction in α-SMA expression compared to the positive control (1.744±1.031 vs 3.962±0.738, p<0.05) (Figure 33C-E). When we cultured with G-MDSCs no significant differences were found between all the conditions (data not shown).

Further, we quantified TGF-β in the co-culture supernatants (described in 3.2.4.3) as it is one of the most important cytokines involved in ECM remodeling . Interestingly, we found that when fibroblasts were co-cultured with M-MDSCs, less TGF-β was found in the supernatant, compared to fibroblasts alone. (274.6±79.89 vs 563.9±249,0, p=0.0571) (Figure 33F). Arguing for a possible TGF-b degradation or cellular uptake.

5 Discussion

Idiopathic pulmonary fibrosis continues to be a clinical challenge with multiple unmet needs. Unfortunately, the absence of early and adequate diagnostic tools delays the initiation of pharmacological treatment to help slow progression, as well as the identification of early candidates for transplantation, the only currently curative treatment.

In recent years, increasing research has helped in understanding pathophysiological changes that contribute to IPF development and progression. Our research and others have highlighted the role of circulating and local myeloid cells and their contribution to lung fibrosis. A retrospective pooled study from several phase III clinical trials showed that elevated monocyte counts were associated with IPF progression and poor outcomes[79]. Moreover, research conducted in our lab has demonstrated that an increase in circulating MDSCs correlates with disease progression and a worse prognosis [1]. Yet, the precise role of MDSCs and their contribution to lung fibrosis remains unknown.

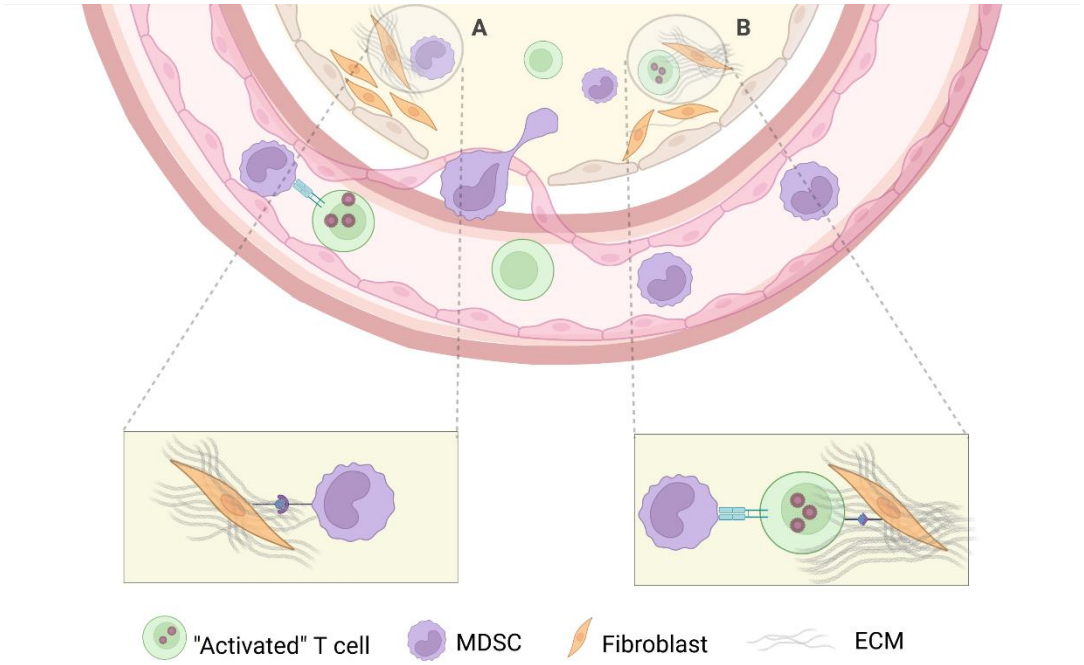

Figure 34. MDSCs Contribution in IPF. A) MDSCs interactions with structural cells (e.g., fibroblasts); **B)** MDSCs interactions with immune cells (e.g. T cells). Graphic created with BioRender.com

Based on preliminary data generated in our laboratory, this work is focused on understanding MDSCs immunomodulatory function (Figure 34B) and their interaction with structural cells in the lung in IPF (Figure 34A)

To facilitate comprehension, the following discussion has been divided into subsections. First, MDSCs abundance in IPF, then their immunoregulatory function in fibrosis, and finally, MDSCs interaction with structural cells.

5.1 MDSCs abundance in IPF

MDSCs have been extensively studied in numerous cancer types because of their association with disease status and progression and have been proposed as a possible biomarker of cancer prognosis[93,115,148]. Some strategies of conventional chemotherapy combined with drugs targeting MDSCs can better control tumor growth[116]. Interestingly, cancer and fibrosis in the lung share pathophysiological phenomena, altered pathways, some risk factors, and even common altered genes. Based on these similarities, our group investigated the presence of circulating MDSCs in IPF patients and demonstrated, for the first time, that there are increased amounts in the circulation and that the increase is associated with worse lung function[1]. In this study, we aimed to validate and quantify the number of circulating MDSCs in a second cohort of patients. In our newly recruited cohort, we also observed that IPF patients have an increase in circulating MDSCs, validating our previous findings (refer to section 4.1.3). Thus, additional validation in independent cohorts, with diverse demographics, are required to determine whether it could serve as a biomarker in IPF.

5.2 MDSCs immunomodulation

MDSCs are well-known for their ability to modulate immunological responses[149–151]. MDSCs can help maintain homeostasis by inhibiting host immune responses in infections, after organ transplantation (preventing organ rejection), and during pregnancy (promoting maternal-fetal tolerance). Yet, their expansion during chronic processes can support, for instance, tumor progression or perpetuate the infection and disease by inhibiting the host immune system. Interestingly, MDSCs are also influenced by tissue niches[85]. They generate a suppressive milieu by interacting with and regulating primarily T cells, but also macrophages, NK cells, TAMs, DCs, and Tregs[152].

In recent years, immune dysregulation has been identified as a driver of IPF[130]. Yet multiple clinical trials with immunosuppressive therapy (e.g., prednisone and azathioprine), demonstrated that blunted immunosuppression can increase mortality[32,153]. T cells are critical for immunity, their role in pulmonary fibrosis is complex, poorly explored, and subtype-dependent [130].

Interestingly, the role of exhausted $CD8^+$ T cells in the fibrotic niche as a result of the suppressive effect of MDSCs during the development of IPF has not yet been investigated. Here, we demonstrate the existence of an exhausted $CD8^+$ T cell phenotype in IPF lung by analyzing the IPF atlas (refer 4.2.1 and 4.2.2), as well as immunohistochemistry, thus we validated the presence of circulating $CD8^+$ T cells, $PD1^+$, $LAG3^+$, and $TIM3^+$ using FACS-based immunophenotyping of IPF blood. We further reveal that T cells expressing PD1 are increased in the lungs of IPF patients and are clustered near $PDL1^+$ M-MDSCs, suggesting the existence of a PD1-PDL1 axis between MDSCs and $CD8^+$ T. Finally, we showed *in vitro*, that IPF M-MDSCs promote exhaustion in autologous $CD8^+$ T cells.

Altogether, we demonstrate that one of the immunostimulatory functions of MDSCs is to promote $CD8^+$ T cell exhaustion, which may be mediated by a PD1-PDL1 axis, the role of which in fibrosis demands further exploration. Yet, we acknowledge that strategies to

target the PD1-PDL1 axis in patients with pre-existing lung disease should be taken with caution due to side effects.

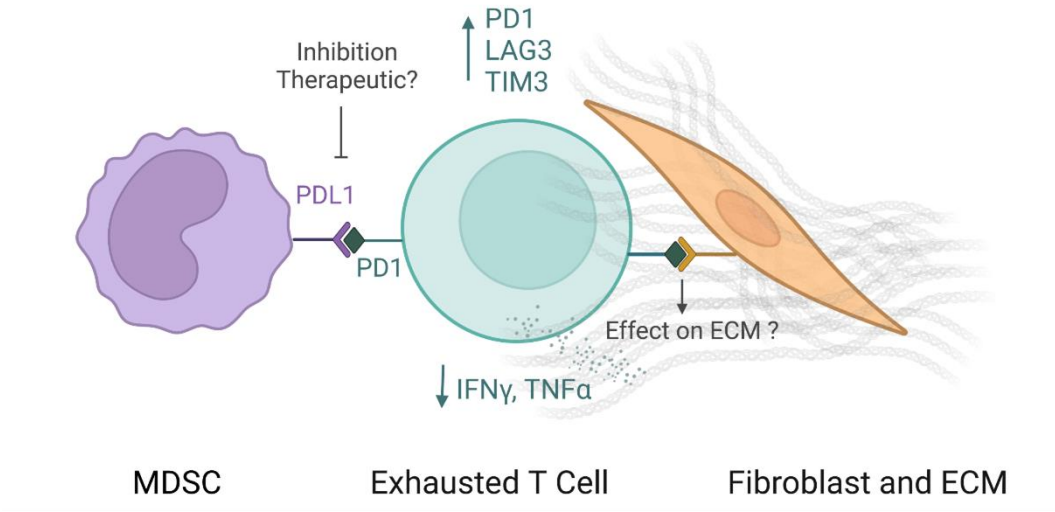

Figure 35. MDSCs immunomodulation theory proposed in IPF development. MDSCs expressing PDL1 ligand bind to the PD1 receptor on $CD8^+$ T cells, resulting in an increase in co-inhibitory receptors (PD1, LAG3, TIM3) and a decrease in cytokine release (IFN-γ, TNF-α), a phenomenon known as *T cell exhaustion*. Consequently, these "exhausted" cells engage with structural cells (such as fibroblasts) via a receptor ligand, modulating ECM deposition. Graphic created with BioRender.com

5.2.1 $CD8^+$ T Exhausted phenotype in IFP

A recent study found that MDSCs metabolically modify $CD8^+$ T cells by transferring cytoplasmic components and reducing $CD8^+$ T effector activity[154], suggesting a complex relationship between these two cell types. MDSCs are well-known for inhibiting T cell proliferation through different mechanisms that have been extensively described[85]. Our group had previously shown MDSCs' ability to suppress $CD8^+$ T cell proliferation in IPF[1]. Interestingly, one of the features of $CD8^+$ T cell exhaustion is the reduction of T lymphocyte proliferative capacity[135]. Here, we sought to investigate the existence of an exhausted $CD8^+$ T cell phenotype in patients with IPF.

Initially, by utilizing web-based data mining, we noted within the IPF cell atlas (ipfcellatlas.com) that IPF lungs displayed characteristics of a $CD8^+$ T cell exhausted phenotype. This was characterized by increased expression of co-inhibitory receptors such as PD1, LAG3, and TIM3. Notably, among all the co-inhibitory receptors examined, PDL1 displayed the highest level of co-expression on $CD8^+$ T cells.

Using immunofluorescence, we confirmed the increase of $CD8^+PD1^+$ T cells in IPF lung tissue compared to controls. Our results are consistent with previous findings that $CD8^+$ T cells co-expressing PD1 are increased in IPF explants[155]. The increased numbers of $CD8^+PD1^+$ T cells in IPF tissue may suggest their involvement in the modulation of the local immune microenvironment, which requires further investigation.

PD1 or programmed cell death protein 1, is an immune checkpoint protein that plays an essential role in regulating the immune system's response, by suppressing T-cell activity and promoting self-tolerance. It is elevated by antigen stimulation and cytokines released by T cells [156]. PD1 modulates diverse aspects of immune activity not just in T cells, but also in B cells, monocytes, and dendritic cells, where it is also present[157,158].

Celada et al. found that elevated levels of $CD4^+PD1^+$ T cells in IPF patients, induced collagen I production in human fibroblast via signal transducer and activator of transcription 3 (STAT3)[139]. This is important since activation of the transcription factor STAT3 occurs not only by $CD4^+$ T cells, yet also in multiple cell types including $CD8^+$ T lymphocytes. In numerous studies STAT3 has been shown to induce ECM production (e.g. via increased TGF-ß and COL1A2), hence contributing to the fibrotic process[159]. It is unknown, however, whether $CD8^+PD^+$ T lymphocytes contribute to fibrosis in a similar mechanism. Indeed, a recent study suggests that $CD8^+PD1^+$ T cells may maintain a balance between immunity and fibrotic sequelae and may play a protective function[155]. The overall evidence suggests that $CD8^+PD1^+$ T cells require deeper investigation in IPF.

After demonstrating the presence of exhausted $CD8^+$ T cells in IPF lung tissue, we aimed to investigate whether this phenotype was already present in the circulation. For that, we used peripheral blood to look for the presence of PD1, LAG3, and TIM3 in circulating $CD8^+$ T cells using FACS analysis. Although these markers were detected in circulation, there were no significant differences in expression between IPF patients and healthy controls. In contrast to our findings, Ni K. et al. found a higher percentage of $PD1^+$ lymphocytes in peripheral blood in pulmonary fibrosis patients compared with healthy control[160]. We hypothesize that divergence is caused by two possible situations First, we demonstrated that these $CD8^+PD1^+$ T cells are detectable in the lungs of IPF patients, suggesting that they might migrate from the circulation to the site of injury or get exhausted in situ. Although in our approach we did not trace circulating exhausted $CD8^+$ T cells, it has been demonstrated that they can migrate to tissues[161] or that they could get exhausted in lung. Second, Ni K. et al. did not identify the type of pulmonary fibrosis that was evaluated, it is likely that non-IPF ILD were included. This is relevant as the pathophysiology of other non-idiopathic forms of fibrosis might be predominantly inflammatory and have a stronger activation at the circulatory level already.

5.2.2 The $CD8^+PD1^+$ - $PDL1^+$ M-MDSCs axis in IPF

Immune checkpoint inhibitors have been used successfully to treat a wide range of cancers. Although drugs that target checkpoint receptors are pharmacologically approved and widely used in patient care, undesirable side effects such as pneumonitis are common[162]. These immune checkpoint pathways regulate immune responses, particularly T lymphocytes through cytokines or receptor-ligand signaling[163]. PD1 and its ligand PDL1 play a crucial role in the regulation of T-cell immunity and have been intensively studied as they are elevated in chronic processes[164]. In IPF they have also been explored in recent years[165]. Tumor cells but also T cells, B cells, DC macrophages, MDSCs, brown adipocytes, epithelial cells, endothelial cells, and mesenchymal cells express PDL1[164,166].

PDL1 has also been linked to IPF, as its inhibition in murine models using neutralizing antibodies reduced collagen deposition and alleviated bleomycin-induced pulmonary fibrosis[139,167]. Moreover, a new study demonstrated that PDL1 mediates the transition of lung fibroblasts to myofibroblasts[18]. Although these IPF studies did not look at PDL1 expression on MDSCs, it has been shown that PDL1 is present and upregulated on the surface of MDSCs in cancer patients and tumor-bearing mice, where it exerts immunosuppressive effects[166]. This immunosuppressive effect of PDL1 in MDSCs can significantly promote tumor growth and influence clinical outcomes[168].

Here, we sought to look into the role of PDL-1 in MDSCs. First, we determined that PDL1 is highly expressed in myeloid cells of ILD patients, based on single-cell RNA data from the IPF atlas (ipfcellatlas.com). This prompted us to check the presence of PDL1 in circulating MDSCs by flow cytometry, which revealed higher PDL1 expression in M-MDSCs, which was later confirmed by cytospins of isolated cells. Our data are supported by results from a recent multicentric study that showed an increase in PDL1 in M-MDSCs[169].

MDSCs exert their suppressive function on T cells through a variety of mechanisms that differ depending on the disease and cell subtype. In the case of M-MDSCs, this function is mostly dependent on nitric oxide (NO), whose immunosuppressive activity on T cells is dependent on cell-to-cell contact[85,93]. Hence, our next approach was to take advantage of multiplexed immunohistochemistry (mIHC) to look for M-MDSCS expressing PDL1 and to determine its distribution and proximity to PD1-expressing lymphocytes ($CD3^+$ $PD1^+$) in lung tissue sections from IPF and non-IPF ILDs. We were unable to differentiate between $CD4^+$ and $CD8^+$ lymphocytes in this experiment due to the limited number of markers that could be employed on the same panel in this technique. First, we observed that in IPF, there was a higher number of MDSCs expressing PDL1 and $PD1^+$ T lymphocytes than in non-IPF ILDs. As previously stated, the presence of increased $PD1^+$ T lymphocytes suggests an exhausted T cell phenotype in IPF lung tissue. New research from Ke Ni et al. supports this finding, by showing increased PD1 expression in lymphocytes and its ligand PDL1 in IPF lung tissue[139,160].

However, Ke Ni et al. did not specify the cell type expressing PDL1, thus we conclude, based on our findings, that a significant fraction of the PDL1 measured was expressed by M-MDSCs. Then, we looked at the proximity between PDL1-expressing MDSCs and $PD1^+$ T lymphocytes. We observed that in IPF, these two cell types were often neighboring each other, suggesting a possible interaction. In our data, we observed that $PD1^+$ T lymphocytes and M-MDSCS expressing PDL1 are less abundant in non-IPF ILDs versus IPF, suggesting that these two cell types expressing these specific markers are less active. We hypothesize that non-IPF ILDs patients were taking immunosuppressive medicine at the time of the tissue collection, which may have influenced their immunological response. Furthermore, as previously stated, these types of fibrosis do not share the same pathophysiology as IPF and thus may have a different immune response, resulting in a slower progression. It is noteworthy to highlight that despite the lack of negative control (healthy donor), we demonstrated a higher expression of $CD8^+$ $PD1^+$ cells in IPF lung tissue compared to healthy donors utilizing the IPF atlas data and the previous experiment using single stains (mentioned above). Yet, this staining is planned to be performed in control tissue. Thus, we believe that our findings show for the first time the existence of the exhausted lymphocyte phenotype $CD8^+$ $PD1^+$ alongside PDL1-expressing M-MDSCs in the lung tissue of IPF patients, hinting towards a local interaction.

T cell exhaustion is characterized by decreased expression of effector cytokines (e.g INF-γ, TNF-α), and increased expression of co-inhibitory immune checkpoint receptors (e.g PD-1, TIM-3, LAG-3), which mediate inhibitory signaling and diminish T cell cytotoxicity[3,124,134,135]. MDSCs have been shown to induce T cell exhaustion[169]. Activated MDSCs express immunological checkpoint proteins, including PD-L1, which may bind to the PD-1 receptor on T cells and suppress T cells[94,95]. Depleting MDSCs, on the other hand, improves T cell response, facilitating tumor eradication and preventing tumor recurrence in mice[170]. We thought this axis/pathway was worth investigating further because we found an exhausted $CD8^+PD1^+$ T cell phenotype in IPF lung tissue in close proximity to PD1-expressing M-MDSCs.

T lymphocytes employ different mechanisms to regulate tissue remodeling in fibrosis, which vary based on their specific subtype[171]. T lymphocytes can influence the development of fibrosis via multiple pathways, including the modulation of chloride channels regulated by cyclic adenosine monophosphate (cAMP) regulated chloride channels[171,172], interactions between Fas and Fas ligands[171,173], as well as T cell exhaustion [171,174]. T cell Exhaustion is characterized by decreased expression of effector cytokines (e.g INF-γ, TNF-α), and increased expression of co-inhibitory immune checkpoint receptors (e.g PD-1, TIM-3, LAG-3), which mediate inhibitory signaling and diminish T cell cytotoxicity[3,131,134,135]. In this study, we initially demonstrated the overexpression of co-inhibitory $CD8^+$ T cell receptors PD1, LAG3, and TIM3 in circulating IPF after 6 days of stimulation with IL-2 and CD3 every 48 hours. Then as a proof of concept, we also demonstrated the reduction in cytokine production on day 6. These findings demonstrated that circulating IPF $CD8^+$ T cells are susceptible to exhaustion.

Then, we determined whether IPF MDSCs can induce $CD8^+$ T cell exhaustion *in vitro*. We were aware that MDSCs have previously been linked to T-cell exhaustion[3,175]. In this approach, we co-cultured $CD8^+$ T cells with autologous MDSCs and stimulated them with IL-2 and CD3 every 48 hours for 6 days. We observed an increase in the expression of the co-inhibitory receptors PD1 and LAG3. Nevertheless, the expected drop in cytokine secretion was not observed. Moreover, no differences were found between healthy controls and IPF patients. We then sought to examine if re-stimulating with CD3 and IL-2 could impact the cytokine secretion response of $CD8^+$ T cells. In the same experimental setting, but without re-stimulation with CD3 and IL-2 every 48 hours, we found an increase in PD1 and LAG3 and a decrease in TNF-α, demonstrating that IPF MDSCs induce $CD8^+$ T cell exhaustion. Notably, we were unable to collect enough similar controls for this condition. Here we consider necessary to discuss the effect of IL-2 on MDSCs in order to understand the disparity between these two conditions. Fas ligand is expressed on $CD8^+$ T cells and is required for suppressor cell apoptosis[176]. MDSCs express Fas receptors in vivo and have been shown to undergo

apoptosis in response to T cell Fas ligand expression[177]. This apoptotic vulnerability may be attributed to factors such as endogenous cytokine overexpression and cytokine nature. Th1 cytokines (e.g., IL2, IFN-γ, IL-12) may promote cell death[176]. Hence, we reasoned that adding "exogenous IL-2" to our experiment made MDSCs more susceptible to apoptosis, resulting in a lack of cells to exert their suppressive function, and therefore the $CD8^+$ T cells were not sufficiently exhausted to diminish their capacity to release cytokines.

These novel findings provide a new perspective on the role of MDSCs in IPF immune dysregulation and enhance our knowledge of the complex immunomodulatory mechanisms underlying fibrotic diseases. However, to fully understand the extent of MDSC-induced $CD8^+$ T cell exhaustion in the context of IPF pathogenesis and its potential therapeutic applications, additional research is required.

5.3 MDSCs and structural cells interactions

Myeloid cells' role in fibrosis and their interaction with structural cells are unclear. Our team was the first to show an increase in MDSCs in IPF, but the lack of MDSCs-specific markers makes them hard to spot from other myeloid cells. By identifying markers expressed by MDSCs that infiltrate lung tissue, we will be able to modulate their communication with structural cells, improving our understanding of their migration to the lung and their influence during the fibrotic process.

Here, we looked into the unique proteins expressed by MDSCs in peripheral blood and lung tissue, their cell subtype invasion patterns, and their influence on the formation of myofibroblasts.

5.3.1 Improving MDSCs phenotyping and detecting their presence in fibrotic lungs

As a first approach, we endeavored to improve MDSCs profiling in order to detect them more precisely in lung tissue. Using mass spectrometry, our laboratory has previously found MDSC-specific markers that distinguish them from monocytes. Based on these findings, we selected the most highly expressed MDSC-specific markers CD263, Neuropilin, and L1CAM, validated their expression by flow cytometry in IPF patients' circulating MDSCs, and compared them to controls. Our results not only validated the presence of these markers in circulating MDSCs in IPF and control but also showed that IPF patients have elevated levels of CD263 and Neuropilin. Other studies have also demonstrated the presence of these markers in MDSCs, supporting our findings[178–180].

MDSCs in the lung have been described and studied in a range of diseases and conditions, including cancer, TB, pulmonary infection, COVID, COPD, cystic fibrosis, pulmonary hypertension, and transplantation, among others[120,152,181,182], and, most recently in IPF[1]. In our study, flow cytometry of lung homogenates and immunostaining revealed that MDSCs expressing CD263 and L1CAM are present in lung tissue, from both ILDs and control. Interestingly, we discovered that CD263 and L1CAM were more abundant in ILD M-MDSCs compared with healthy donors. These findings are significant because, in the context of IPF, better profiling will allow for the identification of potential ligands/receptors on MDSCs, leading to a more accurate characterization of their interactions with surrounding structural and immune cells and, as a result, a better understanding of the role of these cells in the fibrotic process, which is essential for therapeutic purposes.

5.3.2 MDSCs invasiveness profile in IPF

MDSCs are known to increase in cancer by different mechanisms[151] and invade tissues and the tumor microenvironment. There they stimulate angiogenesis, tumor cell invasion, and

metastasis via a variety of soluble factors[183]. MDSCs migration and invasion to the tumor site, as well as their contribution to pre-metastatic niches, have been widely studied, and it appears dependent on MDSCs subsets[184]. M-MDSCs have been linked to early tumor infiltration, whereas G-MDSCs appear to be more active in the metastatic phase[184]. Intercellular communication, chemokine-mediated migration (CXCL1, CXCL2, and CXCL5), interstitial fluid flow, and "spontaneous" migration are all factors that drive MDSC migration to tissue[185,186], however, these data are only known for cancer, and to our knowledge, there are no studies on IPF or any other form of pulmonary fibrosis. Because the presence of MDSCs in fibrotic lung tissue (as previously proven in this study) indicates their ability to migrate and invade, we decided to characterize the invading capability of MDSCs subsets from controls and IPF *in vitro* without the use of any chemoattractant. For this, we developed a 3D collagen-based collagen assay to attempt to reproduce the collagen buildup during fibrosis in vitro. Our data shows that IPF M-MDSCs are more invasive than control M-MDSCs, suggesting that these cells have a greater spontaneous capacity to migrate/invade the lung during IPF development. This tendency, we believe, is the result of metabolic reprogramming of M-MDSCS in IPF, similar to that identified in cancer mouse models[186]. Nevertheless, their pathological and clinical implications require further investigation, and more studies incorporating chemoattractants should be conducted to better understand MDSCs migration/invasion capacity.

In the same experiment, our data suggested that M-MDSCs are more capable than G-MDSCs to invade. However, we believe that the assessment of the invading potential of G-MDSCs in the setting of our experiment is prone to bias. In this assay, we employed cryopreserved cells, and we assume that the cells might die shortly after being seeded, which could explain why there were so few cells in the gel. G-MDSCs are closely related to granulocytes which have a lifespan of 22-26 hours after blood collection[187] and are intolerant to freezing[188]. Previous research has shown that following freezing, G-MDSCs are reduced by more than 50%, while M-MDSCs appear to be more resistant[188]. Contradictorily, other studies found no

difference between the number of frozen and fresh MDSCs[188]. However, we believe our findings may have been influenced by the short lifespan of G-MDSCs after blood sampling and their fragility when cryopreserved.

5.3.3 M-MDSCs and fibroblast interaction

Knowing that M-MDSCs can invade/migrate into lung tissue in IPF, our next step was to study their effect *in situ*. Although MDSCs have been shown to influence fibrosis in numerous tissues (including lungs), little is known about their interaction with fibroblasts. Based on the limited number of tumor-related research, MDSCs are believed to promote fibrosis indirectly rather than directly[189,190]. However, Lebrun and colleagues demonstrated in a murine model of particle-induced lung fibrosis that a specific subgroup of M-MDSCs expressing CCR2 secretes TGF-ß and enhances TIMP-1 secretion, which inhibits the collagenolytic activity of metalloproteinases, leading to increased collagen deposition and fibrosis[121], suggesting a direct fibrogenic effect of MDSCs on fibroblasts.

TGF-ß plays a key role in the differentiation of fibroblasts into myofibroblasts during fibrosis. Increasing evidence shows that myofibroblasts are predominantly engaged in extracellular matrix synthesis[191]. α-SMA is a hallmark of mature myofibroblasts, and its expression may aid in identifying fibroblasts with high ECM remodeling capacity[192]. Here, we examined the expression of α-SMA by immunofluorescence in phFbs co-cultured with M-MDSCs for 48 hours. Our data reveal that when phFbs cultured with TGF-ß in the presence of IPF M-MDSCs, α-SMA expression is lowered when comparing the same condition but without the presence of IPF M-MDSCs (positive control), suggesting that IPF M-MDSCs hinder myofibroblast formation. Furthermore, TGF-ß concentrations were also lower in the supernatants of phFbs co-cultures with IPF M-MDSCs than in cultures containing only phFbs (No TGF-ß added). Our findings suggest that MDSCs have an anti-fibrotic effect, contrary to the pro-fibrotic effect described by Lebrun. Remarkably, a recent murine study found that

M-MDSCs supernatants can decrease α-SMA expression in mesenchymal stem cells (MSC) inhibiting TGF-ß-induced myofibroblast differentiation through IL-5 secretion[193]. Although this study was conducted on MSC, we believe that these data support our findings, because there is evidence that these cells are phenotypically identical to fibroblasts, sharing surface markers, immunomodulatory capabilities, differentiation potential, and morphology[193–196]. Altogether, these results are contradictory. We believe that these differences may be a result of Lebron's use of a model of particle-induced pulmonary fibrosis, which may have resulted in a different inflammatory response that caused M-MDSCs to transform into macrophages[197], which tend to produce large quantities of growth factors that contribute to ECM production during fibrosis[198]. Furthermore, because the study's authors describe a specific subtype of M-MDSCs that express CCR2, we cannot exclude the possibility that the profibrotic effect is subtype-dependent. However, further research is required to determine whether IPF M-MDSCs share the same inhibitory mechanism via IL-5 release, as well as to identify other cytokines that may be involved and therefore, understand the clinical implications.

6 Conclusions and further directions

IPF is a severe and life-threatening lung condition. Despite recent breakthroughs, there are only two antifibrotic medications approved for its therapy (pirfenidone and nintedanib) that slow down disease progression but do not cure disease. Hence, it is essential to deepen the understanding of the molecular and cellular phenomena involved in its development and progression, to enable a prompt diagnosis, preserve organ function, and prevent mortality.

Circulating MDSCs are elevated in IPF patients. Previous work from our group has shown that they are associated with lung function loss and progression. Our *in vitro* experiments reveal that circulating MDSCs express exclusive markers, are capable of invasion/migration, and are detectable in IPF lungs, where they appear to exert an anti-fibrotic effect in situ. Furthermore, exhausted $PD1^{+}$ T cells were detected in close proximity to PDL1-expressing M-MDSCs in IPF lungs, suggesting an interaction that could result in an immunosuppressive milieu.

Although our findings add to the body of knowledge in this field, additional research is needed to determine the role of specific MDSCs subsets and their immune and structural cellular networks in IPF. Here, it is critical to determine how these cells promote or hinder fibrosis progression, if they influence disease outcome, or even whether they represent a possible therapeutic target.

Our recent data has left us with two big questions to address. First, does the increased presence of MDSCs in IPF play a protective (anti-fibrotic) role by reducing CD8+ T-induced damage and limiting ECM deposition in lung tissue? or does it play a deleterious (pro-fibrotic) role by inhibiting the immune response and perpetuating the disease? To address these questions, experiments targeting MDSCs or targeting particular MDSC-expressed proteins are required for interactions with other cell types, which were not performed in this study. These studies could be performed through several approaches, including primary cell co-

culture (in vitro), mouse models (in vivo), and precision cut lung slice PCLS (ex vivo), among others. Furthermore, we can now use cutting-edge technologies like scRNA-seq to help us address this question. This approach will help us not only improve the identification of MDSCs but also better understand their activity by analyzing the expression profiles of specific pathways (e.g. profibrotic or antifibrotic) and detecting possible interactions with other cell types (e.g. T cells).

Second, are MDSCs potential cellular biomarkers predictive of IPF progression? Despite our findings, an independent validation cohort would be required.

7. References

1. Fernandez IE, Greiffo FR, Frankenberger M, et al. Peripheral blood myeloid-derived suppressor cells reflect disease status in idiopathic pulmonary fibrosis. *Eur Respir J*. 2016;48:1171-1183. doi:10.1183/13993003.01826-2015

2. Scott MKD, Quinn K, Li Q, et al. Increased monocyte count as a cellular biomarker for poor outcomes in fibrotic diseases: a retrospective, multicentre cohort study. *Lancet Respir Med*. 2019;7(6):497-508. doi:10.1016/S2213-2600(18)30508-3

3. Wherry EJ, Kurachi M. Molecular and cellular insights into T cell exhaustion. *Nat Rev Immunol*. 2015;15(8):486-499. doi:10.1038/nri3862

4. Eickelberg O, Selman M. Update in Diffuse Parenchymal Lung Disease 2009. *https://doi.org/101164/rccm201001-0124UP*. 2012;181(9):883-888. doi:10.1164/RCCM.201001-0124UP

5. Lederer DJ, Martinez FJ. Idiopathic Pulmonary Fibrosis. Longo DL, ed. *New England Journal of Medicine*. 2018;378(19):1811-1823. doi:10.1056/NEJMra1705751

6. Mura M, Porretta MA, Bargagli E, et al. Predicting survival in newly diagnosed idiopathic pulmonary fibrosis: A 3-year prospective study. *European Respiratory Journal*. 2012;40(1):101-109. doi:10.1183/09031936.00106011

7. Raghu G, Remy-Jardin M, Myers JL, et al. Diagnosis of idiopathic pulmonary fibrosis An Official ATS/ERS/JRS/ALAT Clinical practice guideline. *Am J Respir Crit Care Med*. 2018;198(5):e44-e68. doi:10.1164/rccm.201807-1255ST

8. Travis WD, Costabel U, Hansell DM, et al. An official American Thoracic Society/European Respiratory Society statement: Update of the international multidisciplinary classification of the idiopathic interstitial pneumonias. *Am J Respir Crit Care Med*. 2013;188(6):733-748. doi:10.1164/RCCM.201308-1483ST

9. Hutchinson J, Fogarty A, Hubbard R, Mckeever T. Global incidence and mortality of idiopathic pulmonary fibrosis: a systematic review. *Eur Respir J*. 2015;46:795-806. doi:10.1183/13993003.00958-2015

10. Glassberg MK. THE AMERICAN JOURNAL OF MANAGED CARE ® Supplement S195 Overview of Idiopathic Pulmonary Fibrosis and Evidence-Based Guidelines. *Am J Manag Care*. 2019;25(Suppl 1:S195-S203. Accessed April 17, 2022. www.ajmc.com

11. Selman M, Pardo A. The leading role of epithelial cells in the pathogenesis of idiopathic pulmonary fibrosis. *Cell Signal*. 2020;66. doi:10.1016/j.cellsig.2019.109482

12. King TE, Pardo A, Selman M. Idiopathic pulmonary fibrosis. *The Lancet*. 2011;378(9807):1949-1961. doi:10.1016/S0140-6736(11)60052-4

13. Martinez FJ, Collard HR, Pardo A, et al. Idiopathic pulmonary fibrosis. *Nat Rev Dis Primers*. 2017;3. doi:10.1038/nrdp.2017.74

14. Hocevar BA. TGF-beta induces fibronectin synthesis through a c-Jun N-terminal kinase-dependent, Smad4-independent pathway. *EMBO J*. 1999;18(5):1345-1356. doi:10.1093/emboj/18.5.1345

15. Xu F, Liu C, Zhou D, Zhang L. TGF-β/SMAD Pathway and Its Regulation in Hepatic Fibrosis. *Journal of Histochemistry and Cytochemistry*. 2016;64(3):157-167. doi:10.1369/0022155415627681

16. Gu L, Zhu YJ, Yang X, Guo ZJ, Xu WB, Tian XL. Effect of TGF-β/Smad signaling pathway on lung myofibroblast differentiation. *Acta Pharmacol Sin*. 2007;28(3):382-391. doi:10.1111/j.1745-7254.2007.00468.x

17. Pechkovsky D V., Prêle CM, Wong J, et al. STAT3-mediated signaling dysregulates lung fibroblast-myofibroblast activation and differentiation in UIP/IPF. *American Journal of Pathology*. 2012;180(4):1398-1412. doi:10.1016/j.ajpath.2011.12.022

18. Verrecchia F, Chu ML, Mauviel A. Identification of Novel TGF-β/Smad Gene Targets in Dermal Fibroblasts using a Combined cDNA Microarray/Promoter Transactivation Approach. *Journal of Biological Chemistry*. 2001;276(20):17058-17062. doi:10.1074/jbc.M100754200

19. Kim BN, Ahn DH, Kang N, et al. TGF-β induced EMT and stemness characteristics are associated with epigenetic regulation in lung cancer. *Sci Rep*. 2020;10(1). doi:10.1038/s41598-020-67325-7

20. Königshoff M, Kramer M, Balsara N, et al. WNT1-inducible signaling protein-1 mediates pulmonary fibrosis in mice and is upregulated in humans with idiopathic pulmonary fibrosis. *J Clin Invest*. 2009;119. doi:10.1172/JCI33950

21. Lozano Bolaños A, Mendoza Milla C, Cisneros Lira J, et al. Sonic Hedgehog in idiopathic pulmonary fibrosis. *Am J Physiol Lung Cell Mol Physiol*. 2012;303:978-990. doi:10.1152/ajplung.00184.2012

22. Effendi WI, Nagano T. The hedgehog signaling pathway in idiopathic pulmonary fibrosis: Resurrection time. *Int J Mol Sci*. 2022;23(1). doi:10.3390/ijms23010171

23. Hu B, Phan SH. Notch in fibrosis and as a target of anti-fibrotic therapy Graphical abstract HHS Public Access. *Pharmacol Res*. 2016;108:57-64. doi:10.1016/j.phrs.2016.04.010

24. Katzen J, Beers MF. Contributions of alveolar epithelial cell quality control to pulmonary fibrosis. *Journal of Clinical Investigation*. 2020;130(10):5088-5099. doi:10.1172/JCI139519

25. Lamas DJ, Kawut SM, Bagiella E, Philip N, Arcasoy SM, Lederer DJ. Delayed access and survival in idiopathic pulmonary fibrosis: A cohort study. *Am J Respir Crit Care Med*. 2011;184(7):842-847. doi:10.1164/rccm.201104-0668OC

26. Buendía-Roldán I, Mejía M, Navarro C, Selman M. Idiopathic pulmonary fibrosis: Clinical behavior and aging associated comorbidities. *Respir Med*. 2017;129:46-52. doi:10.1016/j.rmed.2017.06.001

27. King TE, Pardo A, Selman M. Idiopathic pulmonary fibrosis. In: *The Lancet*. Vol 378. Elsevier; 2011:1949-1961. doi:10.1016/S0140-6736(11)60052-4

28. Collard HR, Ryerson CJ, Corte TJ, et al. Acute exacerbation of idiopathic pulmonary fibrosis an international working group report. *Am J Respir Crit Care Med*. 2016;194(3):265-275. doi:10.1164/rccm.201604-0801CI

29. Chahal A, Sharif R, Watts J, et al. Predicting Outcome in Idiopathic Pulmonary Fibrosis: Addition of Fibrotic Score at Thin-Section CT of the Chest to Gender, Age, and Physiology Score Improves the Prediction Model. *Radiol Cardiothorac Imaging*. 2019;1(2):e180029. doi:10.1148/ryct.2019180029

30. Ley B, Brown KK, Collard HR. Biomarkers in Lung Diseases: from Pathogenesis to Prediction to New Therapies: Molecular biomarkers in idiopathic pulmonary fibrosis. *Am J Physiol Lung Cell Mol Physiol*. 2014;307(9):L681. doi:10.1152/AJPLUNG.00014.2014

31. Bowman WS, Echt GA, Oldham JM. Biomarkers in Progressive Fibrosing Interstitial Lung Disease: Optimizing Diagnosis, Prognosis, and Treatment Response. *Front Med (Lausanne)*. 2021;8:574. doi:10.3389/fmed.2021.680997

32. Raghu G, Rochwerg B, Zhang Y, et al. An official ATS/ERS/JRS/ALAT clinical practice guideline: Treatment of idiopathic pulmonary fibrosis: An update of the 2011 clinical practice guideline. *Am J Respir Crit Care Med*. 2015;192(2):e3-e19. doi:10.1164/rccm.201506-1063ST

33. Crestani B, Huggins JT, Kaye M, et al. Long-term safety and tolerability of nintedanib in patients with idiopathic pulmonary fibrosis: results from the open-

label extension study, INPULSIS-ON. *Lancet Respir Med*. 2019;7(1):60-68. doi:10.1016/S2213-2600(18)30339-4

34. Richeldi L, du Bois RM, Raghu G, et al. Efficacy and Safety of Nintedanib in Idiopathic Pulmonary Fibrosis. *New England Journal of Medicine*. 2014;370(22):2071-2082. doi:10.1056/nejmoa1402584

35. Noble PW, Albera C, Bradford WZ, et al. Pirfenidone in patients with idiopathic pulmonary fibrosis (CAPACITY): Two randomised trials. *The Lancet*. 2011;377(9779):1760-1769. doi:10.1016/S0140-6736(11)60405-4

36. Lancaster L, Albera C, Bradford WZ, et al. Safety of pirfenidone in patients with idiopathic pulmonary fibrosis: Integrated analysis of cumulative data from 5 clinical trials. *BMJ Open Respir Res*. 2016;3(1):e000105. doi:10.1136/bmjresp-2015-000105

37. Ley B, Swigris J, Day B mo, et al. Pirfenidone Reduces Respiratory-related Hospitalizations in Idiopathic Pulmonary Fibrosis. *Am J Respir Crit Care Med*. 2017;196(6):756-761. doi:10.1164/RCCM.201701-0091OC

38. Nathan SD, Costabel U, Glaspole I, et al. Efficacy of Pirfenidone in the Context of Multiple Disease Progression Events in Patients With Idiopathic Pulmonary Fibrosis. *Chest*. 2019;155(4):712-719. doi:10.1016/J.CHEST.2018.11.008

39. Jouneau S, Gamez AS, Traclet J, et al. A 2-Year Observational Study in Patients Suffering from Idiopathic Pulmonary Fibrosis and Treated with Pirfenidone: A French Ancillary Study of PASSPORT. *Respiration*. 2019;98(1):19-28. doi:10.1159/000496735

40. Zurkova M, Kriegova E, Kolek V, et al. Effect of pirfenidone on lung function decline and survival: 5-yr experience from a real-life IPF cohort from the Czech EMPIRE registry. *Respir Res*. 2019;20(1). doi:10.1186/s12931-019-0977-2

41. Margaritopoulos GA, Trachalaki A, Wells AU, et al. Pirfenidone improves survival in IPF: Results from a real-life study. *BMC Pulm Med*. 2018;18(1). doi:10.1186/s12890-018-0736-z

42. Hanta I, Cilli A, Sevinc C. The Effectiveness, Safety, and Tolerability of Pirfenidone in Idiopathic Pulmonary Fibrosis: A Retrospective Study. *Adv Ther*. Published online 2019. doi:10.1007/s12325-019-00928-3

43. Vancheri C, Kreuter M, Richeldi L, et al. Nintedanib with add-on pirfenidone in idiopathic pulmonary fibrosis: Results of the INJOURNEY trial. *Am J Respir Crit Care Med*. 2018;197(3):356-363. doi:10.1164/rccm.201706-1301OC

44. Dowman LM, McDonald CF, Bozinovski S, et al. Greater endurance capacity and improved dyspnoea with acute oxygen supplementation in idiopathic pulmonary fibrosis patients without resting hypoxaemia. *Respirology*. 2017;22(5):957-964. doi:10.1111/resp.13002

45. Hoffman M, Mellerick C, Symons K, Glaspole I, Holland AE. Pulmonary rehabilitation for interstitial lung disease: Referral and patient experiences. *Chron Respir Dis*. 2021;18. doi:10.1177/14799731211046022

46. Laporta Hernandez R, Aguilar Perez M, Lázaro Carrasco M, Ussetti Gil P. Lung Transplantation in Idiopathic Pulmonary Fibrosis. *Medical Sciences*. 2018;6(3):68. doi:10.3390/medsci6030068

47. Heukels P, Moor CC, von der Thüsen JH, Wijsenbeek MS, Kool M. Inflammation and immunity in IPF pathogenesis and treatment. *Respir Med*. 2019;147:79-91. doi:10.1016/J.RMED.2018.12.015

48. Takemasa A, Ishii Y, Fukuda T. A neutrophil elastase inhibitor prevents bleomycin-induced pulmonary fibrosis in mice. *European Respiratory Journal*. 2012;40(6):1475-1482. doi:10.1183/09031936.00127011

49. Gregory AD, Kliment CR, Metz HE, et al. Neutrophil elastase promotes myofibroblast differentiation in lung fibrosis. *J Leukoc Biol*. 2015;98(2):143-152. doi:10.1189/jlb.3hi1014-493r

50. Ashitani J ichi, Mukae H, Taniguchi H, et al. Granulocyte-colony stimulating factor levels in bronchoalveolar lavage fluid from patients with idiopathic pulmonary fibrosis. *Thorax*. 1999;54(11):1015-1020. doi:10.1136/thx.54.11.1015

51. Calvente CJ, Tameda M, Johnson CD, et al. Neutrophils contribute to spontaneous resolution of liver inflammation and fibrosis via microRNA-223. *Journal of Clinical Investigation*. 2019;129(10):4091-4109. doi:10.1172/JCI122258

52. Manoury B, Nénan S, Guénon I, Lagente V, Boichot E. Influence of early neutrophil depletion on MMPs/TIMP-1 balance in bleomycin-induced lung fibrosis. *Int Immunopharmacol*. 2007;7(7):900-911. doi:10.1016/j.intimp.2007.02.009

53. Prasse A, Pechkovsky D V., Toews GB, et al. A vicious circle of alveolar macrophages and fibroblasts perpetuates pulmonary fibrosis via CCL18. *Am J Respir Crit Care Med*. 2006;173(7):781-792. doi:10.1164/rccm.200509-1518OC

54. Duru N, Wolfson B, Zhou Q. Mechanisms of the alternative activation of macrophages and non-coding RNAs in the development of radiation-induced lung fibrosis. *World J Biol Chem*. 2016;7(4):231. doi:10.4331/wjbc.v7.i4.231

55. Wynn TA, Chawla A, Pollard JW. Macrophage biology in development, homeostasis and disease. *Nature*. 2013;496(7446):445-455. doi:10.1038/nature12034

56. Wynn TA, Vannella KM. Macrophages in Tissue Repair, Regeneration, and Fibrosis. *Immunity*. 2016;44(3):450-462. doi:10.1016/j.immuni.2016.02.015

57. Shenderov K, Collins SL, Powell JD, Horton MR. Immune dysregulation as a driver of idiopathic pulmonary fibrosis. *J Clin Invest*. 2021;131(2). doi:10.1172/JCI143226

58. Strieter RM, Keeley EC, Burdick MD, Mehrad B. The role of circulating mesenchymal progenitor cells, fibrocytes, in promoting pulmonary fibrosis. *Trans Am Clin Climatol Assoc*. 2009;120:49-59.

59. Deng L, Huang T, Zhang L. T cells in idiopathic pulmonary fibrosis: crucial but controversial. *Cell Death Discov*. 2023;9(1). doi:10.1038/s41420-023-01344-x

60. Kolahian S, Fernandez IE, Eickelberg O, Hartl D. Immune mechanisms in pulmonary fibrosis. *Am J Respir Cell Mol Biol*. 2016;55(3):309-322. doi:10.1165/rcmb.2016-0121TR

61. Engblom C, Pfirschke C, Pittet MJ. The role of myeloid cells in cancer therapies. *Nat Rev Cancer*. 2016;16(7):447-462. doi:10.1038/nrc.2016.54

62. Florez-Sampedro L, Song S, Melgert BN. The diversity of myeloid immune cells shaping wound repair and fibrosis in the lung. *Regeneration*. 2018;5(1):3-25. doi:10.1002/reg2.97

63. Ellson CD, Dunmore R, Hogaboam CM, Sleeman MA, Murray LA. Danger-associated molecular patterns and danger signals in idiopathic pulmonary fibrosis. *Am J Respir Cell Mol Biol*. 2014;51(2):163-168. doi:10.1165/rcmb.2013-0366TR

64. Julier Z, Park AJ, Briquez PS, Martino MM. Promoting tissue regeneration by modulating the immune system. *Acta Biomater*. 2017;53:13-28. doi:10.1016/j.actbio.2017.01.056

65. Boorsma CE, Draijer C, Melgert BN. Macrophage heterogeneity in respiratory diseases. *Mediators Inflamm*. 2013;2013. doi:10.1155/2013/769214

66. Adhyatmika A, Putri KSS, Beljaars L, Melgert BN. The elusive antifibrotic macrophage. *Front Med (Lausanne)*. 2015;2(NOV):81. doi:10.3389/fmed.2015.00081

67. Minutti CM, Knipper JA, Allen JE, Zaiss DMW. Tissue-specific contribution of macrophages to wound healing. *Semin Cell Dev Biol*. 2017;61:3-11. doi:10.1016/j.semcdb.2016.08.006

68. Wynn TA. Integrating mechanisms of pulmonary fibrosis. *Journal of Experimental Medicine*. 2011;208(7):1339-1350. doi:10.1084/jem.20110551

69. Dale DC, Boxer L, Conrad Liles W. The phagocytes: Neutrophils and monocytes. *Blood*. 2008;112(4):935-945. doi:10.1182/blood-2007-12-077917

70. Fernandez IE, Eickelberg O. New cellular and molecular mechanisms of lung injury and fi brosis in idiopathic pulmonary fi brosis. *The Lancet*. 2012;380(9842):680-688. doi:10.1016/S0140-6736(12)61144-1

71. Conte E. Targeting monocytes/macrophages in fibrosis and cancer diseases: Therapeutic approaches. *Pharmacol Ther*. 2022;234. doi:10.1016/j.pharmthera.2021.108031

72. Dal-Secco D, Wang J, Zeng Z, et al. A dynamic spectrum of monocytes arising from the in situ reprogramming of CCR2+ monocytes at a site of sterile injury. *Journal of Experimental Medicine*. 2015;212(4):447-456. doi:10.1084/jem.20141539

73. Suga M, Iyonaga K, Ichiyasu H, Saita N, Yamasaki H, Ando M. *Clinical Significance of MCP-1 Levels in BALF and Serum in Patients with Interstitial Lung Diseases*.

74. Iyonaga K, Takeya M, Saita N, et al. Monocyte chemoattractant protein-1 in idiopathic pulmonary fibrosis and other interstitial lung diseases. *Hum Pathol*. 1994;25(5):455-463. doi:10.1016/0046-8177(94)90117-1

75. Greiffo FR, Viteri-Alvarez V, Frankenberger M, et al. CX3CR1–fractalkine axis drives kinetic changes of monocytes in fibrotic interstitial lung diseases. *European Respiratory Journal*. 2020;55(2). doi:10.1183/13993003.00460-2019

76. Gordon S, Taylor PR. Monocyte and macrophage heterogeneity. *Nat Rev Immunol*. 2005;5(12):953-964. doi:10.1038/nri1733

77. Gibbons MA, MacKinnon AC, Ramachandran P, et al. Ly6Chi monocytes direct alternatively activated profibrotic macrophage regulation of lung fibrosis. *Am J Respir Crit Care Med*. 2011;184(5):569-581. doi:10.1164/rccm.201010-1719OC

78. Moore BB, Fry C, Zhou Y, et al. Inflammatory Leukocyte Phenotypes Correlate with Disease Progression in Idiopathic Pulmonary Fibrosis. *Front Med (Lausanne)*. 2014;1(DEC):56. doi:10.3389/fmed.2014.00056

79. Kreuter M, Lee JS, Tzouvelekis A, et al. Monocyte count as a prognostic biomarker in patients with idiopathic pulmonary fibrosis. *Am J Respir Crit Care Med*. 2021;204(1):74-81. doi:10.1164/rccm.202003-0669OC

80. Fernandez IE, Kass DJ. Do Circulating Monocytes Promote and Predict Idiopathic Pulmonary Fibrosis Progression? *Am J Respir Crit Care Med*. 2021;204(1):9-11. doi:10.1164/rccm.202101-0207ED

81. Ma T, Renz BW, Ilmer M, et al. Myeloid-Derived Suppressor Cells in Solid Tumors. *Cells*. 2022;11(2). doi:10.3390/cells11020310

82. Veglia F, Perego M, Gabrilovich D. Myeloid-derived suppressor cells coming of age review-article. *Nat Immunol*. 2018;19(2):108-119. doi:10.1038/s41590-017-0022-x

83. Hegde S, Leader AM, Merad M. MDSC: Markers, development, states, and unaddressed complexity. doi:10.1016/j.immuni.2021.04.004

84. Ostrand-Rosenberg S. Myeloid-Derived Suppressor Cells: Facilitators of Cancer and Obesity-Induced Cancer. *Annu Rev Cancer Biol 2021*. 2020;5:17-38. doi:10.1146/annurev-cancerbio-042120

85. Li K, Shi H, Zhang B, et al. Myeloid-derived suppressor cells as immunosuppressive regulators and therapeutic targets in cancer. *Signal Transduct Target Ther*. 2021;6(1):1-25. doi:10.1038/s41392-021-00670-9

86. Kumar V, Patel S, Tcyganov E, Gabrilovich DI. The Nature of Myeloid-Derived Suppressor Cells in the Tumor Microenvironment. *Trends Immunol*. 2016;37(3):208-220. doi:10.1016/j.it.2016.01.004

87. Bronte V, Brandau S, Chen SH, et al. Recommendations for myeloid-derived suppressor cell nomenclature and characterization standards. *Nat Commun*. 2016;7(1):1-10. doi:10.1038/ncomms12150

88. Lang S, Bruderek K, Kaspar C, et al. Clinical relevance and suppressive capacity of human myeloid-derived suppressor cell subsets. *Clinical Cancer Research*. 2018;24(19):4834-4844. doi:10.1158/1078-0432.CCR-17-3726

89. Cassetta L, Baekkevold ES, Brandau S, et al. Deciphering myeloid-derived suppressor cells: isolation and markers in humans, mice and non-human primates. *Cancer Immunology, Immunotherapy*. 2019;68(4):687-697. doi:10.1007/s00262-019-02302-2

90. Veglia F, Sanseviero E, Gabrilovich DI. Myeloid-derived suppressor cells in the era of increasing myeloid cell diversity. *Nat Rev Immunol*. 2021;21(8):485-498. doi:10.1038/s41577-020-00490-y

91. Veglia F, Sanseviero E, Gabrilovich DI. Myeloid-derived suppressor cells in the era of increasing myeloid cell diversity. *Nat Rev Immunol*. 2021;21(8):485-498. doi:10.1038/s41577-020-00490-y

92. Li K, Shi H, Zhang B, et al. Myeloid-derived suppressor cells as immunosuppressive regulators and therapeutic targets in cancer. *Signal Transduct Target Ther*. 2021;6(1):1-25. doi:10.1038/s41392-021-00670-9

93. Yang Y, Li C, Liu T, Dai X, Bazhin A V. Myeloid-Derived Suppressor Cells in Tumors: From Mechanisms to Antigen Specificity and Microenvironmental Regulation. *Front Immunol*. 2020;11:1371. doi:10.3389/fimmu.2020.01371

94. Adeshakin AO, Liu W, Adeshakin FO, et al. Regulation of ROS in myeloid-derived suppressor cells through targeting fatty acid transport protein 2 enhanced anti-PD-L1 tumor immunotherapy. *Cell Immunol*. 2021;362. doi:10.1016/j.cellimm.2021.104286

95. Park MJ, Baek JA, Choi JW, et al. Programmed Death-Ligand 1 Expression Potentiates the Immune Modulatory Function Of Myeloid-Derived Suppressor Cells in Systemic Lupus Erythematosus. *Front Immunol*. 2021;12. doi:10.3389/fimmu.2021.606024

96. Ramel E, Lillo S, Daher B, Fioleau M, Daubon T, Saleh M. cells The Metabolic Control of Myeloid Cells in the Tumor Microenvironment. 2021;10:2960. doi:10.3390/cells10112960

97. Li Y, Zhao L, Li XF. Hypoxia and the Tumor Microenvironment. doi:10.1177/15330338211036304

98. Pinton L, Solito S, Damuzzo V, et al. Activated T cells sustain myeloid-derived suppressor cellmediated immune suppression. *Oncotarget*. 2016;7(2):1168-1184. doi:10.18632/oncotarget.6662

99. Gallina G, Dolcetti L, Serafini P, et al. Tumors induce a subset of inflammatory monocytes with immunosuppressive activity on CD8+ T cells. *Journal of Clinical Investigation*. 2006;116(10):2777-2790. doi:10.1172/JCI28828

100. Stiff A, Trikha P, Mundy-Bosse B, et al. Nitric oxide production by myeloid-derived suppressor cells plays a role in impairing Fc receptor–mediated natural killer cell

function. *Clinical Cancer Research*. 2018;24(8):1891-1904. doi:10.1158/1078-0432.CCR-17-0691

101. Pillay J, Tak T, Kamp VM, Koenderman L. Immune suppression by neutrophils and granulocytic myeloid-derived suppressor cells: Similarities and differences. *Cellular and Molecular Life Sciences*. 2013;70(20):3813-3827. doi:10.1007/s00018-013-1286-4

102. Youn JI, Gabrilovich DI. The biology of myeloid-derived suppressor cells: The blessing and the curse of morphological and functional heterogeneity. *Eur J Immunol*. 2010;40(11):2969-2975. doi:10.1002/eji.201040895

103. Lelis FJN, Jaufmann J, Singh A, et al. Myeloid-derived suppressor cells modulate B-cell responses. *Immunol Lett*. 2017;188:108-115. doi:10.1016/j.imlet.2017.07.003

104. Wang Y, Schafer CC, Hough KP, et al. Myeloid-Derived Suppressor Cells Impair B Cell Responses in Lung Cancer through IL-7 and STAT5. *The Journal of Immunology*. 2018;201(1):278-295. doi:10.4049/jimmunol.1701069

105. Shen M, Wang J, Yu W, et al. A novel MDSC-induced PD-1−PD-L1+B-cell subset in breast tumor microenvironment possesses immuno-suppressive properties. *Oncoimmunology*. 2018;7(4). doi:10.1080/2162402X.2017.1413520

106. Poschke I, Mao Y, Adamson L, Salazar-Onfray F, Masucci G, Kiessling R. Myeloid-derived suppressor cells impair the quality of dendritic cell vaccines. *Cancer Immunology, Immunotherapy*. 2012;61(6):827-838. doi:10.1007/s00262-011-1143-y

107. Ostrand-Rosenberg S, Sinha P, Beury DW, Clements VK. Cross-talk between myeloid-derived suppressor cells (MDSC), macrophages, and dendritic cells enhances tumor-induced immune suppression. *Semin Cancer Biol*. 2012;22(4):275-281. doi:10.1016/j.semcancer.2012.01.011

108. Kumar V, Cheng P, Condamine T, et al. CD45 Phosphatase Inhibits STAT3 Transcription Factor Activity in Myeloid Cells and Promotes Tumor-Associated Macrophage Differentiation. *Immunity*. 2016;44(2):303-315. doi:10.1016/j.immuni.2016.01.014

109. Li F, Zhao Y, Wei L, Li S, Liu J. Tumor-infiltrating Treg, MDSC, and IDO expression associated with outcomes of neoadjuvant chemotherapy of breast cancer. *Cancer Biol Ther*. 2018;19(8):695-705. doi:10.1080/15384047.2018.1450116

110. OuYang LY, Wu XJ, Ye SB, et al. Tumor-induced myeloid-derived suppressor cells promote tumor progression through oxidative metabolism in human colorectal cancer. *J Transl Med*. 2015;13(1). doi:10.1186/s12967-015-0410-7

111. Huang B, Pan PY, Li Q, et al. Gr-1+CD115+ immature myeloid suppressor cells mediate the development of tumor-induced T regulatory cells and T-cell anergy in tumor-bearing host. *Cancer Res*. 2006;66(2):1123-1131. doi:10.1158/0008-5472.CAN-05-1299

112. Lee CR, Kwak Y, Yang T, et al. Myeloid-Derived Suppressor Cells Are Controlled by Regulatory T Cells via TGF-β during Murine Colitis. *Cell Rep*. 2016;17(12):3219-3232. doi:10.1016/j.celrep.2016.11.062

113. Gabitass RF, Annels NE, Stocken DD, Pandha HA, Middleton GW. Elevated myeloid-derived suppressor cells in pancreatic, esophageal and gastric cancer are an independent prognostic factor and are associated with significant elevation of the Th2 cytokine interleukin-13. *Cancer Immunology, Immunotherapy*. 2011;60(10):1419-1430. doi:10.1007/s00262-011-1028-0

114. Hao Z, Li R, Wang Y, Li S, Hong Z, Han Z. Landscape of Myeloid-derived Suppressor Cell in Tumor Immunotherapy. *Biomark Res*. 2021;9(1):77. doi:10.1186/s40364-021-00333-5

115. Diaz-Montero CM, Salem ML, Nishimura MI, Garrett-Mayer E, Cole DJ, Montero AJ. Increased circulating myeloid-derived suppressor cells correlate with clinical cancer stage, metastatic tumor burden, and doxorubicin–cyclophosphamide chemotherapy. *Cancer Immunology, Immunotherapy*. 2009;58(1):49-59. doi:10.1007/s00262-008-0523-4

116. De Cicco P, Ercolano G, Ianaro A. The New Era of Cancer Immunotherapy: Targeting Myeloid-Derived Suppressor Cells to Overcome Immune Evasion. *Front Immunol*. 2020;11:1680. doi:10.3389/fimmu.2020.01680

117. Park SJ, Nam DE, Seong HC, Hahn YS. New Discovery of Myeloid-Derived Suppressor Cell's Tale on Viral Infection and COVID-19. *Front Immunol*. 2022;13:275. doi:10.3389/fimmu.2022.842535

118. Crook KR. Role of myeloid-derived suppressor cells in autoimmune disease. *World J Immunol*. 2014;4(1):26. doi:10.5411/wji.v4.i1.26

119. Bryant AJ, Shenoy V, Fu C, et al. Myeloid-derived suppressor cells are necessary for development of pulmonary hypertension. *Am J Respir Cell Mol Biol*. 2018;58(2):170-180. doi:10.1165/rcmb.2017-0214OC

120. Oliveira AC, Fu C, Lu Y, et al. Chemokine signaling axis between endothelial and myeloid cells regulates development of pulmonary hypertension associated with pulmonary fibrosis and hypoxia. *Am J Physiol Lung Cell Mol Physiol*. 2019;317(4):L434-L444. doi:10.1152/AJPLUNG.00156.2019

121. Lebrun A, Lo Re S, Chantry M, et al. CCR2+ monocytic myeloid-derived suppressor cells (M-MDSCs) inhibit collagen degradation and promote lung fibrosis by producing transforming growth factor-ß1. *Journal of Pathology*. 2017;243(3):320-330. doi:10.1002/path.4956

122. Shvedova AA, Tkach A V., Kisin ER, et al. Carbon nanotubes enhance metastatic growth of lung carcinoma via up-regulation of myeloid-derived suppressor cells. *Small*. 2013;9(9-10):1691-1695. doi:10.1002/smll.201201470

123. Pilling D, Zheng Z, Vakil V, Gomer RH. Fibroblasts secrete Slit2 to inhibit fibrocyte differentiation and fibrosis. *Proc Natl Acad Sci U S A*. 2014;111(51):18291-18296. doi:10.1073/pnas.1417426112

124. Verstovsek S, Manshouri T, Pilling D, et al. Role of neoplastic monocyte-derived fibrocytes in primary myelofibrosis. *Journal of Experimental Medicine*. 2016;213(9):1723-1740. doi:10.1084/jem.20160283

125. Suh YG, Kim JK, Byun JS, et al. CD11b+ Gr1+ bone marrow cells ameliorate liver fibrosis by producing interleukin-10 in mice. *Hepatology*. 2012;56(5):1902-1912. doi:10.1002/hep.25817

126. Huaux F. Interpreting Immunoregulation in Lung Fibrosis: A New Branch of the Immune Model. *Front Immunol*. 2021;12:2941. doi:10.3389/fimmu.2021.690375

127. Sun SN, Ni SH, Li Y, et al. G-MDSCs promote aging-related cardiac fibrosis by activating myofibroblasts and preventing senescence. *Cell Death Dis*. 2021;12(6):1-17. doi:10.1038/s41419-021-03874-7

128. Renehan AG, Roberts DL, Dive C. Obesity and cancer: Pathophysiological and biological mechanisms. *Arch Physiol Biochem*. 2008;114(1):71-83. doi:10.1080/13813450801954303

129. Zeng S, Xiao Z, Wang Q, et al. Strategies to achieve immune tolerance in allogeneic solid organ transplantation. *Transpl Immunol*. 2020;58. doi:10.1016/j.trim.2019.101250

130. Shenderov K, Collins SL, Powell JD, Horton MR. Immune dysregulation as a driver of idiopathic pulmonary fibrosis. *Journal of Clinical Investigation*. 2021;131(2). doi:10.1172/JCI143226

131. Habiel DM, Espindola MS, Kitson C, et al. Characterization of CD28 null T cells in idiopathic pulmonary fibrosis. *Mucosal Immunol*. 2019;12(1):212-222. doi:10.1038/s41385-018-0082-8

132. Papiris SA, Kollintza A, Karatza M, et al. CD8+T lymphocytes in bronchoalveolar lavage in idiopathic pulmonary fibrosis. *J Inflamm*. 2007;4. doi:10.1186/1476-9255-4-14

133. Daniil Z, Kitsanta P, Kapotsis G, et al. CD8+ T lymphocytes in lung tissue from patients with idiopathic pulmonary fibrosis. *Respir Res*. 2005;6. doi:10.1186/1465-9921-6-81

134. Saeidi A, Zandi K, Cheok YY, et al. T-cell exhaustion in chronic infections: Reversing the state of exhaustion and reinvigorating optimal protective immune responses. *Front Immunol*. 2018;9(NOV). doi:10.3389/fimmu.2018.02569

135. Gumber D, Wang LD. Improving CAR-T immunotherapy: Overcoming the challenges of T cell exhaustion. *EBioMedicine*. 2022;77. doi:10.1016/j.ebiom.2022.103941

136. Ashley SL, Xia M, Murray S, et al. Six-SOMAmer Index Relating to Immune, Protease and Angiogenic Functions Predicts Progression in IPF. Ding Q, ed. *PLoS One*. 2016;11(8):e0159878. doi:10.1371/journal.pone.0159878

137. Herazo-Maya JD, Noth I, Duncan SR, et al. Peripheral blood mononuclear cell gene expression profiles predict poor outcome in idiopathic pulmonary fibrosis. *Sci Transl Med*. 2013;5(205). doi:10.1126/scitranslmed.3005964

138. Huang Y, Ma SF, Vij R, et al. A functional genomic model for predicting prognosis in idiopathic pulmonary fibrosis. *BMC Pulm Med*. 2015;15(1). doi:10.1186/s12890-015-0142-8

139. Celada LJ, Kropski JA, Herazo-Maya JD, et al. PD-1 up-regulation on CD4+ T cells promotes pulmonary fibrosis through STAT3-mediated IL-17A and TGF-ß1 production. *Sci Transl Med*. 2018;10(460). doi:10.1126/scitranslmed.aar8356

140. Raghu G, Remy-Jardin M, Myers JL, et al. Diagnosis of idiopathic pulmonary fibrosis An Official ATS/ERS/JRS/ALAT Clinical practice guideline. *Am J Respir Crit Care Med*. 2018;198(5):e44-e68. doi:10.1164/rccm.201807-1255ST

141. Miltenyi B. CD8+ T Cell Isolation Kit, human - T cells - MicroBeads and Isolation Kits - Cell separation reagents - MACS Cell Separation - Products - Miltenyi Biotec - USA. Published online 2007. Accessed May 26, 2022. https://www.miltenyibiotec.com/DE-en/products/realease-cd8-microbead-kit-human.html#130-117-036

142. Burgstaller G, Oehrle B, Koch I, Lindner M, Eickelberg O. Multiplex Profiling of Cellular Invasion in 3D Cell Culture Models. *PLoS One*. 2013;8(5). doi:10.1371/journal.pone.0063121

143. Vardhana SA, Hwee MA, Berisa M, et al. Impaired mitochondrial oxidative phosphorylation limits the self-renewal of T cells exposed to persistent antigen. *Nat Immunol*. 2020;21(9):1022-1033. doi:10.1038/s41590-020-0725-2

144. LEGENDplex™. Accessed June 11, 2022. https://www.biolegend.com/en-us/legendplex

145. Marwitz S, Ballesteros-Merino C, Jensen SM, et al. Phosphorylation of SMAD3 in immune cells predicts survival of patients with early stage non-small cell lung cancer. *J Immunother Cancer*. 2021;9:1469. doi:10.1136/jitc-2020-001469

146. Baumann T, Dunkel A, Schmid C, et al. Regulatory myeloid cells paralyze T cells through cell-cell transfer of the metabolite methylglyoxal. *Nat Immunol*. 2020;21(5):555-566. doi:10.1038/S41590-020-0666-9

147. Adams TS, Schupp JC, Poli S, et al. Single-cell RNA-seq reveals ectopic and aberrant lung-resident cell populations in idiopathic pulmonary fibrosis. *Sci Adv*. 2020;6(28). doi:10.1126/sciadv.aba1983

148. Li C, Liu T, Bazhin A V., Yang Y. The Sabotaging Role of Myeloid Cells in Anti-Angiogenic Therapy: Coordination of Angiogenesis and Immune Suppression by Hypoxia. *J Cell Physiol*. 2017;232(9):2312-2322. doi:10.1002/jcp.25726

149. Gabrilovich DI. Myeloid-derived suppressor cells. *Cancer Immunol Res*. 2017;5(1):3-8. doi:10.1158/2326-6066.CIR-16-0297

150. Gabrilovich DI, Nagaraj S. Myeloid-derived suppressor cells as regulators of the immune system. *Nat Rev Immunol*. 2009;9(3):162-174. doi:10.1038/nri2506

151. Condamine T, Gabrilovich DI. Molecular mechanisms regulating myeloid-derived suppressor cell differentiation and function. *Trends Immunol*. 2011;32(1):19-25. doi:10.1016/j.it.2010.10.002

152. Kolahian S, Öz HH, Zhou B, Griessinger CM, Rieber N, Hartl D. The emerging role of myeloid-derived suppressor cells in lung diseases. *European Respiratory Journal*. 2016;47(3):967-977. doi:10.1183/13993003.01572-2015

153. Raghu G, Anstrom KJ, King, Jr. TE, Lasky JA, Martinez FJ. A Double-Blind, Placebo-Controlled, Randomized Trial Of Combined Prednisone, Azathioprine And N-Acetylcysteine In Idiopathic Pulmonary Fibrosis. In: *American Thoracic Society International Conference Meetings Abstracts*. American Thoracic Society; 2012:A6859-A6859. doi:10.1164/ajrccm-conference.2012.185.1_meetingabstracts.a6859

154. Baumann T, Dunkel A, Schmid C, et al. Regulatory myeloid cells paralyze T cells through cell–cell transfer of the metabolite methylglyoxal. *Nat Immunol*. 2020;21(5):555-566. doi:10.1038/S41590-020-0666-9

155. Wang Z, Wang S, Goplen NP, et al. PD-1hi CD8+ resident memory T cells balance immunity and fibrotic sequelae. *Sci Immunol*. 2019;4(36). doi:10.1126/sciimmunol.aaw1217

156. Kulpa DA, Lawani M, Cooper A, Peretz Y, Ahlers J, Sékaly RP. PD-1 coinhibitory signals: The link between pathogenesis and protection. *Semin Immunol*. 2013;25(3):219-227. doi:10.1016/j.smim.2013.02.002

157. Liu J, Chen Z, Li Y, Zhao W, Wu JB, Zhang Z. PD-1/PD-L1 Checkpoint Inhibitors in Tumor Immunotherapy. *Front Pharmacol*. 2021;12. doi:10.3389/fphar.2021.731798

158. Keir ME, Butte MJ, Freeman GJ, Sharpe AH. PD-1 and its ligands in tolerance and immunity. *Annu Rev Immunol*. 2008;26:677-704. doi:10.1146/annurev.immunol.26.021607.090331

159. Kasembeli MM, Bharadwaj U, Robinson P, Tweardy DJ. Contribution of STAT3 to inflammatory and fibrotic diseases and prospects for its targeting for treatment. *Int J Mol Sci*. 2018;19(8). doi:10.3390/ijms19082299

160. Ni K, Liu M, Zheng J, et al. PD-1/PD-L1 pathway mediates the alleviation of pulmonary fibrosis by human mesenchymal stem cells in humanized mice. *Am J Respir Cell Mol Biol*. 2018;58(6):684-695. doi:10.1165/rcmb.2017-0326OC

161. Dustin ML. Tireless surveillance by exhausted T cells. *Journal of Clinical Investigation*. 2021;131(18). doi:10.1172/JCI152382

162. Yin J, Wu Y, Yang X, Gan L, Xue J. Checkpoint Inhibitor Pneumonitis Induced by Anti-PD-1/PD-L1 Therapy in Non-Small-Cell Lung Cancer: Occurrence and Mechanism. *Front Immunol*. 2022;13. doi:10.3389/FIMMU.2022.830631

163. Pardoll DM. The blockade of immune checkpoints in cancer immunotherapy. *Nat Rev Cancer*. 2012;12(4):252-264. doi:10.1038/nrc3239

164. Zerdes I, Matikas A, Bergh J, Rassidakis GZ, Foukakis T. Genetic, transcriptional and post-translational regulation of the programmed death protein ligand 1 in cancer: biology and clinical correlations. *Oncogene*. 2018;37(34):4639-4661. doi:10.1038/s41388-018-0303-3

165. Duitman JW, van den Ende T, Spek CA. Immune checkpoints as promising targets for the treatment of idiopathic pulmonary fibrosis? *J Clin Med*. 2019;8(10). doi:10.3390/jcm8101547

166. Wang JC, Sun L. PD-1/PD-L1, MDSC Pathways, and Checkpoint Inhibitor Therapy in Ph(-) Myeloproliferative Neoplasm: A Review. *Int J Mol Sci*. 2022;23(10). doi:10.3390/ijms23105837

167. Cui L, Chen SY, Lerbs T, et al. Activation of JUN in fibroblasts promotes pro-fibrotic programme and modulates protective immunity. doi:10.1038/s41467-020-16466-4

168. Gabrilovich DI, Ostrand-Rosenberg S, Bronte V. Coordinated regulation of myeloid cells by tumours. *Nat Rev Immunol*. 2012;12(4):253-268. doi:10.1038/nri3175

169. Cassetta L, Bruderek K, Skrzeczynska-Moncznik J, et al. Differential expansion of circulating human MDSC subsets in patients with cancer, infection and inflammation. *J Immunother Cancer*. 2020;8(2):e001223. doi:10.1136/jitc-2020-001223

170. Zhou X, Fang D, Liu H, et al. PMN-MDSCs accumulation induced by CXCL1 promotes CD8+ T cells exhaustion in gastric cancer. *Cancer Lett*. 2022;532:215598. doi:10.1016/j.canlet.2022.215598

171. Zhang M, Zhang S. T Cells in Fibrosis and Fibrotic Diseases. *Front Immunol*. 2020;11:1142. doi:10.3389/fimmu.2020.01142

172. Chen JH, Schulman H, Gardner P. A cAMP-Regulated Chloride Channel in Lymphocytes That Is Affected in Cystic Fibrosis. *Science (1979)*. 1989;243(4891):657-660. doi:10.1126/SCIENCE.2464852

173. Hao Z, Hampel B, Yagita H, Rajewsky K. T Cell–specific Ablation of Fas Leads to Fas Ligand–mediated Lymphocyte Depletion and Inflammatory Pulmonary Fibrosis. *Journal of Experimental Medicine*. 2004;199(10):1355-1365. doi:10.1084/JEM.20032196

174. McKinney EF, Lee JC, Jayne DRW, Lyons PA, Smith KGC. T-cell exhaustion, co-stimulation and clinical outcome in autoimmunity and infection. *Nature 2015 523:7562*. 2015;523(7562):612-616. doi:10.1038/nature14468

175. Messmann JJ, Reisser T, Leithäuser F, Lutz MB, Debatin KM, Strauss G. In vitro-generated MDSCs prevent murine GVHD by inducing type 2 T cells without disabling antitumor cytotoxicity. *Blood*. 2015;126(9):1138-1148. doi:10.1182/blood-2015-01-624163

176. Weiss JM, Subleski JJ, Back T, et al. Regulatory T Cells and Myeloid-Derived Suppressor Cells in the Tumor Microenvironment Undergo Fas-Dependent Cell Death during IL-2/αCD40 Therapy. *The Journal of Immunology*. 2014;192(12):5821-5829. doi:10.4049/jimmunol.1400404

177. Sinha P, Chornoguz O, Clements VK, Artemenko KA, Zubarev RA, Ostrand-Rosenberg S. Myeloid-derived suppressor cells express the death receptor Fas and apoptose in response to T cell-expressed FasL. *Blood*. 2011;117(20):5381-5390. doi:10.1182/blood-2010-11-321752

178. Chen L, Wang Y, Huang J, Hu B, Huang W. Identification of Immune-Related Hub Genes in Parkinson's Disease. *Front Genet*. 2022;13. doi:10.3389/fgene.2022.914645

179. Dominguez GA, Condamine T, Mony S, et al. Selective targeting of myeloid-derived suppressor cells in cancer patients using DS-8273a, an agonistic TRAIL-R2 antibody. *Clinical Cancer Research*. 2017;23(12):2942-2950. doi:10.1158/1078-0432.CCR-16-1784

180. Lim JY, Kim TW, Ryu D Bin, et al. Myeloma-secreted galectin-1 potently interacts with CD304 on monocytic myeloid-derived suppressor cells. *Cancer Immunol Res*. 2021;9(5):503-513. doi:10.1158/2326-6066.CIR-20-0663

181. Heigl T, Singh A, Saez-Gimenez B, et al. Myeloid-Derived Suppressor Cells in Lung Transplantation. *Front Immunol*. 2019;10(APR):900. doi:10.3389/fimmu.2019.00900

182. Koushki K, Salemi M, Miri SM, Arjeini Y, Keshavarz M, Ghaemi A. Role of myeloid-derived suppressor cells in viral respiratory infections; Hints for discovering therapeutic targets for COVID-19. *Biomedicine and Pharmacotherapy*. 2021;144:112346. doi:10.1016/j.biopha.2021.112346

183. Condamine T, Ramachandran I, Youn JI, Gabrilovich DI. Regulation of Tumor Metastasis by Myeloid-derived Suppressor Cells. doi:10.1146/annurev-med-051013-052304

184. Ouzounova M, Lee E, Piranlioglu R, et al. Monocytic and granulocytic myeloid derived suppressor cells differentially regulate spatiotemporal tumour plasticity during metastatic cascade. *Nat Commun*. 2017;8(1):1-13. doi:10.1038/ncomms14979

185. Roberts LM, Perez MJ, Balogh KN, Mingledorff G, Cross J V., Munson JM. Myeloid Derived Suppressor Cells Migrate in Response to Flow and Lymphatic Endothelial Cell Interaction in the Breast Tumor Microenvironment. *Cancers (Basel)*. 2022;14(12). doi:10.3390/cancers14123008

186. Patel S. *A Unique Pattern Of Pmn-Mdsc Migration Inn Cancer*. University of Pennsylvania; 2017. https://repository.upenn.edu/edissertations/2517

187. McKenna KC, Beatty KM, Vicetti Miguel R, Bilonick RA. Delayed processing of blood increases the frequency of activated CD11b+ CD15+ granulocytes which inhibit T cell function. *J Immunol Methods*. 2009;341(1-2):68-75. doi:10.1016/j.jim.2008.10.019

188. Grützner E, Stirner R, Arenz L, et al. Kinetics of human myeloid-derived suppressor cells after blood draw. *J Transl Med*. 2016;14(1):2. doi:10.1186/s12967-015-0755-y

189. Deng X, Li X, Guo X, et al. Myeloid-derived suppressor cells promote tumor growth and sorafenib resistance by inducing FGF1 upregulation and fibrosis. *Neoplasia (United States)*. 2022;28. doi:10.1016/j.neo.2022.100788

190. Kalluri R. The biology and function of fibroblasts in cancer. *Nat Rev Cancer*. 2016;16(9):582-598. doi:10.1038/nrc.2016.73

191. Hill C, Jones MG, Davies DE, Wang Y. *Epithelial-Mesenchymal Transition Contributes to Pulmonary Fibrosis via Aberrant Epithelial/Fibroblastic Cross-Talk Introduction and Discussion*.

192. Arora PD, McCulloch CAG. Dependence of collagen remodeling on α-smooth muscle actin expression by fibroblasts. *J Cell Physiol*. 1994;159(1):161-175. doi:10.1002/jcp.1041590120

193. Cheuk YC, Xu S, Zhu D, et al. Monocytic Myeloid-Derived Suppressor Cells Inhibit Myofibroblastic Differentiation in Mesenchymal Stem Cells Through IL-15 Secretion. *Front Cell Dev Biol*. 2022;10. doi:10.3389/fcell.2022.817402

194. Denu RA, Nemcek S, Bloom DD, et al. Fibroblasts and Mesenchymal Stromal/Stem Cells Are Phenotypically Indistinguishable. *Acta Haematol*. 2016;136(2):85-97. doi:10.1159/000445096

195. Sabatini F, Petecchia L, Tavian M, De Villeroché VJ, Rossi GA, Brouty-Boyé D. Human bronchial fibroblasts exhibit a mesenchymal stem cell phenotype and multilineage differentiating potentialities. *Laboratory Investigation*. 2005;85(8):962-971. doi:10.1038/labinvest.3700300

196. Hanson SE, Kim J, Quinchia Johnson BH, et al. Characterization of mesenchymal stem cells from human vocal fold fibroblasts. *Laryngoscope*. 2010;120(3):546-551. doi:10.1002/lary.20797

197. Shichino S, Abe J, Ueha S, et al. Reduced supply of monocyte-derived macrophages leads to a transition from nodular to diffuse lesions and tissue cell activation in silica-induced pulmonary fibrosis in mice. *American Journal of Pathology*. 2015;185(11):2923-2938. doi:10.1016/j.ajpath.2015.07.013

198. Ogawa T, Shichino S, Ueha S, Matsushima K. Macrophages in lung fibrosis. *Int Immunol*. 2021;33(12):665-671. doi:10.1093/intimm/dxab040

8. Appendix A

8.1 MDSCs MACS-based bead subset isolation

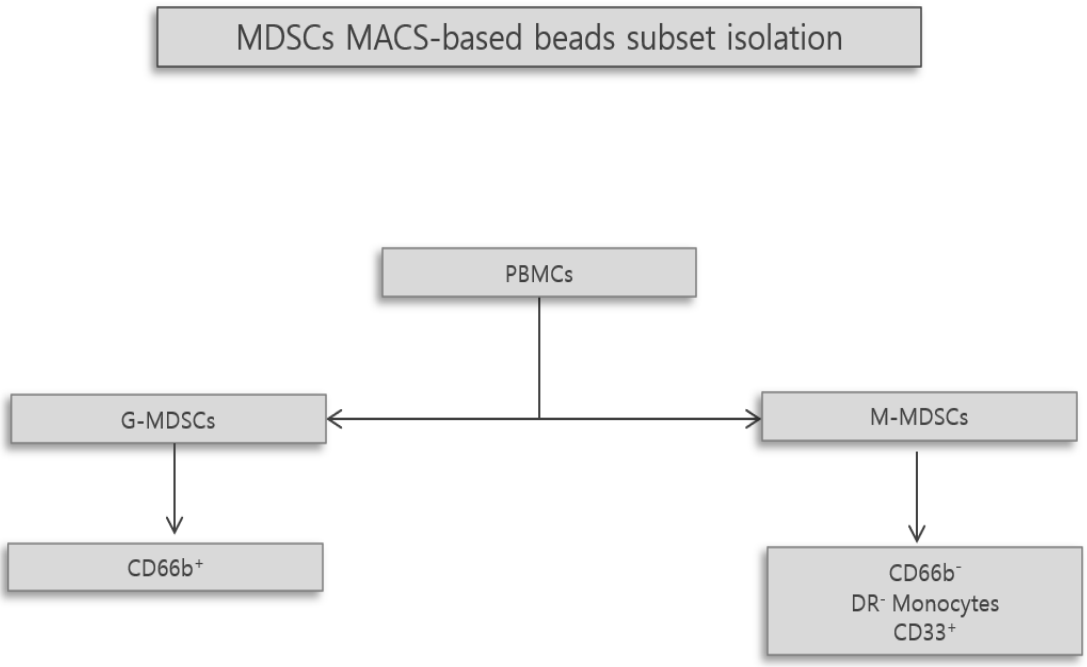

Figure A1. Diagram that summarizes MDSCs MACS-based bead subset isolation. The diagram provides a concise overview of the isolation steps used to isolate G-MDSCs and M-MDSCs using magnetic beads derived from PBMCs.

8.2 M-MDSC purity after bead isolation

During the development of the MDSCs isolation protocol, the purity of M-MDSCs was assessed using FACS, which yielded a purity level of over 94% (refer to Figure S2). The MDSCs cocktail panel 1, as outlined in Section 3.2.6.1, was employed for FACS analysis, without the addition of CD236 and Neuropilin-1 antibodies.

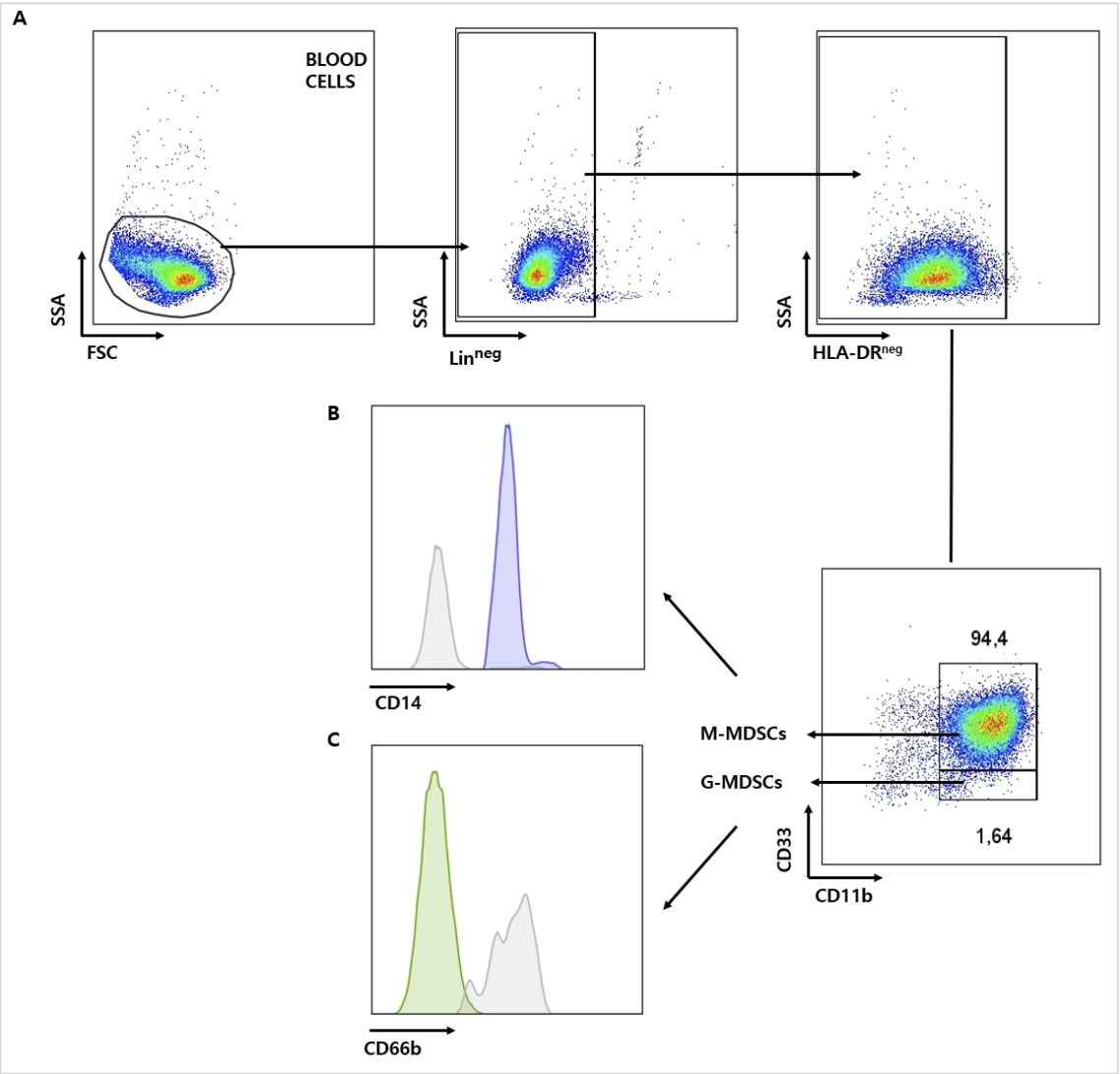

Figure A2. M-MDSCs purity after bead isolation. **A)** M-MDSCs gating strategy in flow cytometry represented by dot-plots graphs of peripheral blood. Lineage negative was used to exclude differentiated and mature cell populations; **B)** M-MDSCs ($CD14^+$) are represented in blue histograms and **C)** G-MDSCs ($CD66b^+$) in green. Isotypes are represented in gray.

Acknowledgments

I would like to express my heartfelt gratitude to all those who have contributed to this chapter of my life. Without your support, guidance, and encouragement, this journey would not have been possible.

First and foremost, my heartfelt thanks go to my supervisor, Dr. Isis Fernandez, whose unwavering support, expert guidance, and invaluable insights have played a pivotal role in shaping this thesis. I genuinely appreciate your mentorship and the confidence you've placed in me throughout this research endeavor.

I am also profoundly grateful to PD. Dr. med. Anne Hilgendorff for her exceptional supervision and support. Prof. Peter Murray, a member of my thesis committee, also deserves my gratitude for his expert feedback and guidance. Anne and Peter, my gratitude for your time and insights is immense. I would also like to acknowledge the efforts of Dr. Marion Frankenberg and Patricia Sklarek in patient recruitment, blood sample collection, and clinical data management.

Daniela Dietel, your role in this journey cannot be overstated. Your technical expertise and unwavering assistance were the very foundation upon which this research was built. Beyond that, I am grateful for the genuine friendship you've offered.

My gratitude extends to CPC Research School, which provided not just resources, but also a nurturing research environment. I'd like to extend a special thank you to PD Dr. Claudia Staab-Weijnitz for her unwavering support throughout these years. Claudia, your understanding and encouragement have made a significant difference for all of us at the Research School.

Gratitude is extended to all those who have been, and continue to be, part of the current lab team. Among them, Flavia, Ivette, Debora, Apurva, and Dmytro, whose collaborative spirit and unwavering dedication have significantly enhanced the quality of this project.

To my fellow Ph.D. students—Erika, Ceylan, Shruthi, Michal, Pushkar, Ashesh, Aydan, Arunima, Anna, and Vijay—I am thankful for the camaraderie, insightful discussions, and shared experiences that have been a source of motivation and learning throughout our journey together.

To my beloved daughter Salwa, your remarkable resilience and understanding have provided me with immeasurable strength. Although I may not have been able to be with you as often as I wished, your unwavering love has been my rock. I hold your patience close to my heart and vow to compensate for all you've given up for me.

I must emphasize the incredible support I've received from my parents, Sonia and Rene. Your unwavering belief in my capabilities, constant encouragement, and the sacrifices you've made have been the driving force behind my academic journey. This achievement is a testament to the depth of your love and support. Your words of encouragement during the most challenging moments, especially when the distance of being in another country made things exceedingly tough, and I found myself on the verge of giving up on my dream, have been etched in my heart. My gratitude is boundless, and I will be eternally thankful.

I also want to thank my sisters, Andrea and Maria Jose, for always believing in me and offering their unwavering support. Additionally, I'd like to express my gratitude to my late grandparents, Sonia and Octavio, who were always my most steadfast advocates and stood by me throughout my journey.

To my boyfriend, Christian, your love and support were the pillars that held me up during the toughest times. Thank you for helping me strike a balance in my life and for your radiant positivity that brightened even my darkest days.

To my friends scattered around the world—Sol, Estefania, David, Sofia, Katherine, Jessi, Lucia, Johana, Cristina, Claudia, Carla, and Adriana—your encouragement, kind words, messages, video chats, and virtual gatherings have been my lifeline. Your support has been unwavering, and I treasure your friendship that knows no bounds.

Affidavit

LMU LUDWIG-MAXIMILIANS-UNIVERSITÄT MÜNCHEN

Dean's Office
Medical Faculty

MMRS

Affidavit

Viteri Alvarez, Sonia Valeria

Surname, first name

Max-Lebsche-Platz 31

Street

81377 München

Zip code, town

Germany

Country

I hereby declare, that the submitted thesis entitled

Myeloid cells immunomodulate tissue niches in Idiopathic Pulmonary Fibrosis

is my own work. I have only used the sources indicated and have not made unauthorised use of services of a third party. Where the work of others has been quoted or reproduced, the source is always given.

I further declare that the dissertation presented here has not been submitted in the same or similar form to any other institution for the purpose of obtaining an academic degree.

Munich, July 10th, 2024

Place, date

Valeria Viteri Alvarez

Signature doctoral candidate

Confirmation of Congruency

LMU LUDWIG-MAXIMILIANS-UNIVERSITÄT MÜNCHEN | Dean's Office Medical Faculty | MMRS

Confirmation of congruency between printed and electronic version of the doctoral thesis

Viteri Alvarez, Sonia Valeria

Surname, first name

Max-Lebsche-Platz 31

Street

81377 München

Zip code, town

Germany

Country

I hereby declare that the electronic version of the submitted thesis, entitled

Myeloid cells immunomodulate tissue niches in Idiopathic Pulmonary Fibrosis

is congruent with the printed version both in content and format.

Munich, July 10th, 2024

Place, date

Valeria Viteri Alvarez

Signature doctoral candidate

List of Publications

Wang X, Zhang H, Wang Y, Bramasole L, Guo K, Mourtada F, Meul T, Hu Q, **Viteri V**, Kammerl I, Konigshoff M, Lehmann M, Magg T, Hauck F, Fernandez IE, Meiners S. DNA sensing via the cGAS/STING pathway activates the immunoproteasome and adaptive T-cell immunity. EMBO J. 2023 Apr 17;42(8):e110597. doi: 10.15252/embj.2022110597. Epub 2023 Mar 13. PMID: 36912165; PMCID: PMC10106989.

Mayr C., Sengupta A., Ansari M., Pestoni J., Ogar P., Angelidis I., Liontos A, Rodriguez-Castillo A,. Lang N, Strunz M, Asgharpour S, Porras-Gonzalez D, Gerckens M, Oehrle B, **Viteri-Alvarez V**, Fernandez I, Tallquist M, Irmler M, Beckers J, Eickelberg O, Mircea Stoleriu G, Behr J, Kneidinger N, Yildirim A, Ahlbrecht K, Morty R, Samakovlis C,. Theis F, Burgstaller G, Schiller H. Autocrine Sfrp1 inhibits lung fibroblast invasion during transition to injury induced myofibroblasts. bioRxiv 2022.07.11.499594; doi: https://doi.org/10.1101/2022.07.11.499594 (preprint)

Greiffo FR, **Viteri-Alvarez V**, Frankenberger M, Dietel D, Ortega-Gomez A, Lee JS, Hilgendorff A, Behr J, Soehnlein O, Eickelberg O, Fernandez IE. CX3CR1-fractalkine axis drives kinetic changes of monocytes in fibrotic interstitial lung diseases. Eur Respir J. 2020 Feb 20;55(2):1900460. doi: 10.1183/13993003.00460-2019. PMID: 31744836.

Koentges C, Pepin ME, Müsse C, Pfeil K, **Alvarez SVV**, Hoppe N, Hoffmann MM, Odening KE, Sossalla S, Zirlik A, Hein L, Bode C, Wende AR, Bugger H. Gene expression analysis to identify mechanisms underlying heart failure susceptibility in mice and humans. Basic Res Cardiol. 2017 Dec 29;113(1):8. doi: 10.1007/s00395-017-0666-6.